Nanoparticles for efficient uptake by Human Dendritic Cells and T Lymphocytes to be used in Adoptive Immunotherapy

Dissertation zur Erlangung des Grades
“Doktor der Naturwissenschaften“
am Fachbereich Biologie
der Johannes Gutenberg-Universität Mainz

vorgelegt von

Oliver Zupke

geboren am 09.02.1982
in Wiesbaden

Mainz, 2012

1. Gutachter:

2. Gutachter:

Tag der mündlichen Prüfung: 26.11.12

Eidesstattliche Erklärung

„Ich erkläre, dass ich die vorgelegte Thesis selbständig, ohne unerlaubte fremde Hilfe und nur mit den Hilfen angefertigt habe, die ich in der Thesis angegeben habe. Alle Textstellen, die wörtlich oder sinngemäß aus veröffentlichten oder nicht veröffentlichten Schriften entnommen sind, und alle Angaben, die auf mündlichen Auskünften beruhen, sind als solche kenntlich gemacht. Bei den von mir durchgeführten Untersuchungen habe ich die Grundsätze guter wissenschaftlicher Praxis, wie sie in der Satzung der Johannes Gutenberg-Universität Mainz zur Sicherung guter wissenschaftlicher Praxis niedergelegt sind, eingehalten."

Mainz, den _____

Contents

List of figures……VI
List of tables……VIII
Abbreviations……IX

1 Abstract 1
Zusammenfassung 2
2 Introduction 4
2.1 The human immune system 4
2.1.1 Innate immune responses 4
2.1.2 Adaptive immunity 4
2.1.2.1 B and T cell receptor 4
2.1.2.2 Human leukocyte antigens 5
2.1.2.3 Antigen processing and presentation 5
2.1.2.4 T lymphocyte activation by APC 7
2.1.2.5 Effector mechanisms of T cells 8
2.1.3 Cellular immunotherapies 9
2.2 Nanoparticles 12
2.2.1 Definition and areas of application 12
2.2.2 Synthesis 12
2.2.3 Nanoparticles in medicine 14
2.2.4 Variation of NP parameters for different biomedical applications 15
2.2.5 Cellular uptake of nanoparticles 17
2.3 Motivation and aims of this work 18
2.3.1 Labeling of dendritic cells with nanoparticles 18
2.3.2 Loading of T lymphocytes with nanoparticles 20
3 Materials & Methods 22
3.1 Materials for cell culture 22
3.1.1 Laboratory equipment 22
3.1.2 Plastic material 23
3.1.3 Substances and solutions 23
3.1.4 Cell culture media 24
3.1.5 Cytokines 24
3.2 Cell culture 24

3.2.1 Isolation of PBMCs from buffy coats by Ficoll density centrifugation 24
3.2.2 Freezing and thawing of cells 25
3.3 Primary cells and cell lines 25
3.3.1 Generation of Dendritic Cells from PBMC 25
3.3.2 Isolation of T lymphocytes from PBMCs 26
3.3.3 Generation of allo-HLA reactive T-cell lines 26
3.3.4 Jurkat T cells 27
3.3.5 CTL clones 27
3.3.6 AML blasts 27
3.3.7 EBV-B (RCC1257) 28
3.3.8 Tumor cell line (RCC1257) 28
3.3.9 Murine T-cell lines 28
3.4 Nanoparticles 29
3.4.1 Materials for nanoparticle synthesis 29
3.4.2 Synthesis of polymeric nanoparticles 30
3.4.3 Characterization of nanoparticles 30
3.5 Loading of cells with nanoparticles 32
3.5.1 DCs 32
3.5.1.1 Particle uptake and protocol optimization 32
3.5.1.2 Particle release 32
3.5.2 T lymphocytes 33
3.5.2.1 Particle uptake and protocol optimization 33
3.5.2.2 Uptake mechanism 34
3.5.2.3 Particle release 34
3.5.3 Human B lymphocytes and murine T cell lines 35
3.6 Analysis of nanoparticle uptake and toxicity by flow cytometry 36
3.6.1 NP uptake of vital cells 36
3.6.2 7-Amino-actinomycin D staining of dead cells for flow cytometry 37
3.6.3 Immunofluorescent staining with monoclonal antibodies for flow cytometry 38
3.7 Confocal laser scanning microscopy of NP-loaded cells 39
3.7.1 DCs 39
3.7.2 T lymphocytes 40
3.8 Transmission electron microscopy of NP-loaded T cells 40
3.9 Phenotypical and functional evaluation of NP-loaded cells 41
3.9.1 DCs 41
3.9.1.1 Phenotypical characterization (by flow cytometry) 41

3.9.1.2 Allogeneic stimulatory capacity (by ^{3}H-thymidine proliferation assay) 41
3.9.1.3 Antigen processing and presentation (by IFN-γ ELISPOT assays) 41
3.9.2 T Lymphocytes 43
3.9.2.1 Recognition of target cells (by IFN-γ ELISPOT assays) 43
3.9.2.2 Specific lysis of target cells (by ^{51}Chromium release assays) 43
3.10 Optimizing NP incorporation and duration of labeling 44
3.10.1 Transfection agents 44
3.10.1.1 Protamine sulfate and Lipofectamine 44
3.10.1.2 PULSIn™ 45
3.10.2 Electroporation 45
3.10.3 Selection of strongly labeled cells by cell sorting 46
3.10.4 Chloroquine 46
3.10.5 Biocoating of NP with Influenza whole virus 46
3.11 Delivery of Cy5-oligonucleotides with biodegradable PBCA nanocapsules 47
4 Results I: Dendritic cells 48
4.1 Labeling of DCs with nanoparticles 48
4.1.1 Labeling efficiency of DCs with polystyrene nanoparticles 48
4.1.2 Optimization of particle concentration 49
4.1.3 Optimization of particle incubation time 50
4.1.4 Verification of nanoparticle uptake by confocal laser scanning microscopy (cLSM) 52
4.1.5 Release of NP by mDCs 53
4.2 Functional evaluation of NP-loaded DCs 53
4.2.1 Expression of cell surface molecules on mDCs 53
4.2.2 Immunostimulatory capacity of labeled mDCs 54
4.2.3 Processing and presentation of viral antigens 55
5 Results II: T lymphocytes 57
5.1 Loading of T cells with nanoparticles 57

5.1.1 Labeling efficiency of T cells with polystyrene nanoparticles 57
5.1.2 Time point of NP loading during T cell re-stimulation cycle....59
5.1.3 Influence of cell culture age on NP uptake capacity 60
5.1.4 Optimization of NP concentration....60
5.1.5 Optimization of incubation time 61
5.1.6 Influence of temperature on NP uptake....62
5.1.7 Influence of human serum on NP uptake 63
5.1.8 Verification of NP uptake by cLSM....64
5.2 Functional evaluation of NP-loaded T lymphocytes: Recognition and lysis of target cells....65
5.3 Uptake mechanism in T cells 67
5.3.1 Influence of pharmacologic endocytosis inhibitors on NP uptake 67
5.3.2 Intracellular localization of NP by TEM....69
5.4 Release of NP by T cells....70
5.4.1 Long-term follow-up of NP-loaded T cells....70
5.4.2 Influence of human serum on NP release 71
5.4.3 NP release during the first 24 h and influence of cell proliferation 71
5.4.4 Influence of adenosine triphosphate binding cassette (ABC)-transporter on NP release....72
5.5 Release of NP by human B cells and murine T cell lines....73
5.6 Optimizing NP incorporation and duration of labeling in human T cell lines 74
5.6.1 Transfection agents....75
5.6.1.1 Protamine sulfate and Lipofectamine....75
5.6.1.2 PULSIn™ 76
5.6.2 Electroporation....78
5.6.3 Selection of strongly labeled cells by cell sorting....80
5.6.4 Chloroquine 81
5.6.5 Transferrin-conjugated nanoparticles....82
5.6.6 Biocoating of NP with Influenza whole virus 82
5.7 Delivery of Cy5-oligonucleotides with biodegradable PBCA nanocapsules....85
6 Discussion.... 87
6.1 Labeling of dendritic cells with nanoparticles....87
6.2 Loading of T lymphocytes with nanoparticles....90
7 Conclusions 96

8 References..... 97
9 Danksagung 109
10 Veröffentlichungen 111
10.1 Publikationen 111
10.2 Postervorträge 111
11 Lebenslauf.....112

List of figures

Figure 1: Schematic of the miniemulsion process 13
Figure 2: TEM picture of polystyrene NP 14
Figure 3: Schematic representation of a nanoparticle with variation possibilities of individual components for different biomedical applications 16
Figure 4: Schematic representation of endocytic pathways and intracellular trafficking of endosomes 18
Figure 5: Generation of monocyte-derived dendritic cells and subsequent labeling with polymeric nanoparticles 48
Figure 6: Uptake of unfunctionalized versus functionalized, fluorescent nanoparticles in immature dendritic cells (iDCs) 49
Figure 7: FACS analysis of immature dendritic cells incubated with different concentrations of the amino-functionalized particle NP-2-NH_2 for 16 h 50
Figure 8: Uptake kinetics as fluorescence intensity of immature dendritic cells after incubation with NP-2-NH_2 for different time periods from 0.5 to 24 h 51
Figure 9: Confocal laser scanning microscopy of DCs after incorporation of NP-2-NH_2 52
Figure 10: Long-term follow-up over 8 days of mature DCs loaded with PMI-containing amino-functionalized nanoparticles (NP-2-NH_2) 53
Figure 11: Phenotypical characterization of NP-labeled mDCs 54
Figure 12: Allogeneic stimulatory capacity of NP-loaded and unlabeled mDCs analyzed in an allo-MLR proliferation assay 55
Figure 13: Processing and presentation of viral antigens 56
Figure 14: Generation of allo-HLA-reactive T lymphocytes and loading of the cells with polymeric nanoparticles. 57
Figure 15: Uptake of unfunctionalized versus functionalized, fluorescent nanoparticles by $CD4^+$ T cells 59
Figure 16: Optimal time point of NP loading during T cell re-stimulation cycle 59
Figure 17: Influence of T cell culture age on particle uptake capacity 60
Figure 18: Optimization of NP concentration 61
Figure 19: Optimization of incubation time 62
Figure 20: Temperature dependence of NP uptake 62
Figure 21: Influence of human serum concentration on NP uptake and T cell viability 64
Figure 22: Confirmation of intracellular localization of NP by confocal laser scanning microscopy 65
Figure 23: Analyzing effector functions of NP-loaded leukemia- and tumor-reactive $CD8^+$ CTL clones as well as of an allo-reactive $CD4^+$ T cell line 66

Figure 24: NP uptake by $CD4^+$ T cell lines in the presence of endocytosis inhibitors 68
Figure 25: TEM analysis on $CD4^+$ T cells after 16 h incubation with NP-9-NH_2 at 1500 µg/mL to allow for maximal loading of intracellular compartments 69
Figure 26: Long-term follow-up of NP-loaded T cells over five days 70
Figure 27: Influence of human serum concentration on NP release.....71
Figure 28: NP release during the first 24 h after re-culture of labeled T cells.....72
Figure 29: Influence of ABC-transporter activity on NP release 73
Figure 30: Uptake and release of NP-9-NH_2 by antigen presenting human B lymphocytes and murine $CD4^+$ and $CD8^+$ T cell lines 74
Figure 31: Uptake of differently charged nanoparticles after pretreatment with cationic transfection agents protamine sulfate and Lipofectamine at various concentrations.....75
Figure 32: Fluorescence intensity of $CD4^+$ T cells after incubation with PULSin treated NP .77
Figure 33: NP delivery to T cell lines by electroporation 79
Figure 34: Selection of strongly and weakly labeled T cells by flow cytometric cell sorting and monitoring of NP release 80
Figure 35: Inhibition of maturation of NP-loaded endodomes by chloroquine 81
Figure 36: Incorporation of transferrin-conjugated NP 82
Figure 37: Improved delivery of NP to dendritic cells and T lymphocytes after ‘biocoating’ with whole virus particles.....83
Figure 38: cLSM of cells loaded with “biocoated” NP.....84
Figure 39: Colocalization studies of Cy5 labeled oligonucleotides delivered by PBCA nanocapsules in T cells with mitochondria by cLSM 85
Figure 40: cLSM of T lymphocytes incubated with PBCA capsules for different time periods 86

List of tables

Table 1: Laboratory instruments 22
Table 2: Plastic material 23
Table 3: Substances and solutions used for cell culture 23
Table 4: Cell culture media 24
Table 5: Cytokines 24
Table 6: Material used for isolation of T lymphocytes from PBMC 26
Table 7: Patient-derived AML blasts 28
Table 8: Composition of additives for culture of murine T cell lines 29
Table 9: Material for nanoparticle synthesis 29
Table 10: Nanoparticles with different characteristics, used for uptake by cells 31
Table 11: Pharmacological inhibitors 34
Table 12: Material used for flow cytometry 37
Table 13: Material used for 7-AAD staining 37
Table 14: Fluorochrome-conjugated monoclonal antibodies 38
Table 15: Material used for cLSM 39
Table 16: Material used for ^{3}H-thymidine proliferation assay 41
Table 17: Material used for IFN-γ ELISPOT assay 42
Table 18: Material used for ^{51}Chromium release assays 43
Table 19: Material and laboratory equipment for optimizing NP incorporation and duration of labeling in T lymphocytes 44
Table 20: Overview of median fluorescence intensity (MFI) of DCs and Jurkat T cells after loading with different particles (conc.: 75 µg/mL, 16 h) as determined by flow cytometry 58

Abbreviations

AA	Acrylic acid
7-AAD	7-Amino-actinomycin D
ABC	Adenosine triphosphate binding cassette
AEC	3-Amino-9-ethyl-carbazole
AEMH	2-aminoethyl methacrylate hydrochloride
ALL	Acute lymphatic leukemia
Allo	Allogeneic
AML	Acute myeloid leukemia
APC	Antigen-presenting cell
APC	Allophycocyanin
ATP	Adenosine triphosphate
BC	Buffy coat
BSA	Bovine serum albumine
BTLA	B and T lymphocyte attenuator
CAR	Chimeric antigen receptor
CD	Cluster of differentiation
CLL	Chronic lymphatic leukemia
CM	Central memory
CMV	Cytomegalovirus
CLIP	Class II associated invariant peptide
cLSM	Confocal laser scanning microscopy
CML	Chronic myeloid leukemia
CTL	Cytotoxic T lymphocyte
CTLA-4	Cytotoxic T-lymphocyte-associated protein 4
CTMA-Cl	Cetyltrimethylammonium chloride
Cy5	Cyanine 5
DC	Dendritic cell
DLI	Donor lymphocyte infusion
DLS	Dynamic light scattering
DMF	N,N-Dimethylformamide
DMSO	Dimethyle sulfoxide
DNA	Desoxyribonucleic acid
E:T	Effector to target ratio
EBV	Epstein Barr virus
EDTA	Ethyendiamine-tetra-acetic acid

EEA1	Early endosome antigen 1
EIPA	5-(N-ethyl-N-isopropyl)amiloride
ELISPOT	Enzyme-linked Immunosorbent Spot assay
EM	Effector memory
ER	Endoplasmatic reticulum
ERAAP	Endoplasmatic reticulum aminopeptidase associated with antigen processing
FACS	Fluorescence activated cell sorting
FasL	Fas ligand
FCS	Fetal calf serum
FITC	Fluorescein isothiocyanate
GM-CSF	Granulocyte/macrophage-colony stimulating factor
GTP	Guanosine triphosphate
GVHD	Graft-versus-host disease
GVL	Graft-versus-leukemia
HLA	Human leukocyte antigen
HS	Human serum
HSCT	Hematopoietic stem cell transplantation
iDC	Immature DC
IFN	Interferon
Ig	Immunoglobulin
IL	Interleukin
IU	International unit
LAMP1	Lysosomal-associated membrane protein 1
LCL	Lymphoblastoid cell line
mAb	Monoclonal antibody
MACS	Magnetic activated cell sorting
mDC	Mature DC
MEM	Minimal Essential Medium
mHag	Minor histocompatibility antigen
MHC	Major histocompatibility medium
MLLC	Mixed lymphocyte/leukemia culture
MLR	Mixed lymphocyte reaction
NC	Nanocapsule
NK	Natural killer

NP	Nanoparticle
PBMC	Peripheral blood mononuclear cell
PBS	Phosphate buffered saline
PD-1	Programmed death-1
PE	Phycoerythrin
PEG	Polyethylene glycol
PerCP	Peridinin-chlorophyll-protein complex
PFA	Paraformaldehyde
PGE 2	Prostaglandin 2
PMI	N-(2,6-diisopropylphenyl)-perylene-3,4-dicarbonacidimide
QD	Quantum Dot
RAB	Ras-related in brain protein
RCC	Renal cell carcinoma
RNA	Ribonucleic acid
Rpm	Rounds per minute
RPMI	Roswell Park Memorial Institute
SD	Standard deviation
SDS	Sodium dodecyl sulfate
SEM	Scanning electron microscopy
siRNA	Small interfering RNA
SPIO	Superparamagnetic iron oxide
TAP	Transporter in antigen processing
TCR	T cell receptor
TEM	Transmission electron microscopy
Tf	Transferrin
Th cell	T helper cell
TIL	Tumor infiltrating lymphocyte
TNF-α	Tumor necrosis factor alpha
Treg	Regulatory T cell

1 Abstract

Dendritic cells (DCs) are the most potent cell type for capture, processing, and presentation of antigens. They are able to activate naïve T cells as well as to initiate memory T-cell immune responses. T lymphocytes are key elements in eliciting cellular immunity against bacteria and viruses as well as in the generation of anti-tumor and anti-leukemia immune responses. Because of their central position in the immunological network, specific manipulations of these cell types provide promising possibilities for novel immunotherapies. Nanoparticles (NP) that have just recently been investigated for use as carriers of drugs or imaging agents, are well suited for therapeutic applications *in vitro* and also *in vivo* since they can be addressed to cells with a high target specificity upon surface functionalization. As a first prerequisite, an efficient *in vitro* labeling of cells with NP has to be established. In this work we developed protocols allowing an effective loading of human monocyte-derived DCs and primary antigen-specific T cells with newly designed NP without affecting biological cell functions. Polystyrene NP that have been synthesized by the miniemulsion technique contained perylenmonoimide (PMI) as a fluorochrome, allowing the rapid determination of intracellular uptake by flow cytometry. To confirm intracellular localization, NP-loaded cells were analyzed by confocal laser scanning microscopy (cLSM) and transmission electron microscopy (TEM). Functional analyses of NP-loaded cells were performed by IFN-γ ELISPOT, ^{51}Chromium-release, and ^{3}H-thymidine proliferation assays.

In the first part of this study, we observed strong labeling of DCs with amino-functionalized NP. Even after 8 days 95% of DCs had retained nanoparticles with a median fluorescence intensity of 67% compared to day 1. NP loading did not influence expression of cell surface molecules that are specific for mature DCs (mDCs) nor did it influence the immunostimulatory capacity of mDCs. This procedure did also not impair the capability of DCs for uptake, processing and presentation of viral antigens that has not been shown before for NP in DCs. In the second part of this work, the protocol was adapted to the very different conditions with T lymphocytes. We used leukemia-, tumor-, and allo-human leukocyte antigen (HLA) reactive $CD8^+$ or $CD4^+$ T cells as model systems. Our data showed that amino-functionalized NP were taken up very efficiently also by T lymphocytes, which usually had a lower capacity for NP incorporation compared to other cell types. In contrast to DCs, T cells released 70-90% of incorporated NP during the first 24 h, which points to the need to escape from intracellular uptake pathways before export to the outside can occur. Preliminary data with biodegradable nanocapsules (NC) revealed that encapsulated cargo molecules could, in principle, escape from the endolysosomal compartment after loading into T lymphocytes. T cell function was not influenced by NP load at low to intermediate concentrations of 25 to 150 µg/mL.

Overall, our data suggest that NP and NC are promising tools for the delivery of drugs, antigens, and other molecules into DCs and T lymphocytes.

Zusammenfassung

Dendritische Zellen (DCs) sind die wichtigsten Antigen-präsentierenden Zellen des Immunsystems. Sie aktivieren naive T-Zellen und veranlassen die Bildung von Gedächtnis T-Zellen. T-Lymphozyten vermitteln Immunität gegen Viren und Bakterien und sind in der Lage, anti-tumorale und anti-leukämische Antworten zu generieren. Die zentrale Stellung dieser beiden Zelltypen im immunologischen Netzwerk macht sie zu einem vielversprechenden Angriffspunkt für die Entwicklung neuer Immuntherapien. Seit einigen Jahren stehen Nanopartikel (NP) vermehrt im Focus biomedizinscher Forschung, da diese als Transportvehikel für Therapeutika und Reportersubstanzen eingesetzt und durch Oberflächenfunktionalisierung an bestimmte Zellpopulationen adressiert werden können. Als Grundvoraussetzung muss jedoch zunächst eine effiziente Beladung der Zellen mit NP *in vitro* etabliert werden. Gegenstand dieser Arbeit ist die Entwicklung von *in vitro* Protokollen zur bestmöglichen Beladung von humanen DCs und T-Zellen mit eigens hergestellten NP ohne deren immunbiologische Funktionalität zu beeinträchtigen. Die verwendeten, mittels Miniemulsion synthetisierten Polystyrol-NP enthalten Perylenmonoimid (PMI) als Fluorochrom, wodurch die Aufnahme in Zellen durchflusszytometrisch quantifiziert werden kann. Die intrazelluläre Lokalisation der NP wurde mit Hilfe von konfokaler Laser-Scanning-Mikroskopie und Transmissionselektronenmikroskopie (cLSM, TEM) überprüft. NP-beladene Zellen wurden in IFN-γ ELISPOT Assays, ^{51}Chrom-Zytotoxizitätstests und ^{3}H-Thymidin Proliferationstests funktionell evaluiert.

Im ersten Teil dieser Arbeit konnte eine effektive Beladung von DCs (generiert aus Monozyten des peripheren Bluts) mit aminofunktionalisierten NP für mindestens 8 Tage erzielt werden, wobei noch 95% der gelabelten Zellen NP besaßen und eine mediane Fluoreszenzintensität von 67% des initialen Wertes aufwiesen. Aufgenommene NP beeinflussten weder die Expression spezifischer Oberflächenmarker reifer DCs (mDCs), noch wurde die Fähigkeit zur Aufnahme, Prozessierung und Präsentation viraler Antigene beeinträchtigt. Dies konnte erstmalig für NP in DCs gezeigt werden. Im zweiten Teil der Arbeit wurde das Protokoll an die unterschiedlichen Kultivierungsbedingungen von antigenspezifischen T-Lymphozyten angepasst. Als Modellsysteme wurden sowohl leukämie- und tumorreaktive als auch alloreaktive, gegen humane Leukozytenantigene (HLA) gerichtete T-Zellen verwendet. Obwohl T-Zellen im Vergleich zu anderen Zellen nur über eine geringe Aufnahmekapazität für NP verfügen, ist es uns dennoch gelungen, diese ebenfalls effizient mit aminofunktionalisierten NP zu beladen. Da jedoch 70-90% der

aufgenommenen NP bereits innerhalb 24 h wieder abgeben wurden, müssen Strategien entwickelt werden, die den NP den Transfer aus dem endolysosomalen Kompartiment in das Zytosol ermöglichen. Erste Ergebnisse mit bioabbaubaren Nanokapseln (NC) zeigen, dass darin verkapselte Moleküle nach NC-Aufnahme prinzipiell dazu in der Lage sind. Die Effektorfunktionen der T-Zellen wurden durch niedrige bis mittlere NP-Konzentrationen zwischen 25 - 150 µg/mL nicht beeinträchtigt.

Die Ergebnisse dieser Doktorarbeit legen nahe, dass sich polymere NP und NC prinzipiell sehr gut als Vehikel für die Einschleusung von Therapeutika, Antigenen und Reportersubstanzen in DCs und T-Zellen eignen.

2 Introduction

2.1 The human immune system

2.1.1 Innate immune responses

The immune system is a complex defense system of lymphoid organs, tissues, cells and other factors that protect against disease causing organisms like viruses, bacteria, fungi or other parasites. Furthermore, it allows the discrimination between body's own and foreign material as well as the control of malfunctioning cells. The human immune system is composed of an innate and an adaptive component. The innate or non specific part is the first hurdle pathogens have to overcome to get into the organism. The innate immune system consists of physical, chemical and microbiological barriers like epithelial surfaces or mucous membranes containing bactericidal substances as a first protection against the invasion and colonization by pathogenic organisms. If pathogens succeed in penetrating first barriers of defence and start to reproduce within the tissues of the host, cellular (e.g. macrophages) and molecular factors (e.g. complement system) of the innate immune system take part in defence of the invaders. When these induced innate responses fail to kill the pathogenic invaders, phagocytic and other cells activated in this immediate non specific immune response, support the development of the specific adaptive immune response (Delves&Roitt 2000).

2.1.2 Adaptive immunity

2.1.2.1 B and T cell receptor

The adaptive immune system is characterized by the high variability of antigen-specific receptors on T and B lymphocytes as well as by the immunological memory function leading to faster and more effective immune responses after repeated exposures to the pathogens. The adaptive immunity consists of a cell mediated and a humoral part. Humoral immunity is mediated by B lymphocytes and directed against extracellular pathogens. Activated plasma cells secrete antibodies into the blood and tissue fluids while membrane bound immune globulines on the B cell's surface serve as antigen receptor (B cell receptor, BCR). The adaptive immune response against intracellular pathogens is mediated by cytotoxic T lymphocytes. In contrast to the humoral part, antigen specific structures exist as membrane bound molecules, namely the T cell receptor (TCR). The TCR cannot bind the intact antigen directly but recognizes peptide fragments of foreign proteins bound on MHC molecules. MHC molecules are ubiquitously expressed on cell surfaces and allow T lymphocytes not only the

recognition of antigenic epitopes but also to discriminate between self and non self. Immune globulines as well as T cell receptors contain highly variable and constant regions and are related in the genetic mechanism that produces their great variability termed somatic DNA recombination. Multiple random rearrangements and splicing of various gene segments as well as the possibility of combination of variable and constant regions result in a repertoire of about 10^{15} specific TCRs and a similar number of different immune globulines (Delves&Roitt 2000; Parkin&Cohin 2001).

2.1.2.2 Human leukocyte antigens

Human leukocyte antigens are membrane bound glycoproteins that are responsible for antigen recognition and presentation of foreign peptides to T cells. HLA proteins are encoded by a family of highly polymorphic genes known as the major histocompatibility complex (MHC) that spans approximately 4 Mb on the short arm of chromosome 6 (Trowsdale 1995). The human MHC is divided into class I, II and III regions. The class I region includes, among other genes, the molecules HLA-A, HLA-B and HLA-C while the class II region consists of genes coded for class II molecules like HLA-DP, -DQ and -DR. These histocompatibility antigens also mediate the rejection of transplants between two allogeneic, genetically different individuals. Class III products are associated with proteins of the complement system and cytokines that are involved in the innate immune responses but not in the rejection of transplants. Class I proteins that are composed of an α- chain and a β2-microglobuline are localized in the membrane of all nucleated cells types, where they present endogenous antigen fragments like virus or tumor associated proteins to cytotoxic $CD8^+$ T cells. This mechanism allows the presentation of antigens indicating viral infection or degeneration of the cell resulting in a subsequent recognition and cytolysis mediated by $CD8^+$ T cells. Class II MHC molecules are composed of two polypeptide chains with an approximately equal length and present exogenous proteins that are derived from extracellular pathogens to $CD4^+$ helper T lymphocytes. Exogenous antigens can also be phagocytosed by professional antigen presenting cells (APC) and subsequently presented by MHC class I molecules to $CD8^+$ cytotoxic T cells in a process termed cross presentation. MHC class II molecules are only expressed by APCs at non inflammatory conditions (Delves&Roitt 2000, Klein&Sato 2000).

2.1.2.3 Antigen processing and presentation

MHC class I and class II molecules deliver peptides to the cell surface from distinct intracellular compartments, since viruses, certain bacteria or tumor associated proteins are localized in the cytosol or in the nucleus, whereas many pathogenic bacteria and parasites replicate in the endolysosomal compartment. Therefore, the antigen presentation requires

different intracellular processing pathways resulting in fragmentation of antigenic proteins, association of those fragments with MHC molecules and the subsequent expression of peptide-MHC molecules at the cell surface allowing the recognition by the T cell receptor of $CD4^+$ or $CD8^+$ T lymphocytes.

MHC class I pathway

Ubiquitinylated endogenous proteins that bind to MHC class I molecules are derived from viruses, tumors, bacteria or defective cells. The proteins are fragmented in the cytosol by a large multicatalytic complex of proteases termed proteasome into smaller fragments. The carboxy terminal ends of the peptides are degraded by proteasome cleavage, while the N-terminus is primarily trimmed in the endoplasmic reticulum (ER) by an aminopeptidase called endoplasmatic reticulum aminopeptidase associated with antigen processing (ERAAP). After fragmentation in the proteasome, the resulting peptides were actively transported from the cytosol to the ER via the transporter associated with antigen processing (TAP) that is localized in the ER membrane. The TAP transporter is a heterodimeric peptide consisting of TAP-1 and -2. As a member of the ABC transporter family TAP is composed of two hydrophobic transmembrane domains that face into the lumen of ER as well as two cytosolic ATP-binding cassette (ABC) domains. The following peptide loading process onto newly synthesized MHC class I peptides is mediated by a complex consisting of calnexin, calreticulin, Erp57 and tapasin. After antigenic peptide has bound to the MHC class I peptide complex, it is transported through the Golgi apparatus to the cell surface for a subsequent presentation of antigen fragments to cytotoxic $CD8^+$ T cells (Williams et al. 2002, Hammer et al. 2006, Janeway 2008).

MHC class II pathway

Exogenous protein antigens derived from extracellular pathogens are presented in association with MHC class II molecules which are expressed mainly by APC including macrophages, dendritic cells (DCs) and B lymphocytes. In a first step, exogenous proteins are recognized by APC and subsequently internalized via phagocytosis or endocytosis. Proteins that bind to surface immunoglobulin on B cells are internalized by receptor mediated endocytosis. Since the antigenic proteins are localized in membrane surrounded vesicles within the APC, they are not accessible to proteasomes in the cytosol. Therefore, those early endosomes containing the antigenic protein as well as inactive proteases become increasingly acidic while progress into the interior of the cell. Acidification of the vesicles resulted in an activation of the proteases leading to a degradation of the protein into peptide fragments. Subsequently, these peptide loaded endosomes fuse with MHC class II-

containing acidic lysosomes. The α and β chains of MHC class II are synthesized and assembled in the endoplasmatic reticulum. The MHC class II-associated protein invariant chain prevents the MHC molecule from binding of peptides or partly folded proteins inside the ER. Newly synthesized MHC class II molecules are then transported through the Golgi apparatus into the antigenic peptides containing acidified vesicle, where the invariant chain is digested by proteases leaving a small CLIP fragment (class II-associated invariant-chain peptide) still bound to the MHC class II molecule. The CLIP fragment is replaced by antigenic peptides from the exogenous protein and finally transported to the cell surface for a subsequent presentation of antigens to $CD4^+$ T cells (Villadangos 2001, Janeway 2008).

Cross presentation

Uptake of exogenous material derived from transformed or virally infected cells by APC, in particular DCs, can also result in presentation of peptides on MHC class I molecules to $CD8^+$ cytotoxic T cells in a process referred to as cross presentation. This alternative pathway leads to CTL responses against tumors that do not originate from DCs or against viruses that are not able to infect DCs (Burgdorf et al. 2008).

2.1.2.4 T lymphocyte activation by APC

Professional APC are very effective in internalizing, processing and presenting antigens, bound to MHC class I or II molecules on their membrane, to $CD4^+$ and $CD8^+$ T cells. The three main types of APCs are dendritic cells, macrophages and B lymphocytes. DCs are key elements in mediating immunity and tolerance, and are essential for linking innate and adaptive immune responses against foreign antigens. They are the most potent cell type for antigen capture, processing, and presentation (Steinman&Banchereau 2007, Villadangos&Schnorrer 2007, Heath et al. 2004). Immature DCs (iDCs) are localized in the skin (as epidermal Langerhans cells) and other tissues at body surfaces, where they recognize and internalize antigens and subsequently migrate to T cell areas of lymphoid organs especially to the lymph nodes and spleen that are primarily responsible for generation of immunity and tolerance. During the migration/maturation phase, DCs lose their capacity to phagocytose but they start the expression of new surface molecules like cluster-of-differentiation (CD) 80, CD83, CD86 allowing an efficient communication with T lymphocytes (Albert et al. 2001, Han et al. 2009). Naïve T cells that have not yet encountered their specific antigen also migrate to the lymphoid tissues. The migration process from blood involves different adhesions molecules and chemokine receptors as well as L-Selectin and other receptors on the T lymphocytes. Naïve T cells encountering the antigenic peptide for which their antigen receptor is specific, begin to proliferate. This clonal expansion of antigen-

specific T cells after antigen priming leads to a primary immune response. Besides the generation of those effector T lymphocytes, matured DCs (mDCs) induce the T cell clone to acquire memory functions allowing maintenance for longer time and the capability of responding rapidly to a repeated exposure to the antigen (secondary immune response). Memory T cells can be subdivided into central memory T cells that are predominantly found in lymphoid organs and effector memory T lymphocytes that are primarily located in the peripheral tissues and sites of inflammation to perform rapid effector functions. They also differ in the expression of surface molecules like L-Selectin or CCR7 as well as in the secretion of effector cytokines like Interferon-γ and IL-4 (Sallusto et al. 2004, Klebanoff et al. 2006).

T cells require two signals to be activated. The specific signal is due to T cell receptor recognition and subsequent binding to MHC peptide complex presented by the APC. The second, costimulatory signal is unspecific and results from interaction of B7 molecules of DCs, e.g. B7.1 (CD80) and B7.2 (CD86), with CD28 receptors on T lymphocytes. Both signals induce cytokine production, especially of IL-2 leading to proliferation and clonal expansion of T cells. Furthermore, several coinhibitory receptors are known that are able to inhibit T cell activation after interaction with B7 ligands of APC, for example the cytotoxic T lymphocyte associated protein 4 (CTLA4), programmed death-1 and -2 (PD-1/2), and the B and T lymphocyte attenuator (BTLA) (Delves&Roitt 2000, Parkin&Cohin 2001, Greenwald et al. 2005).

2.1.2.5 Effector mechanisms of T cells

T lymphocytes are key elements of cell-mediated immune reactions against bacteria and viruses, and are the most potent cell populations for eliciting anti-tumor and anti-leukemia immune responses (Jiang&Chess 2006, Kolb 2008). They also play a major role in destroying foreign cells during allo-transplant rejection or in autoimmune diseases when the immune response is targeting cells of the own body (Issa et al. 2010, Cvetanovich&Hafler 2010). Effector T cells can be categorized into two major groups characterized by their TCR co-receptors. $CD4^+$ T cells are cytokine secreting T helper (Th) cells, while $CD8^+$ T cells primarily kill target cells and therefore named cytotoxic T lymphocytes (CTL). Naïve $CD4^+$ T cells are able to differentiate after activation into the two major functional subsets “Th1” and “Th2” which show characteristic cytokine profiles (Zhu&Paul 2008). After antigen-specific binding, Th1 cells secrete IFN-γ as well as IL-2 and therefore induce T cell proliferation of $CD8^+$ T cells and facilitate the effector functions by activating macrophages and enabling them to destroy intracellular pathogens more efficiently. Furthermore, Th1 cells can boost the cytotoxic effect of natural killer (NK) cells and also activate B lymphocytes to produce opsonizing antibodies belonging to certain immunoglobulin G subclasses. In contrast, Th2

cells secrete the cytokines IL-4, IL-5, IL-6, and IL-10 that stimulate B lymphocytes to produce immunoglobulins of all other subclasses. Therefore, Th2 cells are specialized for the induction of humoral immunity and the elimination of extracellular pathogens (Parkin&Cohen 2001, Janeway 2008). Another set of T helper cells that produce IL-17 and therefore called "Th17" has been described more recently (Weaver et al. 2007). Since the secretion of IL-17 induces several pro-inflammatory cytokines, this T cell subset plays a role in inflammatory immune responses and autoimmunity (Bettelli et al. 2007, Volpe et al. 2008). Additionally, regulatory T cells (Tregs) are able to control effector responses by suppressing the immune system and are therefore also involved in inflammatory mechanisms and autoimmunity (Cvetanovich&Hafler 2010).

$CD8^+$ CTL form the major effector T cell population, being essential in the elimination of virally infected cells and tumor cells, and in the rejection of allografts in transplantation (Zhang&Bevan 2011). CTL-mediated elimination of target cells based on the calcium-dependent release of specialized lytic granules upon recognition of MHC class I associated antigen, that contain the cytotoxic effector proteins perforin and granulysin as well as different proteases called granzymes. Perforin monomers polymerize in the membrane of target cells to form aquaeos channels allowing the other cytotoxic molecules to pass the membrane. Granzymes, which belong to the serine proteases, activate caspases once in the cytoplasm of the target cell resulting in DNA fragmentation and subsequent apoptosis of target cells. Additionally, formation of the perforin pores enabling extracellular ions and water to flow in leading to an osmotic swelling and lysis of the target cell. Furthermore, CTL can eliminate target cells by a perforin-independent mechanism that involves the binding of Fas ligand (FasL, CD95L) on activated CTL to the Fas receptor (Fas, CD95), which is present in the membrane of many target cells. This Fas/FasL interaction also results in an activation of caspases that subsequently induce nucleases leading to adoptosis of the target cells. CTL also act by releasing the cytokines IFN-γ, tumor necrosis factor (TNF) α and β after encountering an antigen presented by APC. These cytokines mainly activate macrophages, induce inflammation and contribute to host defense in further ways (Kavurma&Khachigian 2003, Andersen et al. 2006).

2.1.3 Cellular immunotherapies

DC and T cell based immunotherapies have been applied experimentally both in animal models and in humans to treat many types of hematologic malignancies, solid tumors as well as viral infections in immunosuppressed patiens by using cells that were prepared from autologous or allogeneic blood products (Tacken et al. 2007, Kitawaki et al. 2008, Pedrazzoli et al. 2011, Thomas&Herr 2011). The treatment strategy can be divided into two major

categories: Active cellular immunotherapies using DCs or other antigen presenting cells and the passive, adoptive transfer of T lymphocytes. Professional APC like DCs, macrophages, and B lymphocytes can be loaded with antigens *ex vivo* and subsequently injected back into the patient and thereby elicit anti-tumor responses *in vivo* or used as vehicles for immunotherapeutics. Those DC/APC vaccines should stimulate the patient's immune system to eliminate cells carrying a specific target antigen (O'Neill 2010). DCs can be loaded with different antigen types including whole tumor cells, cell lysats, tumor associated antigens, viral antigens of oncogenic viruses as well as RNA or DNA (Tacken et al. 2007, Gilboa 2007). The desired antigens can be combined with other immunogenic substances/adjuvants leading to a stronger immune response. The use of whole tumor cells or cell lysates allows a vaccination with the complete antigenic content of a tumor and not only with an isolated antigen. DCs can also be pulsed by transfection with nucleic acids encoding tumor antigens whereas the translated protein is loaded on MHC molecules and is finally presented to T lymphocytes (Rosenberg 2004, Pure et al. 2005). The success of the immunotherapy using DCs to treat cancer is dependent on migration to the lymph node as well as the effective activation of antigen specific T cells. It was reported that most of the administered cells (up to 95%) remained at the injection side, died and are cleared by macrophages within 48 hours. Nevertheless, surviving DCs were able to migrate into the T cell areas, where they induced antigen specific T cell responses (Verdijk et al. 2009, Blattman&Greenberg 2004). Despite the fact that the immune responses after DC vaccination are often weak and data on clinical studies are limited, in individual cases treatment was associated with tumor regressions in patients with metastatic melanoma, renal cell carcinoma, B cell lymphoma and cancer of prostate, breast, ovarian, colon and lung (Verdijk et al. 2009, O'Neill et al. 2004).

In contrast to the active vaccination with antigen loaded APC, adoptively transferred tumor specific T cells that were expanded *ex vivo* are characterized by a direct tumor killing activity (Dudley&Rosenberg 2003). Autologous or allogeneic antigen specific T cells can be derived from tumor tissues or from peripheral blood mononuclear cells (PBMCs) in order to generate large numbers of reactive T cell clones *in vitro* from cells that are only present at very low numbers in peripheral blood of the patient or healthy donor. Antigen specific T cells were isolated and cultured in the presence of several cytokines, mainly Interleukin-2 before injecting them back into the patient (Rosenberg et al. 2008). First promising clinical outcomes have been observed in metastatic melanoma and renal cell carcinoma patients after the administration of autologous reactive tumor-infiltrating lymphocytes (TIL, Rosenberg et al. 1988). A further strategy for adoptive immunotherapy is the donor lymphocyte infusion (DLI) after hematopoetic stem cell transplantation (HSCT) representing a mixture of peripheral lymphocytes from the original donor that can stimulate a graft versus leukemia (GvL) reaction

and thus eliminate residual leukemic blasts (Kolb et al. 2008). The transfer of those T cells is a well established strategy in the treatment of recurrent acute and chronic leukemia. It has been reported that the infusion of donor T cells can lead to a complete molecular remission within more than 70% of patients with chronic myeloid leukemia (CML, Kolb et al. 1995), but this beneficial effect is often accompanied with detrimental graft-versus host desease (GvHD). After HLA-matched HSCT, GvL- as well as GvHD effects are mediated by donor derived T cells due to minor histocompatibility antigen (mHag) incompatibilities between patient and stem cell donor. Therefore, hematopoietic expressed mHags as well as leukemia specific/associated antigens, which are exclusively or preferentially expressed on leukemic blasts, are promising target structures for leukemia reactive donor T cells that are able to recognize and eliminate leukemic cells without affecting other cell types (Goulmy 2006, Greiner et al 2006, Bleakley&Riddell 2004). First clinical trials showed that adoptive immunotherapies using leukemia reactive CTL are able to induce leukemia remission (Marijt et al. 2007, Warren et al. 2010).

Furthermore, the administration of allogeneic cytomegalovirus (CMV) and Epstein-Barr virus (EBV) specific T cells to patients after HSCT showed not only a therapeutic but also a protective effect against viral infections (Walter et al. 1995, Thomas&Herr 2011). Additionally, virus specific T cells were successfully used for therapy of EBV-B-associated lymphoma (Rooney et al 1998, Bollard et al. 2004). Cellular immunotherapies also include the transfer of genetic modified T cells carrying previously determined receptors on their surface. Antigen specific T cells can be engineered by transfecting naïve T cells with plasmids or transducing them with viral vectors encoding recombinant tumor specific TCR. Another approach is the introduction of genes encoding chimeric antigen receptors (CARs, O'Neill 2010, Porter et al. 2011). CAR molecules are recombinant artificial TCRs that recognize cancer antigens. They consist of single chain variable fragments derived from specific monoclonal antibodies which are combined with the CD3 domain of the TCR/CD3 complex. CAR transduction by viral vectors deflect lymphocyte specificity to these cancer antigens, allowing recognition of specific antigens expressed on the surface of different types of tumor cells (Pedrazzoli et al. 2011). Clinical studies revealed that the administration of T cells expressing CARs can mediate cancer regression in patients with B-cell hematological malignancies such as CLL, $CD19^+$ ALL, B-Cell lymphomas and Hodgkin's lymphoma (Pedrazzoli 2011, Porter et al. 2011). However, the success of T cell therapy depends on different factors like the *in vivo* persistence, the remaining capacity for migration to sites of disease and the unrestricted functionality of transferred lymphocytes (Yee 2005).

2.2 Nanoparticles

2.2.1 Definition and areas of application

During the past few years there is a growing interest in nanotechnology, since the use of nanomaterials or miniaturized particle based devices provides great opportunities in various fields of life sciences. According to the technical definition by the European Commission's independent Scientific Committee on Emerging and Newly Identified Health Risks (SCENIHR, 2010), a material is considered to be a nanomaterial if more than 0.15% of the number size distribution is below 100 nm. The selective assembly of nanoscaled material and structures of various shapes and surface properties can be used for obtaining novel optical, chemical and mechanical properties that are different from the respective bulk material. Synthetic nanomaterials like nanoparticles (NP) have a size from several up to a few hundred nanometers. Therefore, such particles are considerably smaller than micrometer-sized cells but larger than single molecules, peptides or whole proteins (Mailänder&Landfester 2009). Nanoparticles are already being used as catalysators in the chemical industry and they can also be found in everyday products like cosmetics, e.g. for sun protection with improved properties. Furthermore, nanoparticles are standardly processed in membrane and filter systems used for treatment of waste water, in antireflection coatings of solar cells as well as in paints and varnishes (Limbach et al. 2008, Nagel&Scarpulla 2010).

Additionally, nanoparticles offer great potential in biomedical applications, including rapid biological cell separation, magnetic hyperthermia therapy, magnetic resonance imaging (MRI), and the targeted delivery of drugs into different cells (Miltenyi et al. 1990, Ito&Kobayashi 2008, Wang 2011, Torchilin 2000). Because of their small size, nanoparticles are able to penetrate biological barriers like cell membranes and therefore are ideally suited as transport systems for drugs and biologically active molecules.

2.2.2 Synthesis

The experimental nanoparticles used in this work were synthesized via the so-called “miniemulsion” technique as schematically shown in Figure 1.

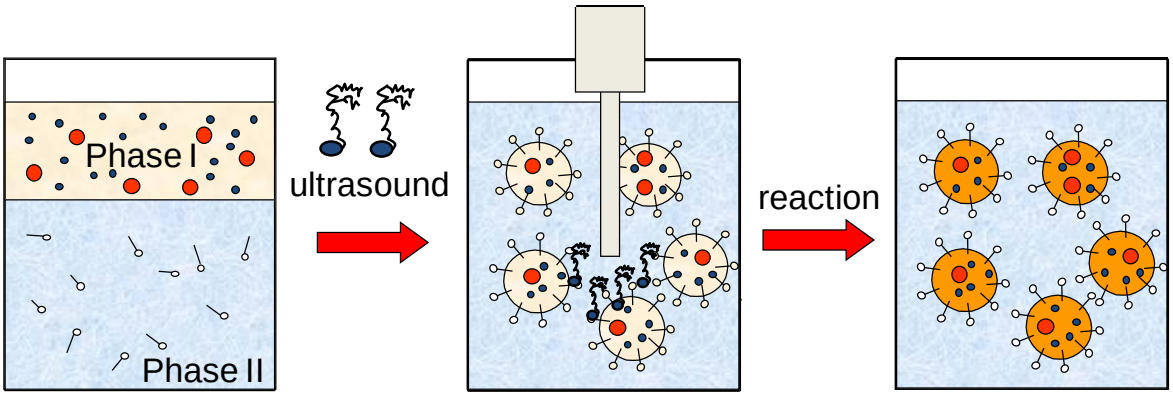

Figure 1: Schema of the miniemulsion process. Stable nanodroplets with narrow size distribution act as individual nanoreactors (adapted and modified from Mailänder & Landfester 2009). Phase I: oily phase containing the co-stabilizer, a reporter substance as well as the monomer; Phase II: surfactant-containing aqueous phase.

The miniemulsion technique allows the synthesis of uniform polymeric nanoparticles with a defined size from 30 to 500 nm (Landfester 2001). Here the direct miniemulsion technique is described (oily droplets in a continuous water phase). For this purpose, two immiscible phases, an organic (oily) phase and an aqueous continuous phase are mixed with a subsequent generation of oil droplets by stirring. The generated droplets still differ in size with diameters up to the micrometer range. For homogenization as well as the formation of nanosized droplets, high shear forces like ultrasound have to be applied. The nanodroplets are very stable due to the combination of an amphiphilic surfactant and an ultrahydrophobe as co-stabilizer that is present in the oil phase. Monomer molecules which have a low but still detectable solubility in the continuous water phase would diffuse from the smaller nanodroplets to the larger ones according to the Laplace pressure. This process is also called Ostwald ripening. The co-stabilizer is characterized by a very much lower solubility in the continuous phase than the rest of the droplet phase and therefore creates an osmotic pressure inside the droplets which opposes the Ostwald ripening process. Therefore, the droplets maintain their homogeneous sizes as well as their contents without interacting with droplets in their immediate vicinity during the whole miniemulsion process. The droplets act as individual nanoreactors suitable for many different chemical reactions. If the organic phase consists of monomers for example styrene they can be polymerized resulting in polystyrene nanoparticles preserving the shape and size of the droplets and also including all substances dissolved in the oily phase (Landfester 2001, 2009). Furthermore, the miniemulsion technique is suitable for the preparation of functional polymeric nanoparticles since not only radical homopolymerization can be performed, but also copolymerization allowing the defined introduction of functional groups to the particle surface. Additionally, even small molecules, liquids or solids can be encapsulated in polymeric shells enabling the

synthesis of various functional nanomaterials that can be used for a wide variety of applications (Weiss & Landfester 2010). Figure 2 shows a transmission electron microscopy (TEM) image of 65 nm sized polystyrene nanoparticles, functionalized with amino groups.

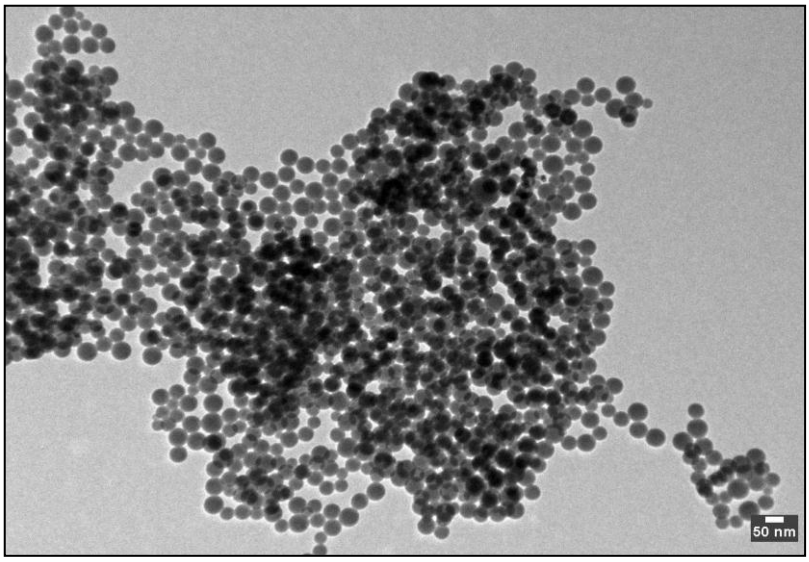

Figure 2: TEM picture of polystyrene NP (particle NP-9-NH_2, TEM micrograph from Dr. Umaporn Paiphansiri, Max Planck Institute for Polymer Research Mainz).

2.2.3 Nanoparticles in medicine

The application of polymeric nanoparticles in medicine, biology and pharmacy appears particularly promising. Commercially available superparamagnetic beads are used today routinely for the magnetic separation of defined cell populations after binding to them via specific antibodies (MACS technique, magnetic activated cell sorting; Miltenyi et al. 1990). Furthermore, superparamagnetic iron oxide (SPIO) particles are already in clinical use as safe contrast agents for MRI. The particles consist of an iron oxide core coated with dextran or carboxydextran and have a diameter of 60-180 nm (Wang 2011). After intravenous administration, clinical approved SPIO particles are quickly removed from circulating blood by phagocytosis of the reticuloendothelial system resulting in an accumulation in the normal liver, spleen, bone marrow, and lymph nodes (Wang 2011) and therefore allowing an imaging of these organs. SPIO particles were also used for an *in vivo* monitoring of single cells enabling the detection of migration and homing of the cells after a previous *ex vivo* labeling procedure. Subsequently, SPIO loaded cells can be injected into mice or other model organisms (Mou et al. 2011) and monitored by MRI. Additionally, superparamagnetic particles offer great potential for use in hyperthermia therapy of solid tumors like prostate cancer (Johannsen et al. 2005). For this purpose, nanoparticles have to be accumulated inside the tumor (e.g. by injection) and after application of an external alternating magnetic field heat is induced. The temperature in the targeted tumor tissue increases what resulted in necrosis of tumor cells while the surrounding normal tissues are not damaged (Ito&Kobayashi 2008, Lacroix et al. 2009).

Furthermore, the pharmaceutical use of targeted nanoparticulate drug delivery seems to be particularly promising for future therapeutic treatment of many diseases, since substances can be encapsulated into different polymers. The shell of the nanoscaled carrier system protects the incorporated drug from early degradation or metabolization after application and allows a controlled retarded release of the freight in the body. The use of nanocarriers as vehicles for delivery of drugs also enables the targeting of a defined cell population via specific surface functionalizations (Torchilin 2000), such as cancerous cells. Since targeting as well as the controlled release leads to an increasing efficiency of drugs, dosage can be reduced resulting in a better tolerance of drugs with less side-effects (Haag&Kratz 2006). Furthermore, the use of biodegradable nanovehicles seems to be particularly interesting for use in genetic therapy for improving specific cell functions or to modify the metabolism of degenerated cells after delivery of nucleic acids encoding for respective molecules. Here, the surface of the nanocapsules can also be functionalized with specific antibodies and receptors. The composition and functionalization of the carriers enable the targeting of e.g. a genetic freight into defined cell subsets and organelles as well as the prolonged release for sustained gene expression.

2.2.4 Variation of NP parameters for different biomedical applications

The nanoparticles can be equipped with different functionalities and therefore the process of synthesis depends on the field of application. For an intracellular delivery of substances, a previous interaction of the nanoparticulate transport system with the outer membrane of the cell is required and results -in the best case scenario- in a subsequent incorporation of the particles by the cell. Thus, the properties of the nanoparticles, especially the form, size, charge, surface and materials used for synthesis play a crucial role for an effective uptake (Chithrani et al. 2006, Musyanovych et al. 2008). Additionally, the influence of the nanoparticles on cell viability must be considered since the particles could be potentially toxic and can induce apoptosis of the cell, for example caused by their size or residual surfactants on the particles' surface that were used for synthesis (Nel et. al 2006). Since cytotoxicity not only depends on physico-chemical characteristics of NP, but also on the sensitivity of the respective cell type, different NP have to be tested to identify the particle type that show a strong incorporation into the cells of interest without toxic effects or significant inhibition of important physiological functions (Lorenz et al. 2008, Rabolli et al. 2010, Zhao et al. 2011).

The substances that are supposed for introducing into cells can be packed into a biocompatible or biodegradable material. Biodegradable polymeric nanocapsules consist of poly-butylcyanoacrylate (PBCA), starch or other biological envelope material allowing an enzymatically degradation of the shell with a retarded release of the freight

(Musyanovych&Landfester 2008, Baier et al. 2010). In contrast to biodegradable material, polymers like polystyrene show long term stability since they cannot be degraded inside the cell. The miniemulsion technique of synthesis allows a broad variation of the polymer, the surface functionality, the size and the inner core. This route of synthesis can yield monodisperse nanoparticles and their diameter can easily be varied up to 500 nm. Different reporters can be unproblematically embedded into this nanomaterial. Especially fluorescent reporters for cell und animal studies, for example N-(2,6-diisopropylphenyl)-perylene-3,4-dicarbonacidimide (PMI) as well as contrast agents for MRI or hyperthermia applications (e.g. iron oxide) have been incorporated (Holzapfel et al. 2006). The surface of the nanoparticulate carriers can be altered by addition of a co-monomer that, for example, results in a functionalization with carboxylic groups when acrylic acid is used or alternatively yields amino groups after adding aminoethyl methacrylate hydrochloride (AEMH). The density of functional groups can be enhanced by increasing the concentration of the co-monomer. Further modifications like the addition of amino acids or even peptides or proteins (e.g. transferrin) can be performed, whereby the carboxyl group or amino group acts as anchor for coupling reactions (Holzapfel et al. 2006, Mailänder&Landfester 2009). The coupling of polyethylene glycol (PEG) chains to nanoparticles' surface reduces the unspecific *in vivo* uptake by the mononuclear phagocytes system and increases the circulation time to effectively target diseased cells (Zahr et al. 2006). Figure 3 shows an overview of the particles' parameters have to be altered in respect to the field of application the nanocarriers wanted to be used.

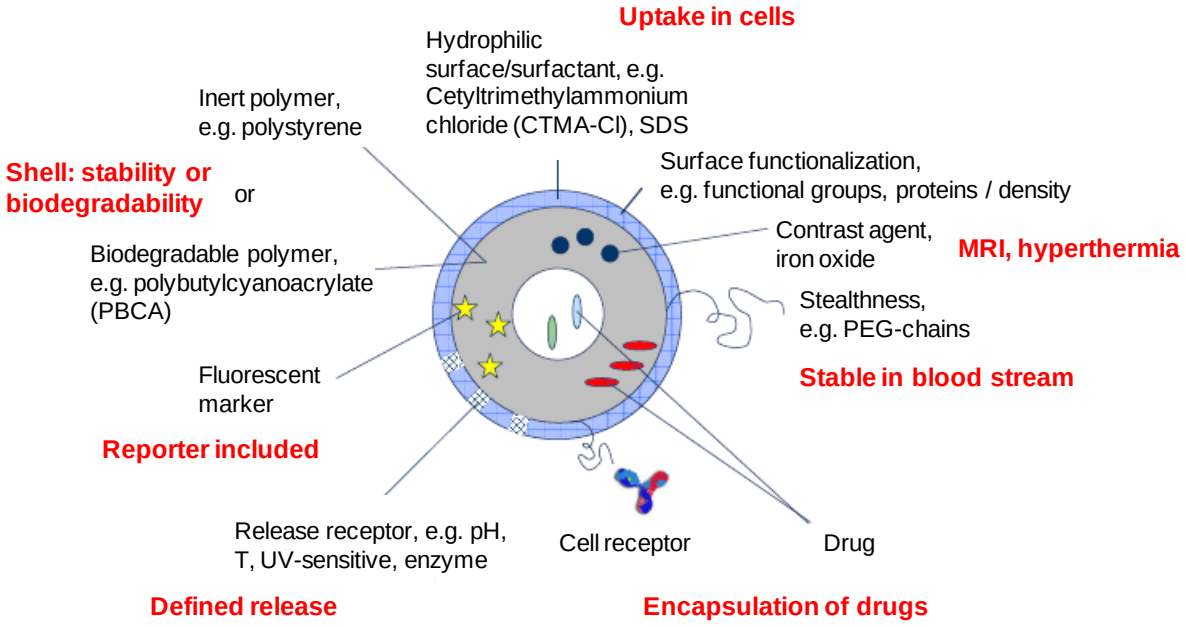

Figure 3: Schematic representation of a nanoparticle with variation possibilities of individual components for different biomedical applications (Figure modified from Mailänder&Landfester 2009).

2.2.5 Cellular uptake of nanoparticles

Because of their small size, nanoparticles can be incorporated by cells after incubation. The uptake mechanisms as well as the intracellular fate of these nanoparticles are of great interest, since insights into the routes of incorporation and their intracellular behavior could enable manipulations of the uptake process of the nanomaterials into cells or even allow a targeted delivery of the freight to specific subcellular compartments, especially the nucleus or cytoplasm (Dausend et al. 2008). Particles with a size from some nanometers up to some hundred nanometers are known to be taken up by endocytosis. There exist several endocytic pathways that are based on formation of intracellular vesicles after invagination of the cell membrane or membrane ruffling. Phagocytosis is a mechanism used for uptake of larger particles like bacteria and therefore primarily performed by specialized cells of the immune system (APC) allowing an effective elimination of those pathogens as well as cell debris (Savina&Amigorena 2007, Conner&Schmid 2003). In contrast, the internalization of fluid surrounding the cell is termed pinocytosis, while substances in the fluid can also be incorporated simultaneously by this way mostly after binding to a cell surface receptor like the binding of transferrin to the transferrin receptor (Iversen et al. 2011). One very well studied uptake pathway is mediated by clathrin-coated pits. The resulting vesicles are characterized by a protein network consisting of clathrin triskelion assemblies that covers those pits and vesicles (Conner&Schmid 2003). A further class of vesicles is coated with the protein caveolin. The caveolin-mediated pathway is derived from membrane domains that are called lipid rafts consisting of phospholipids, glycosphingolipids and cholesterol (Anderson 1998, Quinn 2010). Additionally, uncoated vesicles can also arise from those lipid raft regions or by macropinocytosis that occurs when membrane protrusions fuse back with the cell membrane and form large (>1 µm) vesicles enabling the unspecific internalization of larger particles (Kirkham&Parton 2005). Furthermore, particles can be incorporated by receptor mediated endocytosis, for example via lectin, opsonin and scavenger receptors (Raynal et al. 2004). There exist a lot of several factors like actin, dynamin or cholesterol, which participate in different uptake mechanism. Besides these major endocytic pathways, particles can be incorporated by not fully understood mechanisms (Lu et al. 2009, Lai et al. 2007, Conner&Schmid 2003, Masilamani et al. 2008). Figure 4 shows an overview of main endocytic pathways and intracellular routes.

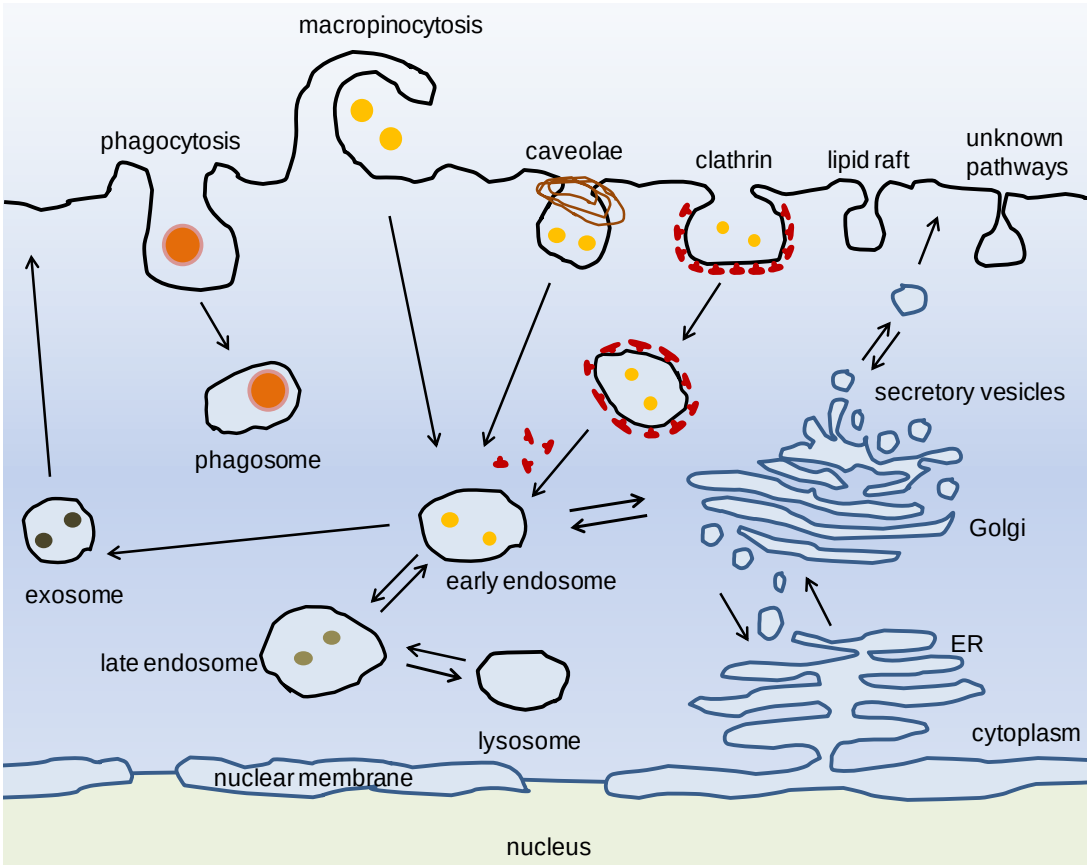

Figure 4: Schematic representation of endocytic pathways and intracellular trafficking of endosomes. Golgi, Golgi apparatus; ER, endoplasmic reticulum (adapted and modified from Sieczkarski&Whittaker 2002).

Furthermore, the uptake mechanisms can be different for several nanoparticles with changing properties (Jiang et al. 2011). In contrast, a particle type can be incorporated by different cell lines in a variety of ways (Dausend et al. 2008, Lunov et al. 2011). The use of pharmacological inhibitors that are specific for different pathways of endocytosis can help to identify the possible route of particles' entrance into the cell. Since not only the uptake mechanism and the intracellular traffic but also specific functions of the cells can be altered by different nanoparticle properties, it has to be examined if particle loaded cells are still functional (Mailänder&Landfester 2009).

2.3 Motivation and aims of this work

2.3.1 Labeling of dendritic cells with nanoparticles

DCs are the most potent cell type for antigen capture, processing, and presentation. They exist as multiple distinct subsets, and are able to activate naïve T cells as well as to initiate memory immune responses. Tumors may cause severe dysfunction of DCs *in vivo* (Pinzon-Charry 2005). In order to overcome this limitation, many groups have implemented *ex vivo*

generation protocols for DCs for vaccination in malignant diseases and viral infections (Tacken et al. 2007, Herr et al. 2000, Mackensen et al. 2000, Ranieri et al. 1999). Until now effectiveness of DC vaccination is limited (Palucka et al. 2010). DCs are also involved in allogeneic reactions against foreign cells like in graft versus host disease. This is especially interesting as immature DCs of the skin (i.e. Langerhans cells) have been shown to play a crucial role in the development of GvHD in a mouse model (Merad et al. 2004). Migration and homing of DCs play a crucial role for DC functions. Hindering the entrance of DCs into lymph nodes, for example, can avert GvHD (Beilhack et al. 2008). Thus, a deeper insight into homing and migration of DCs should enable us to understand differences between DC subpopulations, their physiological migration patterns and how the function of *ex vivo* generated DCs can be tailored and influenced in order to enhance their therapeutic effect or how DCs can be silenced in order to treat autoimmune diseases and GvHD.

In order to follow the migration of DCs in vivo, a platform that enables different labeling techniques of DCs with a variety of readouts would be desirable. The labeling technique should be suitable for small animal studies and studies in humans as well. Such a labeling procedure would be especially interesting for *ex vivo* generated DC preparations used as cellular therapeutics. For animal studies the stable transfection of DCs with a bioluminescent protein is easily achieved. Here luciferase modified mice as DCs donors have been used (Creusot et al. 2009). Such approaches cannot be implemented for human studies for safety and regulatory reasons. They also have the disadvantage that light - even in small animals like mice - is absorbed once the cell is deeply located in the body like in the gut. Other methods for following DCs migration noninvasively are scintigraphy, positron emission tomography (PET), single photon emission computed tomography (SPECT) and MRI (Baumjohann&Lutz 2006). In any of these methods, the amount of the imaging agent is determining the detection limit. Therefore increasing the uptake of reporter molecules should enhance the ability to detect low numbers of DCs. As DCs constantly sample their environment by phagocytosis they take up structures larger than molecules (Ishimoto et al. 2008). Artificially designed particles therefore hold great promise for delivery of antigens into DCs (Elamanchili et al. 2007) or labeling of DCs (Lim et al. 2008, Noh et al. 2008). Particles in the range of some micrometer down to some nanometer have been tested for their uptake into DCs (Manolova et al. 2008). Particles in the range of 20-200 nm can easily migrate from the site of injection through the draining lymphatic vessels to the lymph node while larger particles remain mostly at the site of injection and are only transported to the lymph node by DCs and macrophages. In contrast, the smaller nanoparticles can be taken up by resident DCs like the Langerhans cells and by DCs residing in the lymph node (Manolova et al. 2008). By choosing nanoparticles in the range of 20-200 nm it therefore should be possible to target

not only the DCs in the skin or tissues but also in the lymph node. Nanoparticles can be used as carriers for antigen delivery (Elamanchili et al. 2007, Demento et al. 2009) as well as for cell labeling in order to determine homing and migration of DCs as it has been also shown by other groups with quantum dots (Cambi et al. 2007, Sen et al. 2008). This work will form the basis for both future adoptive immunotherapy trials and the monitoring of administered cells *in vivo* over time.

As a first prerequisite an effective *in vitro* labeling protocol of DCs has to be established. For this purpose, a broad panel of fluorochrome containing nanoparticles with different properties has to be screened in order to identify the NP that is most suitable for DC labeling. Subsequently, different protocol parameters like NP concentration and incubation time will be optimized in this work. For studying normal DC physiology, DC functions should not be affected by the labeling agent. Thus, functional evaluation of labeled DCs will be performed to ensure that the biological role of DCs as professional APC is not inhibited by the NP load.

2.3.2 Loading of T lymphocytes with nanoparticles

The central position of T lymphocytes in the immunological network explains why nearly every immunotherapeutic strategy aims to specifically manipulate them, either to enhance immunity (e.g. in infection and cancer) or to reduce existing misdirected function (e.g. in autoimmunity and transplant rejection). A widely used strategy for manipulation of T cells is genetic engineering, where genes of interest are transferred into T cells to modulate the *in vivo* performance of these cells with regard to their trafficking, homing, persistence, and function. While several gene transfection strategies have been developed that allow for efficient *in vitro* manipulation of T cells, none of them can be applied directly in living recipients. Here nanoparticles offer considerable advantages, because they are suitable not only to transport drugs such as nucleic acids and contrast agents, but can also be functionalized on the surface to enable the targeting of specific cell types *in vivo* (Davis et al. 2008, Petros&DeSimone 2010). The additional use of biodegradable NP components even provides the possibility that drug delivery and release can be customized with regard to time point, duration, and intracellular localization (Panyam&Labhasetwar 2003).

Nanoparticles and their uptake into cells have mainly been analyzed in cell lines, typically malignant or transformed ones (Chithrani&Chan 2007, Dausend et al. 2008, Basu et al. 2009). Rarely this has been done in primary cells and only limited literature is dealing with NP uptake into T cells. Most investigators analyzed murine T cells that were loaded with iron oxide *in vitro* to demonstrate homing of adoptively transferred T cells into sites of tumor infiltration or autoimmune disease by MRI in animals *in vivo* (Moore et al. 2002, Kircher et al. 2003, Anderson et al. 2004). As these studies focus on the detectability and proof of concept

for the visualization of T cells, only few data were provided whether T cells are still functional upon NP labeling (Iida et al. 2008, Janic et al. 2009). While most studies showed that labeling is durable even after days (Kircher et al. 2003, Kaufman et al. 2003), others reported significant loss of MRI signal by approximately 40% during 24 h, which was attributed to ongoing division of T cells during this period (Smirnov et al. 2006). There are also interesting reports on the use of NP-loaded T cells for delivering chemotherapeutic drugs to tumor sites (Steinfeld et al. 2006). However, it remains unclear whether these murine data can be translated into the human setting, because human T cells have been rarely analyzed for NP uptake so far. Some investigators have shown that the efficiency in particle uptake is considerably lower in human T cells than in other cell types, even if transfection agents are being used (Janic et al. 2009, Arbab et al. 2003).

Analogous to the procedure of NP loading to DCs, we will analyze a broad panel of established and newly designed fluorescent polymeric nanoparticles for their uptake into human T cells. Since T lymphocytes are strongly proliferating cells without professional phagocytic activity, the developed NP loading protocol will be adapted to the very different conditions compared to DCs. Additionally, we will use various transfection reagents as well as inhibitors of endosomal trafficking and compare different labeling techniques to identify the most effective NP loading strategy. The uptake mechanism will be investigated by using different pharmacological inhibitors that are specific for components of the main endocytic pathways. Furthermore, the influence of NP loading on essential T cell effector functions will be tested. Finally, experiments with newly designed biodegradable nanocapsules will be performed for evaluating their suitability as nanovehicles and subsequent release of their freight into T lymphocytes.

3 Materials & Methods

3.1 Materials for cell culture

3.1.1 Laboratory equipment

Table 1: Laboratory instruments

Instruments / Utensils	Model / Provider
1-10 µl pipette 2-20µl, 20-200µl, 200-1000µl pipette 5-50µl, 25-200µl Multichannel pipettes	Eppendorf, Hamburg, D Gilson, Limburg, D Dunn Labortechnik, Asbach, D
Autoclave	VX-150, Systec, Wettenberg, D
Axiovert 25 microscope	Carl Zeiss AG, Jena, D
^{137}Caesium source	Gammacell-GC2000, Molsgaard Medical, Gansloe, DK
Cell counting chamber	Fuchs-Rosenthal, Marienfeld, Lauda-Königshofen, D
Cell culture tube-racks	VWR, Darmstadt, D
Centrifuges (Megafuge 1.0R)	Hereaus, Hanau, D
CO_2-Incubators	Binder, Tuttlingen, D; Heraeus, Hanau, D
Cover slip	Menzel, Braunschweig, D
Cryo tube-racks	VWR, Darmstadt, D
FACS tube-racks	Roth, Karlsruhe, D
Freezer (-80°C)	Hera freeze, Heraeus, Hanau, D
Ice machine	Ziegra, Isernhagen, D
Water deionization machine	Purelab Classic, Elga LabWater, Celle, D
Nitrogen cryo bank	Air Liquide DMC, Marne-la-Vallée, F
Nitrogen reservoir tank	Taylor Wharton XL-180, Tec Lab, Husum, D
Pipettor	Pipetboy acu, Integra Biosciences, Fernwald, D
Precision scale	EW150-3W, Kern, Balingen
Refrigerator Freezer Combo (+4°C / -20°C)	Liebherr, Ochsenhausen, D Bosch, München, D
Sterile work bench	Nuaire, Plymouth, USA; Haereus, Hanau, D
Vortex mixer	MS2 Minishaker, IKA, Staufen, D
Water bath heater	GFL, Burgwedel, D

3.1.2 Plastic material

Table 2: Plastic material

Material	Model / Provider
Cell culture flasks (50 mL/25 cm^2, 250 mL/75 cm^2)	Greiner, Frickenhausen, D
Cell culture plates (6-/24-/48-/96-well)	Greiner, Frickenhausen, D
Cryo boxes	Nalgene Freezing Containers, Nunc, Wiesbaden, D
Cryo tubes	Greiner, Frickenhausen, D
Cytotox tubes 0.6 mL	Greiner, Frickenhausen, D
FACS tubes	BD Biosciences, Heidelberg, D
Falcon tubes (15 mL, 50 mL)	Greiner, Frickenhausen, D
Ficoll separation tubes	Leucosep tubes, Greiner, Frickenhausen, D
Ice bucket	Neolab, Heidelberg, D
Microtiter plates (96-well flat-, round-, V-bottom)	Greiner, Frickenhausen, D
Petri dishes (35/60/95 mL)	Greiner, Frickenhausen, D
Pipettes single use (1/2/5/10/25/50 mL)	Greiner, Frickenhausen, D
Pipette tips (0.5-10 µl, 1-200 µl, 200-1000 µl)	TipOne Pipette Tips, Starlab GmbH, Ahrensburg, D
Reaction tubes (0.5 mL, 1.5 mL, 2 mL)	Eppendorf, Hamburg, D
Sterile filter (0.22 µm, 0.45 µm)	Steritop, Millipore, Eschborn, D

3.1.3 Substances and solutions

Table 3: Substances and solutions used for cell culture

Material	Provider
AIM-V medium	Invitrogen, Karlsruhe, D
Dimethyle sulfoxide (DMSO)	Carl Roth, Karlsruhe, D
Ethylendiamine-tetra-acetic acid (EDTA)	Sigma-Aldrich, Steinheim, D
Fetal calf serum (FCS)	PAA Laboratories, Pasching, A
Ficoll lymphocyte separation medium	PAA Laboratories, Pasching, A
Heparin	Ratiopharm, Ulm, D
Human albumin	CSL Behring, Marburg, D
Human serum (HS)	Isolated from blood of 10-20 healthy donors; pooled, heat-inactivated, sterile filtrated
Penicillin/Streptomycin (Pen/Strep)	Invitrogen, Karlsruhe, D
Phosphate buffered saline (PBS, without $CaCl_2$, $MgCl_2$)	Invitrogen, Karlsruhe, D
RPMI 1640 medium (+ L-Glutamine)	Invitrogen, Karlsruhe, D
Trypan blue	Merck, Darmstadt, D
Trypan blue (solution for cell counting)	75 mL stock solution (2 g ad 1 l H_2O) diluted 1:4 with 125 mmol saline for use
Trypsin-EDTA (0.05%)	Invitrogen, Karlsruhe, D

3.1.4 Cell culture media

Table 4: Cell culture media

Medium	Supplement
AIM-V freezing medium	8% human albumin, 10 U/mL heparin, 10% DMSO
AIM-V medium (T cell culture)	1-10% HS
RPMI medium (culture of immortalized cell lines)	10% FCS, 1% Pen/Strep
RPMI medium^{DC} (culture of dendritic cells)	2% HS, 1% Pen/Strep

3.1.5 Cytokines

Table 5: Cytokines

Cytokines	Provider
IL-1β	Miltenyi Biotec, Bergisch Gladbach, D
IL-2	Novartis, Nürnberg, D
IL-4	Miltenyi Biotec, Bergisch Gladbach, D
IL-6	Miltenyi Biotec, Bergisch Gladbach, D
IL-7	R&D Systems, Wiesbaden, D
IL-15	R&D Systems, Wiesbaden, D
GM-CSF (Granulocyte-monocyte colony stimulating factor)	Bayer, Leverkusen, D
PGE2 (prostaglandin 2)	Sigma-Aldrich, Steinheim, D
TNF-α (Tumor necrosis factor-α)	PromoCell, Heidelberg, D

3.2 **Cell culture**

Cells were cultivated under sterile conditions at 37°C and 5% CO_2.

3.2.1 Isolation of PBMCs from buffy coats by Ficoll density centrifugation

Buffy coat products were obtained from healthy donors after informed consent according to the declaration of Helsinki. Peripheral blood mononuclear cells were isolated from buffy coats by standard Ficoll density centrifugation. Briefly, blood was transferred from donation bag into sterile 50 mL Falcon tubes and diluted with the same volume of PBS. Then, the blood/PBS mixture was aliquoted as 20 mL portions into Leucosep tubes containing 15 mL of Ficoll lymphocyte separation medium underneath a porous barrier (frit). After centrifugation for 20 min at 1300 g without brake the interphase consisting of PBMCs was collected and transferred into new Falcon tubes for further washing steps with RPMI. Finally, PBMC were counted and seeded for generation of monocyte derived dendritic cells or

immunomagnetically separation of $CD4^+$ and $CD8^+$ T lymphocytes. Remaining PBMC were frozen and stored in liquid nitrogen until further use.

3.2.2 Freezing and thawing of cells

For cryo-preservation, cells were centrifuged for 5 min at 470 g and resuspended in 1 mL of freezing medium containing 10% DMSO. Cells were then transferred to cryo-tubes that were placed in cryo-boxes containing isopropanol allowing a controlled-rate freezing over night at -80°C. For long term storage in liquid nitrogen cells were placed in the nitrogen bank. For thawing of stored cells, cryo-tubes were removed from the nitrogen bank and frozen cells were rapidly thawed by adding pre-warmed medium to obtain the suspension. Cells were then diluted into growth medium and centrifugated for 5 min at 470 g to remove DMSO. After discarding the supernatant cells were counted and seeded in fresh growth medium for experimental use.

3.3 **Primary cells and cell lines**

3.3.1 Generation of Dendritic Cells from PBMC

Dendritic cells (DCs) were generated from blood monocytes of buffy coat products obtained from healthy donors. First, PBMCs were isolated from buffy coats by standard Ficoll separation as described above. For monocyte isolation by plastic adherence, PBMCs were distributed into 6-well plates at a cell density of $2x10^7$ PBMCs/well. Monocytes were allowed to adhere at 37°C for 1 h in 1 mL $medium^{DC}$ (RPMI supplemented with 2% heat-inactivated human serum, 100 U/mL penicillin, 100 µg/mL streptomycin and 2 mM L-Glutamine). Non-adherent cells were removed by washing the adherent cells twice with warm PBS and stored overnight at 37°C in $medium^{DC}$. On the next day medium was replaced with $medium^{DC}$ containing 800 U/mL granulocyte/macrophage-colony stimulating factor (GM-CSF) and 1000 U/mL interleukin (IL)-4 at day 1 and again with $medium^{DC}$ containing 1600 U/mL GM-CSF and 1000 U/mL IL-4 on day 3 and 5. Immature DCs (iDCs) were harvested at day 6 with cold PBS, pooled and counted. iDCs were directly used in experiments or frozen and stored in liquid nitrogen until further use. For experimental use, freshly generated or thawed iDCs were seeded in $medium^{DC}$ containing 800 U/mL IL-4 and 500 U/mL GM-CSF in 48-well plates. For maturation of DCs, medium was complemented with 10 ng/mL IL-1β, 1000 U/mL IL-6, 10 ng/mL tumor necrosis factor (TNF)-α and 1 µg/mL prostaglandine E2 (PGE2). iDCs were allowed to mature for 48 h at 37°C/5% CO_2 before analysis or use as antigen presenting cells (mature DCs) in functional assays.

3.3.2 Isolation of T lymphocytes from PBMCs

$CD8^+$ and $CD4^+$ T cells were isolated from PBMCs by immunomagnetic cell separation (MACS™, Miltenyi Biotec) according to the manufacturer's instructions. Briefly, $CD8^+$ T cells were first labeled with CD8 MicroBeads and purified by positive selection using MS columns. The $CD8^{neg}$ fraction was subsequently used to isolate $CD4^+$ T cells after labeling with CD4 MicroBeads in a similar procedure. The purity of the isolated cell populations was determined by flow cytometry. $CD8^+$ and $CD4^+$ T cells were directly used in experiments or frozen and stored in liquid nitrogen until further use.

Table 6: Material used for isolation of T lymphocytes from PBMC

Material	Provider
CD4 MicroBeads, human	Miltenyi Biotec, Bergisch Gladbach, D
CD8 MicroBeads, human	Miltenyi Biotec, Bergisch Gladbach, D
LS columns	Miltenyi Biotec, Bergisch Gladbach, D
MS columns	Miltenyi Biotec, Bergisch Gladbach, D
MACS Multistand	Miltenyi Biotec, Bergisch Gladbach, D
MACS buffer	PBS, 0.5% BSA, 2 mM EDTA sterile filtrated
MiniMACS Separator unit	Miltenyi Biotec, Bergisch Gladbach, D
MidiMACS Separator unit	Miltenyi Biotec, Bergisch Gladbach, D
Preseparation filter	Miltenyi Biotec, Bergisch Gladbach, D
Bovine serum albumin (BSA)	Carl Roth, Karlsruhe, D
Ethylendiamine-tetra-acetic acid (EDTA)	Sigma-Aldrich, Steinheim, D

3.3.3 Generation of allo-HLA reactive T-cell lines

Primary human allo-HLA-reactive $CD4^+$ and $CD8^+$ T-cell lines were generated by mixed lymphocyte reaction (MLR). First, $CD4^+$ and $CD8^+$ T lymphocytes were isolated immunomagnetically from PBMC of healthy blood donors as described above. T cells were then stimulated in 24-well plates with allogeneic, HLA class I mismatched, irradiated (100 Gy) Epstein-Barr Virus (EBV)-transformed B lymphoblastoid cell lines (B-LCL) at a ratio of 1:1 in AIM-V medium (Invitrogen) supplemented with 5% human serum ($1x10^6$ T cells and $1x10^6$ EBV B-LCL per well in a total volume of 2 mL). Interleukin-2 at 100 U/mL was added on day (d) 3. T cells were restimulated weekly with irradiated B-LCL cells in fresh medium supplemented with human serum and cytokines.

3.3.4 Jurkat T cells

The human lymphoblastoid T cell-line Jurkat served as a first model system for T lymphocytes. Jurkat cells were originally established from the peripheral blood of a 14 year old boy with an acute lymphoblastic leukemia (ALL, Schneider et al. 1977). The immortal and in suspension growing cells were cultivated at a cell density of $0.4x10^6$/mL in RPMI medium containing 10% heat-inactivated FCS and 1% penicillin/streptomycin in 250 mL cell culture flasks. Cells were counted twice a week and subcultured at an initial density of $0.4x10^6$ cells per mL.

3.3.5 CTL clones

Acute myeloid leukemia (AML)-reactive cytolytic T lymphocyte (CTL) clones were generated from naïve $CD8^+$ T cells of healthy donors by stimulation with HLA-identical AML blasts in mixed lymphocyte/leukemia cultures (MLLC, Distler et al. 2008, Albrecht et al. 2011). The following CTL clones were used in protocol optimization and functional assays: 2A7, 5B2, 4D7, 2D10, and 8F11. The renal cell carcinoma (RCC)-reactive $CD8^+$ T cell clone MLTC BC-V was generated in mixed lymphocyte tumor cell cultures (MLTC) by stimulation of healthy donor $CD8^+$ T cells with allogeneic, HLA identical RCC cells (Dörrschuck et al. 2004).
For weekly re-stimulation, $1x10^6$ AML- or RCC-reactive CTL clones were co-cultured in 24-well plates with their respective, irradiated stimulator cells ($1x10^6$ AML blasts or $1x10^5$ RCC tumor cells) in a total volume of 2 mL per well. Re-stimulation of AML-reactive CTL was performed in AIM-V medium supplemented with 10% HS, 100 U/mL IL-2, 5 ng/mL IL-7, and 5 ng/mL IL-15, while medium for RCC-reactive CTL was only supplemented with 5% HS and 250 U/mL IL-2.

3.3.6 AML blasts

AML blasts, that were originally isolated from peripheral blood or leukaphereses of patients at the time point of initial diagnosis by standard Ficoll separation, act as stimulator and target cells in functional evaluation of NP-loaded antigen-specific CTL clones. For this purpose, blasts were thawed one day before use and seeded in petri dishes at cell numbers of $2x10^6$/mL in AIM-V medium supplemented with 10% human serum before overnight culture at 37°C/5% CO_2. Subsequently, AML blasts were washed out and irradiated with 35 Gy before using them as stimulator cells for antigen-specific CTL clones or were directly used as target cells in functional assays. Table 7 shows the patient-derived AML blasts and the respective AML-reactive CTL clone used in this work.

Table 7: Patient-derived AML blasts

model	CTL clone
MZ201-AML	4D7, 2A7
MZ653-AML	8F11, 5B2
MZ987-AML	2D10

3.3.7 EBV-B (RCC1257)

Epstein-Barr Virus (EBV)-transformed B lymphoblastoid cell lines (B-LCL, Tatsumi, 1992) served as stimulator cells for allo-HLA-reactive $CD4^+$ and $CD8^+$ T lymphocytes. The immortalized suspension cell-line derived from the renal cell carcinoma patient MZ1257 was cultivated at a cell density of $0.4x10^6$/mL in RPMI medium containing 10% heat-inactivated FCS and 1% penicillin/streptomycin in 250 mL cell culture flasks. Cells were counted twice a week and subcultured at an initial density of $0.4x10^6$ cells per mL. EBV-B cells were irradiated with 100 Gy before using them as stimulator cells for T lymphocytes in allogeneic MLR and for weekly re-stimulation.

3.3.8 Tumor cell line (RCC1257)

The adherent growing RCC1257 cell-line derived from the renal cell carcinoma patient MZ1257 was cultivated in RPMI medium containing 10% heat-inactivated FCS and 1% penicillin/streptomycin in cell culture flasks of 25 cm^2. Cells were counted once a week and sub-cultivated at a density of about 10^4 cells per cm^2 after trypsinization of adherent cells. For this purpose, adherent cells were washed with PBS and incubated for 5 min at 37°C/5% CO_2 with 3 mL trypsin-EDTA. Detached cells were resuspended and diluted in RPMI medium. After centrifugation for 5 min at 470 g the supernatant was discarded and cells seeded in fresh medium. RCC1257 cells were irradiated with 100 Gy before using them as stimulator cells for antigen-specific CTL clone MLTC BC-V or were directly used as target cells in functional assays.

3.3.9 Murine T-cell lines

Murine T cells were obtained from Priv. Doz. Dr. Udo Hartwig (Department of Medicine III, Medical Center of the Johannes Gutenberg-University, Mainz). Briefly, splenocytes derived from spleens of 8 – 12 weeks old C57BL/6 mice were used to isolate $CD4^+$ and $CD8^+$ T cells by immunomagnetic cell separation using anti-CD4 and anti-CD8 microbeads, respectively. Purified (>95%) T cells were then polyclonally stimulated with immobilized anti-CD3 mAb (clone 145-2C11) at 0.8 – $1x10^7$ cells/well in RPMI medium supplemented with 10% FCS,

5% ”additives” (see Table **8**) and 100 U/mL human recombinant IL-2 for 72 h at 37°C in Ab-coated 6-well plates (3 µg Ab/mL) using a total volume of 3 mL complete medium.

Table 8: Composition of additives for culture of murine T cell lines

Chemicals	Provider
100 mL Pen/Strep	Invitrogen, Karlsruhe, D
100 mL β-mercaptoethanol (175x 10^6 U diluted in 500 mL PBS)	Sigma-Aldrich, Steinheim, D
100 mL 1 M Hepesbuffer	Invitrogen, Karlsruhe, D
100 mL Sodium pyruvate	Invitrogen, Karlsruhe, D
100 mL L-Glutamine (200 mM)	Biochrom AG, Berlin, D
60 mL Non-essential amino acids	Invitrogen, Karlsruhe, D

3.4 Nanoparticles

3.4.1 Materials for nanoparticle synthesis

Nanoparticles were synthesized in the group of Prof. Dr. Katharina Landfester at the Max Planck Institute for Polymer Research (MPIP), Mainz. Chemicals that were used for nanoparticle synthesis are shown in Table 9:

Table 9: Material for nanoparticle synthesis

Chemicals	Provider
2,20-azobis(2-methylbutyronitrile) (V59)	Wako Chemicals, Neuss, D
Acrylic acid (AA)	Sigma-Aldrich, Steinheim, D
2-aminoethyl methacrylate hydrochloride (AEMH)	Sigma-Aldrich, Steinheim, D
Cetyltrimethylammonium chloride (CTMA-Cl, 25 wt.% in aqueous solution)	Sigma-Aldrich, Steinheim, D
Hexadecane (HD)	Sigma-Aldrich, Steinheim, D
N-(2,6-diisopropylphenyl)-perylene-3,4-dicarbonacidimide (PMI)	BASF, Ludwigshafen, D
Sodium dodecyl sulfate (SDS)	Sigma-Aldrich, Steinheim, D
Styrene	Merck, Darmstadt, D

3.4.2 Synthesis of polymeric nanoparticles

Composite latex particles with incorporated fluorescent dye were prepared by miniemulsion polymerization (Holzapfel et al. 2005). For the preparation of the carboxyl functionalized latex particle, a mixture of styrene, the functional co-monomer acrylic acid, initiator (V59), hydrophobe (hexadecane) and PMI was added to the aqueous phase containing SDS and demineralized water. In the case of the amino-functionalized particle synthesis, the amino monomer AEMH was dissolved in the aqueous phase consisting of water and ionic surfactant CTMA-Cl. Polystyrene particles synthesized in the presence of SDS or CTMA-Cl were used as reference for carboxyl and amino-functionalized particles, respectively. After 1 h of pre-emulsification by stirring at 1000 rpm, the mixture was sonicated in an ice-cooled bath for 120 s at 90% amplitude (Branson sonifier W450 digital, 1/200 tip, Branson, USA). The copolymerization was performed for 20 h at 72°C with the stirring rate fixed at 500 rpm

3.4.3 Characterization of nanoparticles

Nanoparticles were characterized as described earlier (Holzapfel et al. 2005, Musyanovych et al. 2007). Briefly, the solid content of the final particle dispersion was measured gravimetrically. The polymer particles were purified from water-soluble oligomers and surfactants by dialysis. The particle sizes of the purified samples as well as the zetapotential were measured by means of dynamic light scattering (DLS). Visually verification of the particles was performed by scanning electron microscopy (SEM). The surface charge density on purified latex samples was determined by streaming potential titration. The UV-Vis absorption spectra of the latex particles were obtained by UV/Vis spectrometry. The particles used in this work are listed in Table 10.

Table 10: Nanoparticles with different characteristics, used for uptake by cells

Nanoparticle	Original name	Monomer / Co-monomer	Surfactant	Size, nm	ζ-potential, mV	Functional groups	Functional groups/nm^2	Amount of PMI, mg/g polymer
NP-1	DB010-PS-(AA)g	styrene	SDS	110	-52.1	-	-	0.20
NP-1-COOH	DB010-PS-AAd	styrene / AA	SDS	115	-51.5	COOH	0.45	0.37
NP-2	DB011-PS-(AEMH)f	styrene	CTMA-CL	107	50	-	-	0.20
NP-2-NH_2	DB-011-PS-AEMHc	styrene / AEMH	CTMA-CL	144	45.3	NH_2	0.58	0.27
NP-3	GB-PS-6	styrene	Lutensol	130	-8.7	-	-	0.44
NP-3-COOH	GB-PS-8 (AA)	styrene / AA	Lutensol	135	-31	COOH	0.22	0.4
NP-3-NH_2	GB.PS.10 (AEMH)	styrene / AEMH	Lutensol	135	4.3	NH_2	0.07	0.43
NP-4-COOH	GB-PS-24(AA)	styrene / AA	Lutensol	155	-31	COOH	0.66	0.4
NP-4-NH_2	GB-PS-26(AEMH)	styrene / AEMH	Lutensol	145	8.7	NH_2	0.17	0.43
NP-5	AM-SC-PM	styrene	CTMA-CL	100	49	-	-	0.50
NP-5-NH_2	AM-NSC5-2PM	styrene / AEMH	CTMA-CL	120	53	NH_2	0.13	0.50
NP-6	AM-SL-PM	styrene	Lutensol	175	-4	-	-	0.58
NP-6-NH_2	AM-NSL3-2PM	styrene / AEMH	Lutensol	182	8	NH_2	0.23	0.40
NP-7	AM-SS-PM	styrene	SDS	116	-45	-	-	0.47
NP-7-COOH	AM-ASS5-PM	styrene / AA	SDS	121	-46	COOH	0.5	0.28
NP-8	UPAM2	styrene	CTMA-CL	117	36.5	-	-	0.44
NP-8-NH_2	UPAM1	styrene / AEMH	CTMA-CL	125	42.5	NH_2	0.25	0.39
NP-9	UPAM4	styrene	CTMA-CL	78	44.3	-	-	0.41
NP-9-NH_2	UPAM3_N2	styrene / AEMH	CTMA-CL	65	49.2	NH_2	0.04	0.55
NP-9-PEG-CH_3	UPAM3F2	styrene / AEMH	CTMA-CL	71	4.2	PEG-CH_3	10.5 g attached to 100 g NP	0.39
NP-9-PEG-CH_3/NH_2	UPAM3F3	styrene / AEMH	CTMA-CL	63	3.5	PEG-CH_3/NH_2	22 g attached to 100 g NP	0.39
NP-9-Transferrin	UPAM3F7N2	styrene / AEMH	CTMA-CL	64	3.2	Transferrin	372 molecules/NP	0.39
NP-10	UPS1sds	styrene	SDS	32	-36.6	-	-	0.17

First letters of original NP name are initials of the manufacturers' names: DB, Dr. Daniela Baumann; GB, Dr. Grit Baier; AM, Dr. Anna Musyanovych; UP, Dr. Umaporn Paiphansiri.

3.5 Loading of cells with nanoparticles

3.5.1 DCs

3.5.1.1 Particle uptake and protocol optimization

For labeling with nanoparticles, $1x10^5$ iDCs were seeded in 1 mL $medium^{DC}$ containing 800 U/mL IL-4 and 500 U/mL GM-CSF in 48-well cell culture plates. After 1-2 h, particles were added at a concentration of 25 µg/mL if no other concentration is indicated. NP-loading was performed with particle NP-2-NH_2 if not mentioned otherwise. Cells were incubated with particles for 16 h at 37°C/5% CO_2 if not noted otherwise. After this labeling period, non-incorporated particles were removed by washing with warm (37°C) PBS and cells were prepared for flow cytometry. In order to analyze NP incorporation by DCs, cells were stained with APC-conjugated monoclonal antibody against the DC-specific marker CD11c. Hereby DCs can be distinguished from other cell types as well as from large aggregates of nanoparticles that may have formed during incubation in the cell culture medium.

In a first step, NP with different characteristics were incubated with DCs at an initial concentration of 75 µg/mL for 16 h as it has been suggested by the producers at the MPIP for use in preliminary uptake tests since those NP loading conditions led to an adequate uptake by HeLa cells in previous experiments (personal communication). Uptake of different particles was analyzed by flow cytometry in order to identify the best particle that can be used for subsequent protocol optimization.

In experiments determining the concentration dependence of nanoparticle uptake, the most suitable NP was used for labeling of DCs at various concentrations from 0.75 to 150 µg/mL for 16 h. To investigate the optimal incubation time, iDCs were incubated with NP at optimized concentration of 25 µg/mL for different time periods from 0.5 to 24 h.

3.5.1.2 Particle release

A long-term follow-up of mature DCs loaded with PMI-containing nanoparticles was performed over 8 days. After an incubation period of 16 h (concentration: 25 µg/mL), non-incorporated particles were removed by rinsing with warm (37°C) PBS and iDCs matured over 48 h. The fluorescence intensity of incorporated particles was measured by flow cytometry on day 1, 2, 3, 4, 5, and 8 after maturation for monitoring release of NP.

3.5.2 T lymphocytes

3.5.2.1 Particle uptake and protocol optimization

For labeling with NP, $3x10^5$ T cells were seeded in 1 mL in 48-well plates at day 2 after the second antigen-specific re-stimulation (day 14+2, if not otherwise indicated). Medium was AIM-V regularly supplemented with 1% human serum if not noted otherwise. NP-loading was performed with particle NP-9-NH_2 if not mentioned otherwise. Nanoparticles were added at a concentration of 75 µg/mL if no other concentration is indicated. Cells were incubated with particles for 16 h at 37°C/5% CO_2 if not otherwise stated. After this labeling period, non-incorporated particles were removed by centrifugation for 5 min at 470 g.

First, nanoparticles with different characteristics were screened for their suitability as labeling agent for T lymphocytes and also for comparing uptake of particles by T cells with NP incorporation by dendritic cells. For this purpose, NP were loaded to T cells at a concentration of 75 µg/mL for 16 h. Uptake of different particles was analyzed by flow cytometry in order to identify the best particle that can be used for subsequent protocol optimization for achieving an efficient incorporation by T lymphocytes.

To ascertain the optimal time point of NP loading during the T cell re-stimulation cycle, allo-reactive $CD4^+$ and $CD8^+$ T-cell lines (culture day 21) as well as leukemia-reactive CTL clones 2A7 (culture day 77) and 5B2 (culture day 42) were incubated with 500 µg/mL NP for 16 h at day 2, day 4 or day 6 after antigen-specific re-stimulation in AIM-V medium supplemented with 10% HS.

In experiments determining the concentration dependence of nanoparticle uptake, NP were added to $CD8^+$ T cells on day 2 after re-stimulation at concentrations ranging from 25 to 2400 µg/mL in AIM-V medium supplemented with 10% HS. In order to find the optimal incubation time, T cell lines were incubated with 500 µg/mL particles for different periods from 2 to 24 h.

For investigating the influence of human serum on NP uptake antigen-specific $CD4^+$ T-cell lines were incubated with NP in AIM-V medium containing different amounts of human serum from 0-10%.

For investigating the influence of cell culture age on NP uptake and to compare NP uptake by $CD4^+$ and $CD8^+$ T-cell lines, cells were cultivated over two to four weeks with NP loading on the respective day two after antigen specific re-stimulation.

In order to analyze the influence of temperature on NP uptake, $CD4^+$ and $CD8^+$ T-cell lines were incubated with NP at 37°C or 4°C for different time periods from 0.5 h to 16 h. For this purpose, cells were seeded in pre-heated (37°C) or pre-cooled (4°C) medium respectively, before NP were added.

3.5.2.2 Uptake mechanism

For investigating the possible NP uptake mechanism, T cells were incubated with NP in the presence of pharmacological drugs that inhibit components of the three classical endocytic pathways: macropinocytosis, clathrin- and caveolin-mediated endocytosis (Table 11). In preliminary dose finding studies cells were incubated with various concentrations of dynasore (1-160 µM), chlorpromazine (6.13-100 µM), 5-(N-ethyl-N-isopropyl)amiloride (EIPA, 1.25-160 mM), and cytochalasin D (0.25-20 µM) to determine the maximum non-toxic concentration that could be used for inhibition studies. Cell viability was analyzed by flow cytometry after 7-amino-actinomycin D (7-AAD) staining of dead cells. In subsequent inhibition experiments $CD4^+$ and $CD8^+$ T cells were preincubated with different concentrations of the respective drug in PBS^+ (with Ca^{2+} and Mg^{2+}) for 30 min at 37°C. Subsequently, NP (75 µg/mL) were added and incubated with T cells in presence of inhibitors for further 60 min at 37°C. For investigating the uptake mechanism, NP incubation time was shortened to 60 min since blocking of one endocytic pathway could allow NP incorporation via other routes (Conner&Schmid 2003). NP incorporation and cell viability was measured by flow cytometry and verified visually by confocal laser scanning microscopy (cLSM).

For blocking intracellular trafficking of vesicles, $CD4^+$ T cells were incubated with NP in the presence of different concentrations of the Golgi inhibitors brefeldin A (0.1-16 µg/mL) and monensin (0.1-16 µM). Experimental setup was the same as described above.

Table 11: Pharmacological inhibitors

Material	Inhibition / site of action	Provider
5-(N-ethyl-N-isopropyl)amiloride	Membrane Na^+/H^+ exchanger	Sigma-Aldrich,
Brefeldin A	Vesicle transport between ER and Golgi	Sigma-Aldrich,
Chlorpromazine	Assembly of clathrin (Wang et al. 1993)	Sigma-Aldrich,
Cytochalasin D	Polymerization of actin	Sigma-Aldrich,
Dynasore	GTPase activity of dynamin	Sigma-Aldrich,
Monensin	Trans-Golgi transport	Sigma-Aldrich,
PBS^+ (with Ca^{2+} and Mg^{2+})		Invitrogen, Karlsruhe, D

3.5.2.3 Particle release

In preliminary experiments, particles were incubated with $CD4^+$ T cells at a concentration of 500 µg/mL for 16 h in AIM-V + 10% HS. After incubation non-incorporated particles were removed by centrifugation. An aliquot of the labeled cells was directly analyzed by flow cytometry for NP uptake (day 1). Residual cells were re-cultured at $3x10^5$ per well (48-well plate) in particle free AIM-V medium supplemented with 10% HS and 100 U/mL IL-2 for a

long-term follow-up over five days. The content of residual NP was analyzed by flow cytometry on every single day during the experimental course. In two further experiments, NP release during the first 24 h was monitored by analyzing NP content 0.5, 2, 4, 8, 24 h after re-culture of NP-loaded cells in particle free AIM-V medium supplemented with 1% HS. Release of NP during short-term follow-up of labeled cells was stopped by centrifugation and subsequent fixation of the labeled cells with PBS containing 1% paraformaldehyde (PFA) and 0.1% BSA.

In order to investigate the influence of human serum on release of incorporated NP, $CD4^+$ T cells were incubated with particles at a concentration of 500 µg/mL for 16 h. After this incubation period, non-incorporated particles were removed by centrifugation and NP-loaded cells re-cultured for further 24 h at 37°C in particle free AIM-V medium supplemented with different concentrations of human serum from 0% to 10%.

For analyzing the influence of temperature and cell proliferation on NP release, $CD4^+$ T cells were incubated with particles in the presence of 1% HS for 16 h at 37°C. After the incubation period, non-incorporated particles were removed by centrifugation and NP-loaded cells were re-cultured for further time periods from 0.5 h to 24 h at 37°C or 4°C. NP-labeled cells were seeded in pre-heated (37°C) or pre-cooled (4°C) medium respectively for investigating influence of temperature on NP exocytosis during the first 24 h after re-culture in particle free medium. Additionally, cell proliferation was monitored by counting the number of cells in each well before and after re-culture.

For investigation of a possible influence of adenosine triphosphate binding cassette (ABC)-transporter activity on NP exocytosis, 500 µg/mL NP were pulsed onto flow-cytometric sorted central memory ($CCR7^+$ $CD45RA^-$) and effector memory ($CCR7^-$ $CD45RA^-$) T cells, since those T-cell subsets have been described to strongly express such multidrug resistance efflux transporter proteins (Turtle et al. 2009). Sorted naïve ($CCR7^+$ $CD45RA^+$) T cells served as controls. After sorting (for more details see below), T cells were activated nonspecifically with anti-CD3/CD28 Dynabeads™ (Invitrogen, Karlsuhe, D) during 72 h of incubation at 37°C/5% CO_2 in AIM-V medium supplemented with 5% HS and 50 U/mL IL-2 (15 µL Dynabeads™ per 10^6 cells). After removal of magnetic Dynabeads™, NP were loaded to cells over 16 h at 37°C. After removal of excess nanoparticles by centrifugation, NP-loaded cells were seeded in particle free medium for monitoring NP release over three days.

3.5.3 Human B lymphocytes and murine T cell lines

For labeling with NP, EBV-B LCLs ($3x10^5$ cells per well) were incubated with 75 µg/mL NP in AIM-V medium supplemented with 1% HS for 16 h at 37°C.

For NP-loading of murine $CD4^+$ and $CD8^+$ T cell lines, cells were incubated at $3x10^5$ per well with 75 µg/mL NP in RPMI medium supplemented with 5% FCS and 100 U/mL IL-2 at day 3 after polyclonal stimulation for 16 h at 37°C. After the labeling period, non-incorporated particles were removed by centrifugation for 5 min at 470 g and prepared for analysis by flow cytometry. To investigate release of incorporated particles, NP-loaded EBV-B LCLs were re-cultured at $3x10^5$ per well in particle free AIM-V medium supplemented with 1% HS. NP-labeled murine T cell lines were re-cultured at $3x10^5$ per well in RPMI medium supplemented with 5% FCS and 100 U/mL IL-2 for monitoring NP release.

3.6 Analysis of nanoparticle uptake and toxicity by flow cytometry

Flow cytometry (FACS, fluorescence-activated cell sorting) uses the principles of light scattering, light excitation, and emission of fluorochrome molecules to identify, analyze, or sort different populations of cells. A flow cytometer measures fluorescence on single cells and is able to determine the number of cells expressing the molecule to which a fluorescent probe binds. Additionally, the expression level of a certain molecule on a cell population as well as the uptake level of fluorescently labeled particles can be evaluated by detecting the fluorescence intensity. First, cells have to be stained by incubating with fluorochrome-conjugated antibodies or particles. Prepared cells, suspended in a buffer, are injected into a stable stream that forces cells to travel one by one through a fluorimeter with a laser-generated incident beam of a designated wavelength. Light that is reflected back from the samples will be analyzed for fluorescence as well as for side and forward scatter allowing discrimination of cells by the respective markers, their size, and internal complexity.

3.6.1 NP uptake of vital cells

Nanoparticle uptake and toxicity was analyzed by flow cytometry as described earlier (Lorenz et al. 2006, Philpott et al. 1996). Briefly, fluorescent intensity of PMI containing particles taken up by DCs and T lymphocytes was measured in the FL1 channel (filter 530/30 nm) after excitation with 488 nm light (argon laser). For analyzing particle uptake, only vital cells ($7\text{-}AAD^{neg}$) were gated, since dying and dead cells could bind NP unspecifically. The median fluorescence intensity (MFI) of the FL1 channel was used for statistical determination of the particle uptake. Analysis was performed using the flow cytometer BD FACS Canto. After gating of viable lymphocytes, at least 10.000 events were measured and analyzed applying the BD FACS Diva software. Results represent means of duplicates with standard deviations indicated. As the particles contained different amounts of the fluorescent dye (incorporated

dye (icDye) given as w/w), the FL1-MFI was normalized by the following formula in order to compare the efficiency of uptake between different particle types:

$$\text{Normalized FL1} = n\text{FL1}_{(\text{particle } X)} = \frac{\text{Median FL1}_{(\text{particle } X)}}{\text{Median FL1}_{(\text{uncharged particle})} \frac{\text{icDye}_{(\text{particle } X)} /}{\text{icDye}_{(\text{uncharged particle})}}} .$$

The material used for flow cytometry is shown in Table 12:

Table 12: Material used for flow cytometry

Material/Devices	Description/Provider
AIM-V medium	Invitrogen, Karlsruhe, D
Bovine serum albumin (BSA)	Carl Roth, Karlsruhe, D
FACS buffer	PBS (without $CaCl_2$ / $MgCl_2$), 0.1% BSA
Flow Cytometer	BD FACS Canto, Becton Dickinson Biosciences, Heidelberg, D
Software	BD FACS Diva, vers. 6.1.3, Becton Dickinson Biosciences, Heidelberg, D

3.6.2 7-Amino-actinomycin D staining of dead cells for flow cytometry

Staining of dying and dead cells with 7-amino-actinomycin D (7-AAD) was used to evaluate particle toxicity. The red fluorescent cell viability dye 7-AAD allows the discrimination of dying and dead cells after passing through the cell membrane and intercalation between cytosine and guanine bases of the DNA whereas cell membranes of intact cells are not permeable to 7-AAD (Philpott 1996). For this purpose, cells were stained with 12.5 µg/mL 7-AAD for 15 min at 4°C. After incubation, cells were washed with 1 mL AIM-V medium, resuspended in 0.3 mL FACS buffer, and measured immediately by flow cytometry. 7-AAD was excited with the 488 nm argon laser and fluorescence intensity was measured using a 630 nm long pass filter. The materials used for 7-AAD staining of cells are shown in Table 13:

Table 13: Material used for 7-AAD staining

Material	Provider
7-amino-actinomycin D	Sigma-Aldrich, Steinheim, D
AIM-V	Invitrogen, Karlsruhe, D
PBS^+ (with $CaCl_2$ + $MgCl_2$)	Invitrogen, Karlsruhe, D

3.6.3 Immunofluorescent staining with monoclonal antibodies for flow cytometry

For immunofluorescent staining, $1x10^5$ cells were washed with 1 mL FACS buffer and incubated for 15 min at 4°C with 2-20 µL FITC-, PE-, PerCP- or APC-conjugated monoclonal antibodies (mABs) specific for indicated surface antigens in a total volume of approximately 30 µL. After washing off unbound antibody with 1 mL FACS buffer, stained cells were resuspended in 0.3 mL FACS buffer. Immunofluorescent staining of NP-loaded as well as of unlabeled cells was performed prior to 7-AAD staining. The mouse anti-human monoclonal antibodies used for immunophenotyping of cell populations by flow cytometry, are shown in Table 14. All mABs were titrated in order to find the optimal concentration to be used in the experiments. Antibodies were stored at 4°C, and handled under sterile conditions.

For flow-cytometric sorting, cells were stained using about 50 to 60 µL of mABs per $100x10^6$ cells. Subsequently, cells were washed with 30 mL sort buffer and resuspended in 2 mL sort buffer. Cells were then passed through a 30 µm nylon mesh filter (Miltenyi Biotec). Sort buffer was added until a concentration of $10\text{-}20x10^6$ cells per mL was reached. Cells were separated by flow cytometric cell sorting at 4°C under sterile conditions.

Table 14: Fluorochrome-conjugated monoclonal antibodies

Antibody specificity	Clone	Fluorochrome	Provider	Volume (in µL)
Isotype control mouse IgG1	MOPC-21	FITC, PE, APC	Beckman Coulter, Krefeld, D	2-20
CD3	UCHT1	FITC, PE, APC	Beckman Coulter, Krefeld, D	3
CD4	13B8.2	FITC, PE, APC	Beckman Coulter, Krefeld, D	2
CD8	B9.11	FITC, PE, APC, PerCP	Beckman Coulter, Krefeld, D	3
CD11c	B-ly6	APC	BD Biosciences, Heidelberg, D	5
CD16	3G8	FITC, PE	Beckman Coulter, Krefeld, D	5
CD45RA	T6D11	APC	Miltenyi, Bergisch Gladbach, D	5
CD56	B159	FITC, PE	Beckman Coulter, Krefeld, D	5
CD80	MEM-233	APC	EuroBiosciences, Friesoythe, D	20
CD83	HB15e	APC	BD Biosciences, Heidelberg, D	5
CD86	2331(FUN-1)	APC	BD Biosciences, Heidelberg, D	5
CD197 (CCR7)	150503	FITC, APC	BD Biosciences, Heidelberg, D	5
HLA-DR	G46-6	APC	BD Biosciences, Heidelberg, D	5

The last column shows the volume of mAbs in µL used for staining of 10^5 cells. For negative controls the volume of immunoglobulin (Ig) G1 antibody was the same as the highest volume of another mAb that was used in the experiment and conjugated to this dye.

3.7 Confocal laser scanning microscopy of NP-loaded cells

In contrast to conventional light microscopes, a confocal laser scanning microscope (cLSM) is equipped with a laser light source, a laser scanning head, and an automatic focusing unit. The laser is moved across a specimen to create optical sections using visible light. The confocal arrangement of illumination and detector pinholes enables that only information from the focal plane reaches the detector. The optical slices are used to provide a three-dimensional (3D) reconstruction of samples that can also be stained with fluorescent dyes.
Intracellular localization of particles was confirmed by cLSM at the core facility "cLSM" of the Forschungszentrum Immunologie (FZI), Mainz. The membrane stain CellMask™ Orange was excited by the 543 nm helium-neon laser. The argon laser (488 nm) was used for excitation of PMI, and the nucleus stain Hoechst 33342™ was excited by the blue violet diode laser (405 nm). Additionally, excitation of Cy5 labeled oligonucleotides was performed at 633 nm (helium-neon laser) while MitoTracker™ was excited by the argon laser at 488 nm in colocalization studies with biodegradable nanocapsules (see also below).

Table 15: Material used for cLSM

Material/Devices	Description/Provider
CellMask™ Orange	Invitrogen, Karlsuhe, D
Hoechst 33342™	Invitrogen, Karlsuhe, D
Lab-Tek 8-well chamber slides	Thermo Fisher Scientific, Bremen, D
MitoTracker™ Green FM	Invitrogen, Karlsuhe, D
Microscope	LSM 710 NLO confocal laser scanning microscope, Carl Zeiss, Jena, D
Objective	Plan-Apochromat 63x/1.4 Oil DIC, Carl Zeiss, Jena, D
Software	Zen 2009, Carl Zeiss, Jena, D

3.7.1 DCs

For cLSM analysis of mDCs, cells were incubated with particles in 48-well culture plate, matured as described above and $1x10^5$ cells in 300 µL medium per well were transferred into Lab-Tek 8-well chamber slides. For cLSM analysis of iDCs, $1x10^5$ cells were cultured directly in chamber slides. After particle incubation, non-incorporated particles were washed off with 37°C warm PBS. Nuclear staining was performed by incubating the cells with 200 nM Hoechst 33342™ (final concentration) in a total volume of 300 µL PBS for 30 min at 37°C. After washing with the same volume of PBS, 300 µL PBS was added into the well and

immediately before microscopy cell membranes were stained with 2.5 µg/mL CellMask™ Orange plasma membrane stain.

3.7.2 T lymphocytes

T cells were incubated with particles in 48-well culture plate as described above. After removal of non-incorporated particles by centrifugation, $2x10^5$ cells were resuspended in 300 µL PBS and transferred to a 15 mL tube for subsequent nuclear staining with 200 nM Hoechst 33342™ (final concentration) for 30 min at 37°C. After washing, cells were transferred in 300 µL medium per well into Lab-Tek 8-well chamber slides. Immediately before microscopy, cell membranes were stained with 1.67 µg/mL CellMask™ Orange plasma membrane stain.

3.8 Transmission electron microscopy of NP-loaded T cells

Transmission electron microscopy (TEM) is based on conventional light microscopy but uses electrons instead of light. The electrons are focused with electromagnetic lenses into a narrow, high energy electron beam travelling through a vacuum in the column of the microscope before interacting with the ultra thin specimen as it passes through. Transmitted electrons collected by a detector are used to produce a high resolution image of the sample.
TEM studies of NP-loaded $CD4^+$ T cells were performed in collaboration with Dr. Martin Dass (AK Prof. Dr. Katharina Landfester, Max Planck Institute for Polymer Research, Mainz). For TEM analyses, T cells were loaded with NP as described above but with particle concentrations of 500 to 2000 µg/mL. After washing off unbound particles, cells were fixed with a high pressure freezer Compact 1 (Wohlwend GmbH, Switzerland) and freeze-substituted in a Leica EM AFS 2 device (Leica Microsystems, Germany). Therefore a substitution medium of acetone, 0.2% osmiumtetroxide, 0.1% uranylacetate and 5% water content was used (all chemicals from Merck). The medium was pre-cooled to -90°C before samples were added and afterwards the temperature was increased stepwise to 0°C during 20 h. After the freeze substitution the samples were placed at room temperature, the substitution medium was displaced by pure acetone and the samples were washed two times with acetone. A 50:50 mixture of acetone and EPON 812 embedding medium (Fluka/Sigma Aldrich) was added to the samples for 3 h and afterwards replaced by 100% EPON 812 embedding medium and stored over night. All samples were embedded in fresh EPON 812 and polymerized at 60°C for 3 days. Ultrathin sections (60 nm) were prepared with a microtome (Leica Ultracut UCT Ultramicrotome). To improve contrast of polystyrene, sections were treated for 1 min with ruthenium tetroxide (Structure Probe, spi Supplies, Pennsylvania,

USA; Trent et al. 1983). For electron microscopic analysis a Zeiss 912 Omega transmission electron microscope operated at 120 kV was used.

3.9 Phenotypical and functional evaluation of NP-loaded cells

3.9.1 DCs

3.9.1.1 Phenotypical characterization (by flow cytometry)

For analyzing the expression of further cell surface markers, NP-loaded as well as unlabeled cells were stained with APC-conjugated mAbs specific for indicated antigens (CD11c, CD80, CD83, CD86, HLA-DR, CCR7, CD80; see also above under 3.6.3).

3.9.1.2 Allogeneic stimulatory capacity (by ^{3}H-thymidine proliferation assay)

The ^{3}H-thymidine proliferation assay enables the quantification of cell proliferation by measuring ^{3}H-thymidine incorporation into newly synthesized DNA (Ahern et al. 1976). Particle-loaded DCs as well as unlabeled DCs served as stimulator cells in an allogeneic mixed lymphocyte reaction (MLR). MACS-isolated T cells ($5x10^{4}$/well) were co-cultured with irradiated (30 Gy) HLA class I-mismatched mDCs ($5x10^{3}$/well) in 96-well round-bottomed microtiter plates in a total volume of 160 µL of AIM-V medium supplemented with 5% HS for 5 days at 37°C and 5% CO_2. Unstimulated T cells served as controls. ^{3}H-thymidine (0.5 µCi/well) was added 18 h before assay termination, and incorporation was measured in a TopCount scintillation counter. Results represent means of triplicates with standard deviations (SD) indicated.

Table 16: Material used for ^{3}H-thymidine proliferation assay

Material	Description/Provider
^{3}H-thymidine	Amersham Biosciences, Freiburg, D
TopCount scintillation counter	Wallac, Turku, FIN

3.9.1.3 Antigen processing and presentation (by IFN-γ ELISPOT assays)

The enzyme-linked immunosorbent spot (ELISPOT) assay is a method used for monitoring immune responses by detecting the cytokine secretion of effector cells. Interferon-γ (IFN-γ) ELISPOT assays were performed as described earlier (Britten et al. 2002, Herr et al. 1997, Distler/Blötz et al. 2011, Albrecht et al. 2011). Briefly, multiscreen HTS™ IP plates were coated with 10 µg/mL mAb anti-hIFN-γ 1-DIK over night at 4°C. Plates were washed with PBS to remove unbound antibody. Serum-containing medium was used to block unspecific

binding. T cells and DCs were seeded in 100 µL medium per well and were incubated for 24 to 40 h at 37°C/5% CO_2. After incubation, captured IFN-γ was detected by biotinylated mAb anti-hIFN-γ 7-B6-1 at 2 µg/mL. Spots were developed by the sequential addition of avidin-peroxidase complex (Vectastain Kit) and 3-amino-9-ethyl-carbazole. Spot numbers were counted with computer-assisted video image analysis system KS ELISPOT 4.9. Results represent means ± standard deviations of duplicate values.

For investigating the T cell reactivity against cytomegalovirus (CMV) antigens presented by particle-loaded DCs, labeled mDCs of a CMV-seropositive donor seeded with $1x10^4$ per well in AIM-V medium supplemented with 10% HS, were incubated with 1 µg/mL CMV peptide mix (JPT Peptide Technologies, Germany) for 30 min at 37°C/5% CO_2. After addition of $5x10^4$ autologous $CD4^+$ or $CD8^+$ T cells, respectively, ELISPOT plate was incubated for 24 h at 37°C/5% CO_2. To analyze T cell recognition of influenza antigens processed and presented by nanoparticle-loaded DCs, iDCs were first incubated (16 h) with nanoparticles. Six hours before ending of the incubation time, 10 µg/mL of an inactivated influenza A (H3N2) whole virus preparation (Baxter, Vienna, Austria) was added to the medium. Subsequently, DCs were rinsed with warm PBS and matured for 48 h as described above. In ELISPOT assay wells, $1x10^4$ mDCs were incubated in AIM-V medium with $2x10^5$ autologous T cells for 40 h at 37°C/5% CO_2.

Table 17: Material used for IFN-γ ELISPOT assay

Material/Devices	Description / Provider
3-Amino-9-ethyl-carbazole (AEC) tablets	Sigma-Aldrich, Steinheim, D
Axioplan 2 microscope (ELISPOT reader)	equipped with imaging system and software KS ELISPOT 4.9; Carl Zeiss, Jena, D)
Acetate buffer	615.8 mL H_2O + 1,8 g Na acetate + 9.2 mL acetic acid (99%)
Anti-human Interferon-γ mAB 1-DIK (Capture Ab)	Mabtech AB, Nacka, S
Anti-human Interferon-γ mAB 7-B6-1-Biotin (Detection Ab)	Mabtech AB, Nacka, S
Bovine serum albumin (BSA)	Carl Roth, Karlsruhe, D
Buffer for secondary mAb	PBS, 0.5% BSA
Ethanol >99,8%	Carl Roth, Karlsruhe, D
H_2O_2 30% (w/w) solution	Sigma-Aldrich, Steinheim, D
MultiScreen HTS Filter Plates	Millipore, Eschborn, D
Natrium acetate	Sigma-Aldrich, Steinheim, D
N,N-Dimethylformamide (DMF)	Sigma-Aldrich, Steinheim, D
PBS (without Ca^{2+} and Mg^{2+})	PBS Powder (9.55 g/l), Biochrom, Berlin, D
Tween 20	AppliChem, Darmstadt, D
Vectastain ABC-Kit (reagents A + B)	Vector Laboratories, Burlingame, USA
Wash buffer	PBS, 0.05% Tween 20

3.9.2 T Lymphocytes

3.9.2.1 Recognition of target cells (by IFN-γ ELISPOT assays)

IFN-γ ELISPOT assays were performed as described above. T cell lines were incubated with NP concentrations from 25 to 500 µg/mL for 16 h on day 2 after antigen-specific re-stimulation. After removal of excessive particles, NP-loaded T cells were used as effector cells in IFN-γ ELISPOT assays, while unlabeled T cells served as controls. T cells were seeded at 0.1–2x10^4/well and target cells at 5x10^4/well in AIM-V medium supplemented with 5% human serum in ELISPOT plates in a total volume of 200 µl. ELISPOT plate was incubated for 20 h at 37°C/5% CO_2.

3.9.2.2 Specific lysis of target cells (by ^{51}Chromium release assays)

^{51}Chromium (^{51}Cr) release assays were performed to evaluate the cytolytic activity of NP-loaded $CD8^+$ T lymphocytes towards a radioactively labeled target cell. When the target cells are recognized and killed, the incorporated radionuclide is released to the medium and can be quantified by gamma-counting. Leukemia- and tumorreactive CTL clones 8F11 (d 42) and MLTC BC-V (d 56) were incubated with NP concentrations from 25 to 500 µg/mL for 16 h as explained above. For functional evaluation by ^{51}Chromium release assays, 1x10^6 target cells were incubated for 1.5–2 h at 37°C with 100 µCi of $Na_2{}^{51}CrO_4$. After washing, labeled target cells were plated at 1–1.5x10^3 per well in conical 96-well plates. T cells were added in duplicates at indicated effector-to-target (E:T) ratios in a total volume of 160 µL. Target cells with medium only or with detergent instead of T cells served as negative (spontaneous release) or positive (maximum release) controls. After 5 h assay incubation at 37°C, plates were centrifuged and 80 µL supernatant was collected and counted in a Wizard 2 Gamma-counter (Perkin Elmer). Percent specific lysis was calculated with the following equation:
% specific lysis = 100 x (experimental release – spontaneous release)/(maximum release – spontaneous release). Data are mean ± SD of duplicates.

Table 18: Material used for ^{51}Chromium release assays

Material/Devices	Provider
AIM-V	Invitrogen, Karlsruhe, D
Cytotox tubes	Greiner, Frickenhausen, D
$Na_2{}^{51}CrO_4$	Amersham Biosciences, Freiburg, D
Triton X	Sigma-Aldrich, Steinheim, D
Wizard 2 gamma counter	Perkin Elmer, Rodgau, D

3.10 Optimizing NP incorporation and duration of labeling

The material and laboratory equipment that was used for optimizing NP incorporation and duration of labeling in T lymphocytes is listed in Table 19.

Table 19: Material and laboratory equipment for optimizing NP incorporation and duration of labeling in T lymphocytes

Material/Devices	Provider
AIM-V	Invitrogen, Karlsruhe, D
Cell sorter	BD FACS Aria, Becton Dickinson Biosciences, Heidelberg, D
Chloroquine	Sigma-Aldrich, Steinheim, D
Electroporation cuvettes 4 mm	peqLab, Erlangen, D
Ethylendiamine-tetra-acetic acid (EDTA)	Sigma-Aldrich, Steinheim, D
Gene Pulser Xcell™ electroporator	Bio-Rad Hercules, CA, USA
H_2O	Braun, Melsungen, D
Influenza A (H3N2) whole virus vaccine	Baxter, Wien, A
Lipofectamine 2000	Invitrogen, Karlsruhe, D
OptiMEM medium	Invitrogen, Karlsruhe, D
Protamine sulfate	Sigma-Aldrich, Steinheim, D
PULSIn™	PolyPlus Transfection, Illkirch, F
Software	BD FACS Diva, Becton Dickinson Biosciences, Heidelberg, D
Sort buffer	PBS (without $CaCl_2$ / $MgCl_2$), 1% HS, 2 mM EDTA

3.10.1 Transfection agents

3.10.1.1 Protamine sulfate and Lipofectamine

$CD8^+$ T cells were stimulated by allogeneic B-LCLs for 48 h at 37°C. For complex formation with positively charged transfection agents, particles with different surface charges as well as uncharged particles (NP-5-NH_2, NP-7-COOH, NP-7) were preincubated with 1, 3 and 5 µg/mL protamine sulfate or 5, 10 or 20 µg/mL Lipofectamine for 15 min at 37°C. After preincubation, complexes were added to cells for 16 h incubation at 37°C in AIM-V supplemented with 10% HS. Uptake of NP after treatment with transfection agents was verified visually by cLSM.

3.10.1.2 PULSIn™

$CD4^+$ T cells were stimulated by allogeneic B-LCLs for 48 h at 37°C. For complex formation, 4 µL, 20 µL and 40 µL of PULSin™ reagent were preincubated with 75 µg/mL particles at room temperature in a similar way as described in the literature (Delehanty et al. 2010). After pretreatment, NP-PULSin™ complexes were added to cells for an incubation period of 16 h at 37°C in serum free medium. In further experiments, the amount of PULSin™ reagent was reduced to 1 µL, 4µL and 20 µL for minimizing toxicity. Additionally, the incubation period of cells with NP-PULSin™ complexes was shortened to 4 h and 1 h. In these tests, particle-loading and analysis of NP uptake by $CD4^+$ T cells (day 21) was performed on day 3 after re-stimulation. In parallel studies, incorporation of NP-PULSIn™ complexes by T cells was verified by cLSM.

3.10.2 Electroporation

Electroporation was performed for achieving a cytoplasmic delivery of particles via electric field induced membrane pores. For electroporation of allo-reactive T lymphocytes, cells were stimulated by allogeneic B-LCLs for 72 h at 37°C since read out of NP uptake was usually performed on day 3 after re-stimulation. In preliminary experiments with the robust Jurkat T-cell line, $5x10^6$ cells were electroporated in 200 µL OptiMEM medium in the presence of 75 µg/mL particles at different electric puls conditions (500 V, 5 ms duration; 350 V, 12 ms; 350 V, 5 ms; 50 V, 5 ms; and 5 pulses â 50 V, 5 ms with 100 ms intervals between single pulses). Immediately after electroporation, cells were transferred into 2 mL of prewarmed OptiMEM medium for a 30 min regeneration phase at 37°C. After regeneration, excess particles were removed by centrifugation and cells prepared for flow cytometric analysis of NP incorporation and viability. Alternatively, 75 µg/mL NP were loaded to cells by incubation as described above and also analyzed for NP uptake and viability. Subsequent electroporation experiments were performed with Jurkat and allo-reactive T cells in order to optimize protocol parameters like particle concentration during electroporation or the cultivation temperature during the regeneration phase of electroporated cells. For investigating the influence of the cell number in the cuvette, 1, 2.5 or $5x10^6$ $CD8^+$ T cells were resuspended in 500 µL pre-cooled (4°C) OptiMEM medium and transferred into cuvettes. Immediately after addition of 750 µg/mL particles, the electroporation pulse was given to the cells (350 V/5 ms) by Gene Pulser Xcell™ electroporator. After application of the electric pulse, electroporated cells were washed out and re-cultured in AIM-V+1% HS at 4°C for at least 30 min allowing the membrane pores to close. Subsequently, excess particles were removed by centrifugation and NP-loaded cells re-cultured in particle free medium for monitoring NP release over three days by flow cytometry. For determining the effectiveness of electroporation, a control was

used but without application of an electroporation pulse to the cuvette containing cells and particles. For analyzing labeled cells by cLSM, NP were loaded to $2.5x10^6$ Jurkat T cells by application of a 350 V/5 ms pulse in the presence of 750 µg/mL NP. Cells that were incubated with 75 µg/mL NP for 16 h at 37°C served as a control.

3.10.3 Selection of strongly labeled cells by cell sorting

$2x10^7$ $CD4^+$ T cells were incubated with particles for 16 h as described above and $4x10^7$ $CD4^+$ T cells were electroporated in the presence of 750 µg/mL NP by application of an electric pulse of 350 V for 5 ms ($5x10^6$ cells/cuvette). After labeling, non-incorporated NP were removed by centrifugation and cells were resuspended in 2 mL sort buffer. To remove cell and particle clumps, cells were then passed through a 30 µM nylon mesh filter (Miltenyi Biotec). Sort buffer was added until a concentration of 10–$20x10^6$ cells per mL was reached. Strongly as well as weakly labeled cells were separated by flow cytometric cell sorting at 4°C under sterile conditions. After sorting, the differently labeled cells were re-cultured in particle free medium for monitoring and comparing NP release over three days.

3.10.4 Chloroquine

$CD4^+$ T cells were stimulated by allogeneic B-LCLs for 72 h at 37°C before NP loading and flow cytometric analysis of NP uptake and cell viability. Based on the literature, cells were incubated with particles for 3 h at 37°C in the presence of 10 µM, 100 µM and 200 µM chloroquine in serum free medium (Muro et al. 2003, Sêe et al. 2009). After the incubation period, excess particles and chloroquine was removed by centrifugation and labeled cells re-cultured in AIM-V medium supplemented with 1% HS for monitoring NP release over three days.

3.10.5 Biocoating of NP with Influenza whole virus

T cells were stimulated by allogeneic B-LCLs for 72 h at 37°C since read out of NP uptake was usually performed on d3 beyond re-stimulation. After preliminary dose finding studies, amino-functionalized NP were preincubated with a 244.5 µg/mL (hemagglutinin protein content) preparation of an inactivated influenza A (H3N2) whole virus vaccine (Baxter, Vienna, Austria) for 0.5 h at 37°C allowing an electrostatic attachment of whole virus on NP surface (1.91 µg whole virus per 75 µg/mL NP). Afterwards, the NP-virus complexes were incubated with $CD4^+$ T lymphocytes or dendritic cells in serum free medium for further 2 h at 37°C. After removal of excessive particles by centrifugation, NP-loaded cells were re-cultured in particle free medium for a long-term follow-up over 3 to 9 days. NP delivery and release

was analyzed by flow cytometry. Incorporation of NP-virus complexes by T cells and DCs was verified by cLSM after co-staining of cell membranes and nuclei as described above.

3.11 Delivery of Cy5-oligonucleotides with biodegradable PBCA nanocapsules

For studying the uptake of poly-butylcyanoacrylate (PBCA) capsules by T lymphocytes, $CD4^+$ T cells were first incubated with 150 µg/mL capsules for 24 h. To investigate the time dependent release of Cy5-labeled oligonucleotides, nanocapsules were incubated with T cells for shorter time periods (1 h – 8 h) as well as for longer periods (24 h – 72 h) in two further experiments. After the incubation period, excess capsules were removed by centrifugation and cells prepared for cLSM. Since an accumulation of those oligonucleotides in the mitochondria has been reported earlier (Baier et al. 2011, Lorenz et al. 2011), costaining of the mitochondria was performed by incubating the cells with 200 nM MitoTracker™ Green FM for 30 min at 37 °C. After washing, cells were transferred in 300 µL AIM-V medium per well into Lab-Tek 8-well chamber slides. Immediately before microscopy, cell membranes were stained with 1.67 µg/mL CellMask™ Orange plasma membrane stain.

4 Results I: Dendritic cells

4.1 Labeling of DCs with nanoparticles

4.1.1 Labeling efficiency of DCs with polystyrene nanoparticles

In a first set of experiments, different pairs of PMI containing polystyrene nanoparticles (NP) without or with functional groups at their surface were analyzed. Copolymerization of monomers with carboxy or amino groups resulted in functionalized nanoparticles with the respective charged groups in a distinct density on their surface. The nanoparticles were characterized for their diameter, which demonstrated to be in the range of 100-150 nm. The amount of encapsulated PMI was determined for normalization (see Materials and Methods). These nanoparticles were investigated for their uptake by human immature dendritic cells (iDCs). For that purpose, iDCs generated over 6 days with IL-4 and GM-CSF from blood monocytes of healthy donors (Figure 5) were incubated over 16 h with 75 µg/mL of the respective particle type.

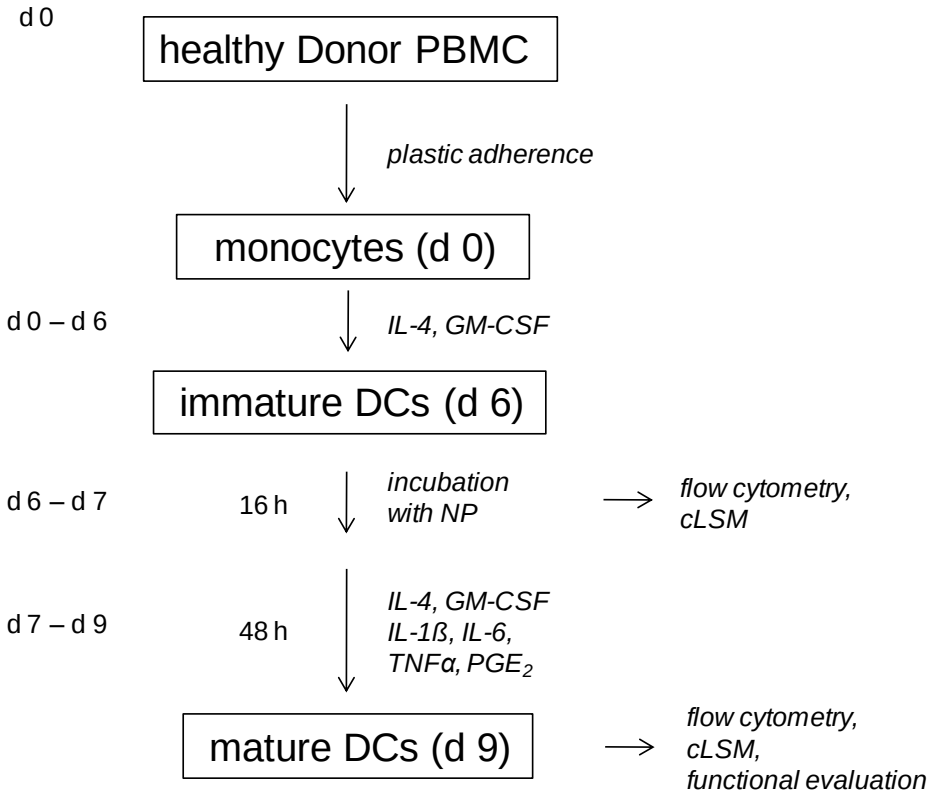

Figure 5: Generation of monocyte-derived dendritic cells and subsequent labeling with polymeric nanoparticles. For cLSM studies as well as long-term follow ups and functional evaluation, NP-loaded iDCs were matured over 48 h by adding the indicated cytokines.

After washing off NP that were not taken up or at least did not adhere firmly, cells were analyzed by flow cytometry for uptake of PMI-containing particles, measurable in channel FL1 on the flow cytometer (excitation with 488 nm laser line, emission filter 530/30 nm). Staining for CD11c was applied for gating on DCs. 7-AAD was used to exclude dead cells and to determine toxic effects. After normalization of median fluorescence intensity (MFI) values - which was necessary due to different PMI contents - data showed that carboxy functionalization did not improve uptake of NP by iDCs (Figure 6A).

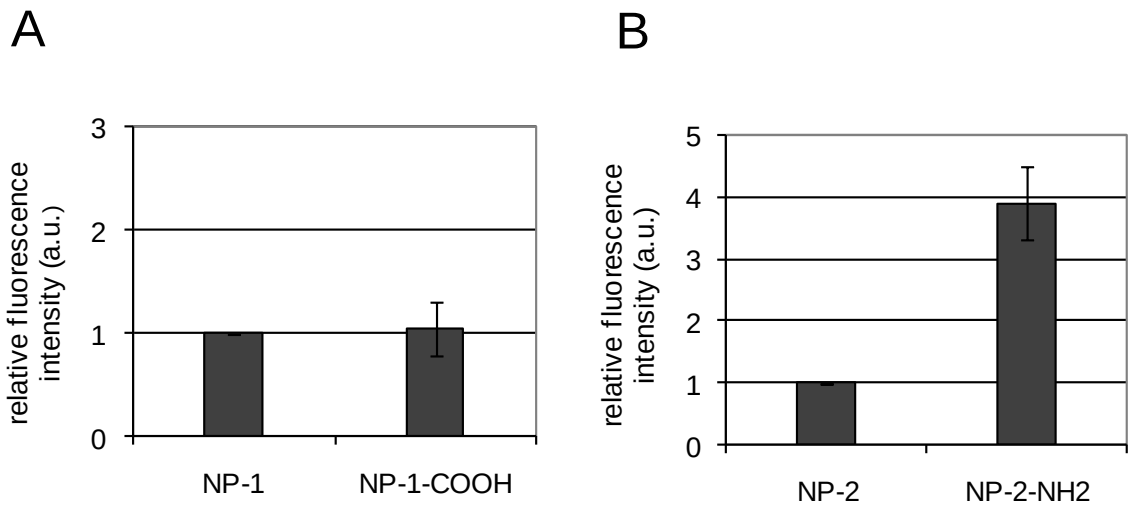

Figure 6: Uptake of unfunctionalized versus functionalized, fluorescent nanoparticles in immature dendritic cells (iDCs). Relative fluorescence intensity is shown in arbitrary units (a.u.). Cells were incubated with particles (conc. 75 µg/mL) for 16 h. Results are expressed as means of three independent experiments with DCs generated from different donors. (A) Uptake of nanoparticles unfunctionalized and functionalized with carboxyl groups (NP-1-COOH). (B) Uptake of the amino-functionalized particles (NP-2-NH_2) versus unfunctionalized particles. Data published in Zupke et al. 2010.

In contrast, amino-functionalized particles were found to be four-fold more effective in labeling iDCs compared to the unfunctionalized counterpart (Figure 6B). This result was consistent in independent experiments with iDCs from three healthy donors. Thus, the amino-functionalized particle NP-2-NH_2 was used in all subsequent experiments with dendritic cells.

4.1.2 Optimization of particle concentration

As a first step in developing an optimal protocol for labeling iDCs with NP-2-NH_2 particles, NP concentration was varied from 0.75 to 150 µg/mL, while all other parameters were kept constant. After 16 h of incubation, viable iDCs were analyzed for fluorescence intensity due to particle uptake. A significant increase in fluorescence intensity was noticeable between 7.5 and 25 µg/mL NP that even rose when higher concentrations of 75 or 150 µg/mL were applied (Figure 7A).

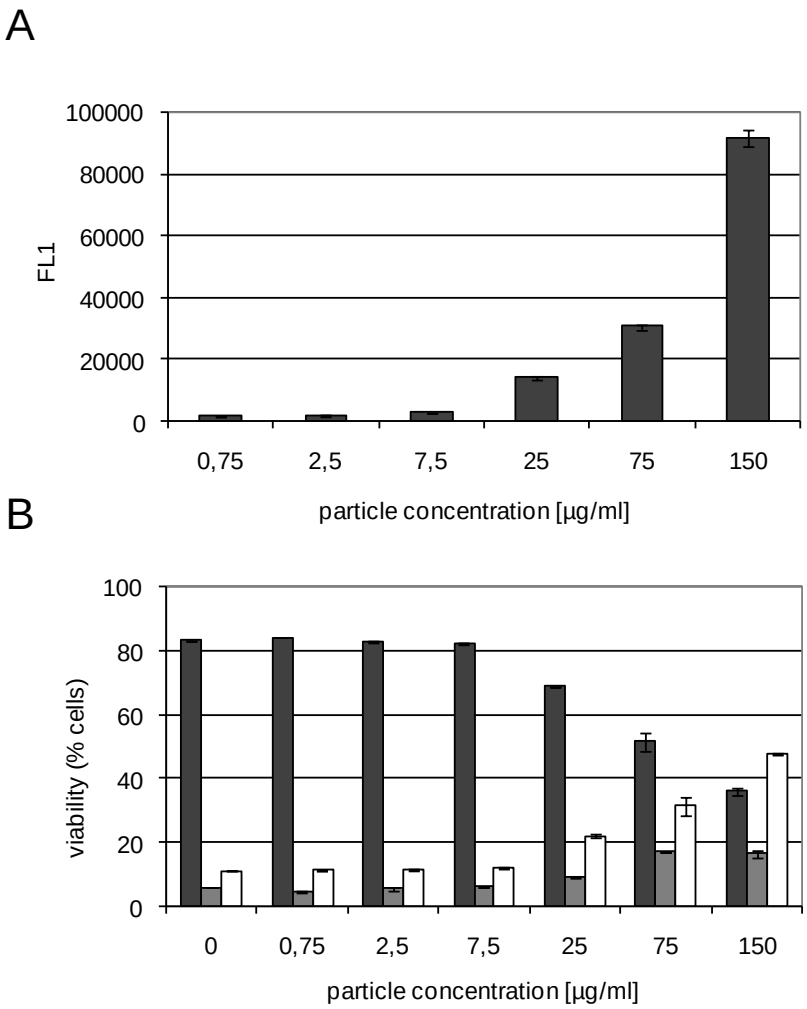

Figure 7: FACS analysis of immature dendritic cells incubated with different concentrations of the amino-functionalized particle NP-2-NH_2 for 16 h. (A) Increasing the concentration of the particle correlates with higher fluorescence intensity of the cells. (B) Toxicity of the particle at different concentrations (dark bars: 7-AAD^{neg}/vital cells, light grey bars: 7-AAD^{low}/dying cells, white bars: 7-AAD^{pos}/dead cells). FL1 is the median fluorescent intensity of PMI fluorochrome contained within DCs. Data published in Zupke et al. 2010.

Since the percentage of dead (7-AAD^{pos}) cells markedly increased with particle concentration higher than 25 µg/mL (Figure 7B), 25 µg/mL was chosen as standard concentration in all further testings. As reproduced in experiments with DCs from three donors, this concentration allowed the determination of a comparably strong fluorescence signal, while cell viability remained in an acceptable range of >70%.

4.1.3 Optimization of particle incubation time

Subsequently the impact of the incubation time of NP-2-NH_2 particles on the uptake by iDCs was analyzed. For these tests, NP concentration was kept constant at 25 µg/mL, as defined in the previous set of experiments. The period of NP incubation was varied between 0.5 and 24 h. Results in 5 different donors revealed saturated particle uptake at an incubation time between 8 and 24 h (Figure 8C), with a reliable cell viability >85% for all time periods

(representative example shown in Figure 8B). Since three of five donors showed highest particle uptake after 16 h of incubation (Figure 8C, representative example shown in Figure 8A), all subsequently performed experiments were done with this incubation period.

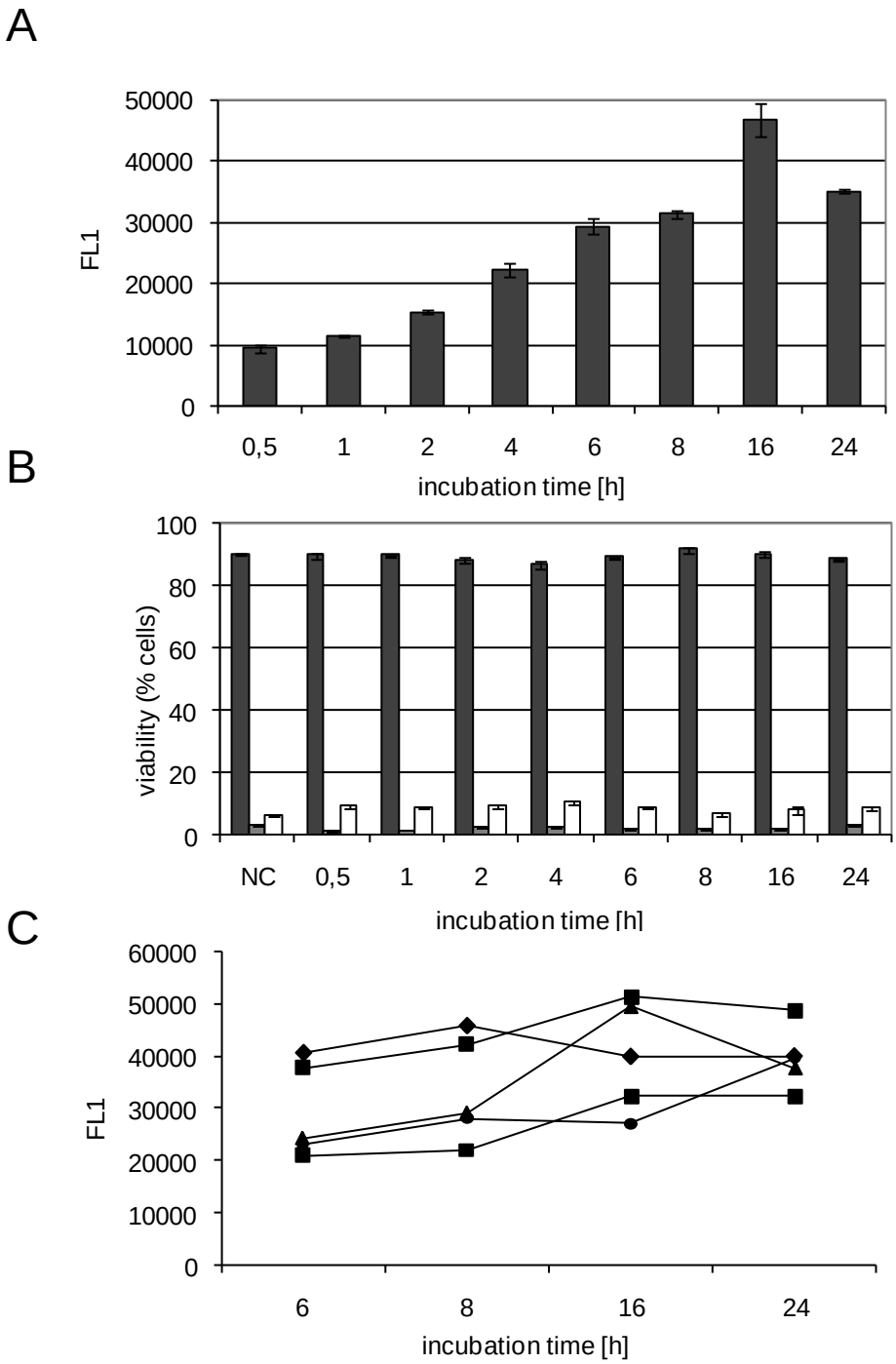

Figure 8: Uptake kinetics as fluorescence intensity of immature dendritic cells after incubation with NP-2-NH_2 for different time periods from 0.5 to 24 h. (A) An incubation time of 16 h leads to the strongest fluorescent intensity. (B) Toxicity of the particle after incubation with cells for different time periods (dark bars: 7-AAD^{neg}/vital cells, light grey bars: 7-AAD^{low}/dying cells, white bars: 7-AAD^{pos}/dead cells). No significant toxicity is detectable. (C) Fluorescence intensity of iDCs from five donors after incubation with fluorescent nanoparticles for different time periods (6, 8, 16, and 24 h). In most cases, an incubation time of 16 h led to strongest fluorescent intensity. There was no significant toxicity detectable (data not shown). FL1 is the median fluorescent intensity of PMI fluorochrome contained within DCs. NC, negative control. Data published in Zupke et al. 2010.

4.1.4 Verification of nanoparticle uptake by confocal laser scanning microscopy (cLSM)

Flow cytometric measurement of cells loaded with fluorescent nanoparticles does not necessarily lead to fluorescent signals exclusively resulting from particles incorporated by cells. It might also be the case that particles are only attached to the cell surface. In order to confirm intracellular localization and to exclude mere attachment of NP at the cell surface, immature and mature DCs loaded with NP-2-NH_2 were analyzed by confocal laser scanning microscopy. As shown in Figure 9A, immature DCs incorporated intermediate to high amounts of green-fluorescent NP-2-NH_2 particles. Some cells also showed particles attached at the surface, observable by the overlap of green (PMI) particle fluorescence and red stained cell membranes, resulting in yellow regions. In contrast, DCs that have been matured after incubation with NP-2-NH_2 particles, showed clear incorporation of NP without any residual attachment at the outer surface (Figure 9B). Besides the incorporation of the nanoparticles, also the dendrites as characteristic signs of mature DCs could be detected in Figure 9B. Based on these cLSM results, it was confirmed that fluorescent signals measured by flow cytometry on mature DCs can definitively be attributed to incorporated NP.

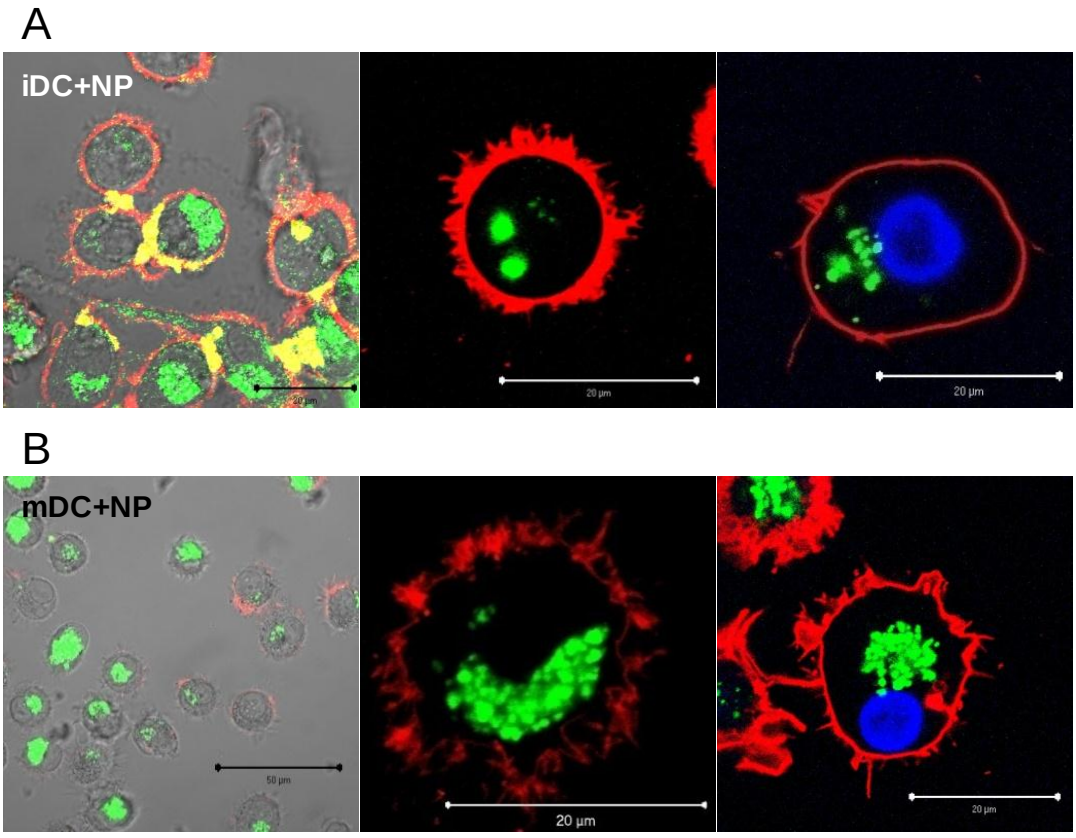

Figure 9: Confocal laser scanning microscopy of DCs after incorporation of NP-2-NH_2. The particles contain PMI as green-fluorescent dye; cell membranes were stained with CellMask Orange (red). In some experiments the nucleus was stained with Hoechst 33342 (blue). (A) Immature dendritic cells. (B) Mature dendritic cells. Representative examples of one donor are shown. Data published in Zupke et al. 2010.

4.1.5 Release of NP by mDCs

One future aim of our study is to use nanoparticle-loaded DCs for *in vivo* trafficking studies. Thus, an efficient and enduring labeling of cells is necessary in order to monitor administered cells over several days. Therefore flow cytometry analyses of mature DCs cultured over a period of 8 days after labeling with NP-2-NH_2 particles were performed. Obtained data revealed that mDCs even after 8 days still contained considerably high amounts of NP; the median fluorescent intensity decreased only to approximately two thirds of the initial value (Figure 10). More than 95% of cells were still positive for the fluorescent marker incorporated into the nanoparticles. This result could be confirmed with DCs from three healthy donors.

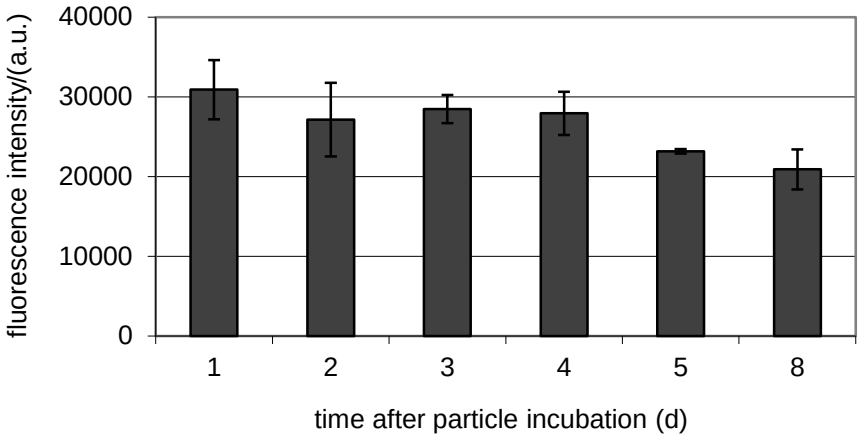

Figure 10: Long-term follow-up over 8 days of mature DCs loaded with PMI-containing amino-functionalized nanoparticles (NP-2-NH_2). After particle incubation (16 h), DCs were matured over 48 h. The fluorescence intensity of incorporated particles was measured on day 1, 2, 3, 4, 5, and 8 after maturation. The graph shows the mean values of mDCs from three different donors. Mature DCs retained particles for at least eight days. No significant toxicity was detectable (data not shown). Data published in Zupke et al. 2010.

4.2 Functional evaluation of NP-loaded DCs

4.2.1 Expression of cell surface molecules on mDCs

Mature dendritic cells can be phenotypically characterized by the expression of several markers for maturation, homing and costimulation molecules, which are indispensable for their function as professional antigen presenting cells. For that reason, it is necessary to analyze if loaded nanoparticles have an influence on the surface expression of these markers. Mature DCs that had been labeled with NP-2-NH_2 particles were analyzed in parallel with unlabeled mDCs of the same donor for the expression of HLA-DR (antigen presentation), CD80, CD86 (costimulation), CD83 (maturation), CCR7 (homing) and CD11c (unknown function). Here, no significant differences in the expression level of any of these

molecules were observed (Figure 11A and B). This observation was made with mDCs derived from three different healthy donors (Figure 11B). Thus, it could be excluded that the incubation of DCs with NP-2-NH_2 particles interferes with mDC phenotype.

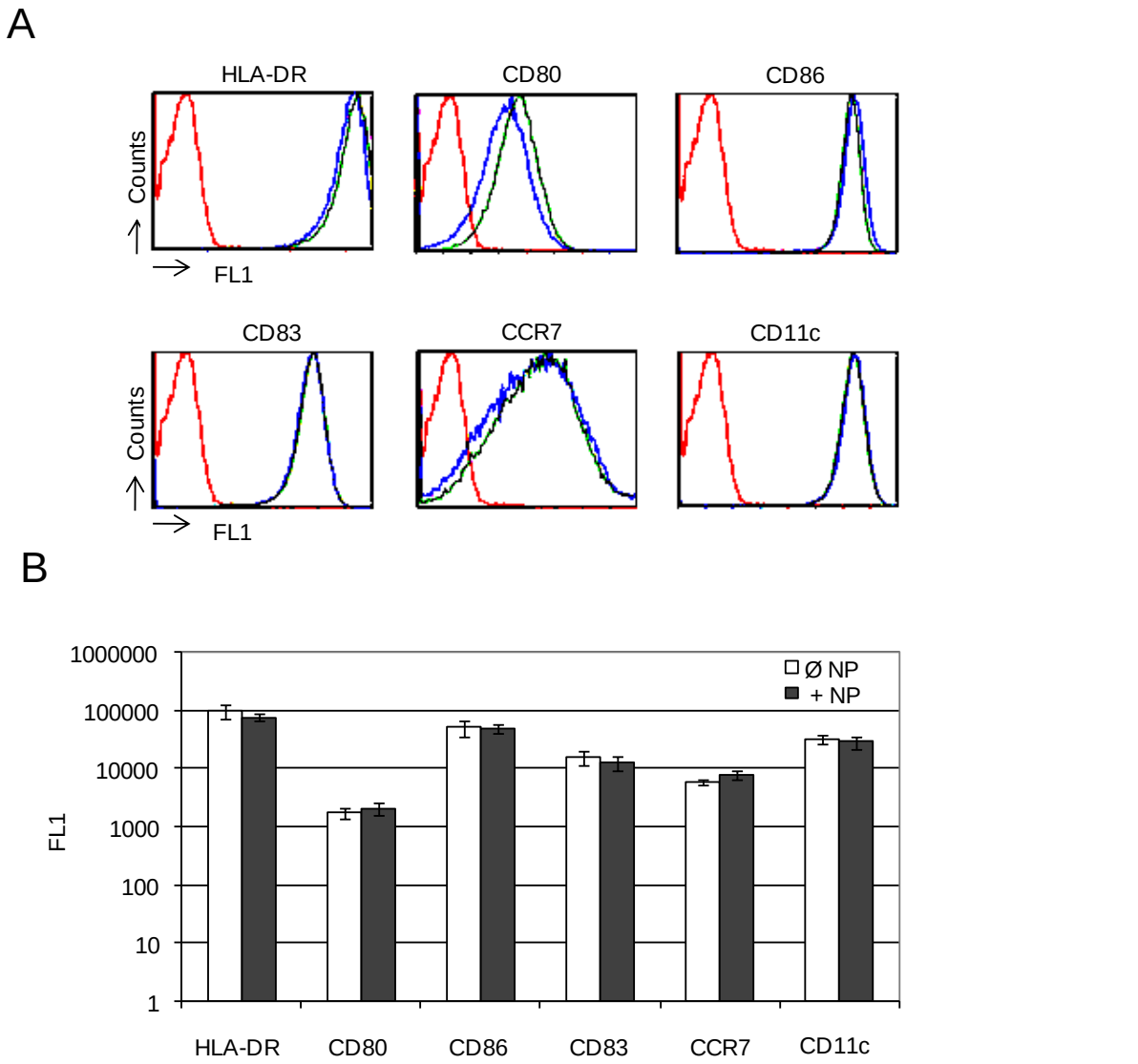

Figure 11: Phenotypical characterization of NP-labeled mDCs. Immature DCs were incubated with amino-functionalized particles (NP-2-NH_2, 25 µg/mL) for 16 h and were afterwards matured for 48 h. Expression of HLA-DR, costimulatory molecules CD80 and CD86, maturation marker CD83, chemokine receptor CCR7, and CD11c as marker for dendritic cells were analyzed by flow cytometry. (A) Representative example of marker expression on mDCs of one donor (blue line: NP-labeled mDCs, green line: unlabeled mDCs, red line: isotype control). (B) Mean MFI values of mDCs from three different donors. Data published in Zupke et al. 2010.

4.2.2 Immunostimulatory capacity of labeled mDCs

Loading of DCs with nanoparticles should not adversely affect their immunological function as antigen presenting cells. To investigate this aspect, ^{3}H-Thymidin proliferation studies were performed using mDCs with or without NP labeling as stimulator cells for immunomagnetically isolated $CD4^{+}$ and $CD8^{+}$ T lymphocytes of a completely human

leucocyte antigen (HLA)-disparate donor. By ^{3}H-Thymidin labeling at day 5 of the assay, it could be observed that T cells stimulated with NP-2-NH_2 labeled, HLA-mismatched DCs demonstrated comparably strong proliferation compared to stimulations with unlabeled DCs (Figure 12). On the basis of this result a possibly negative influence of NP loading on the allo-immunostimulatory capacity of DCs could be excluded.

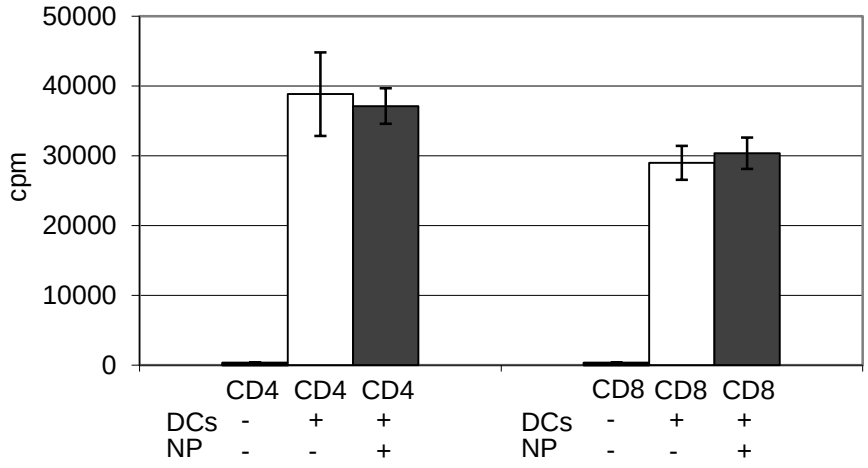

Figure 12: Allogeneic stimulatory capacity of NP-loaded and unlabeled mDCs analyzed in an allo-MLR proliferation assay. 5x10^{3} mDCs were co-cultured with 5x10^{4} CD8^{+} or CD4^{+} HLA class I-mismatched T cells for 5 days. T cell proliferation was measured by ^{3}H-thymidin uptake for the last 18 h of incubation on day 5. Unstimulated T cells as well as NP-labeled and unlabeled mDCs without responder cells served as controls. Data published in Zupke et al. 2010.

4.2.3 Processing and presentation of viral antigens

Functional aspects of NP-loaded DCs were further investigated in IFN-γ ELISPOT assays determining reactivity of T cells stimulated with viral antigens presented by DCs. For that purpose, immature DCs derived from blood monocytes of a cytomegalovirus (CMV)-seropositive donor were first incubated with NP-2-NH_2 particles, before cytokine maturation over 48 h and loading with a peptide mix containing CD4^{+} and CD8^{+} T cell epitopes of CMV. Mature DCs were subsequently used in an IFN-γ ELISPOT assay as targets for immunomagnetically isolated autologous CD8^{+} and CD4^{+} T cells. Loading of DCs with NP did not impair CMV peptide presentation, since IFN-γ spot production by CD4^{+} and CD8^{+} T cells was comparably strong, irrespective of NP loading of the antigen presenting DCs (Figure 13A). To investigate not only the peptide presentation capacity of NP labeled DCs, but in addition their ability to process viral proteins, an inactivated whole virus preparation of an Influenza A H3N2 strain was used as antigen source in further IFN-γ ELISPOT assays. Here, iDCs were incubated with or without NP-2-NH_2 particles and viral preparation, before cytokine maturation over 48 h. Matured DCs were subsequently used as target cells in an ELISPOT assay. Effector cells were CD4^{+} T cells isolated from PBMC of the same donor.

Since we did not observe any noticeable difference in the number of IFN-γ spots produced by T cells stimulated with labeled or unlabeled dendritic cells, it can be concluded that the incorporation of NP-2-NH_2 particles by DCs does not impair their ability for processing viral protein antigens and their presentation via MHC II molecules to $CD4^+$ T cells (Figure 13B).

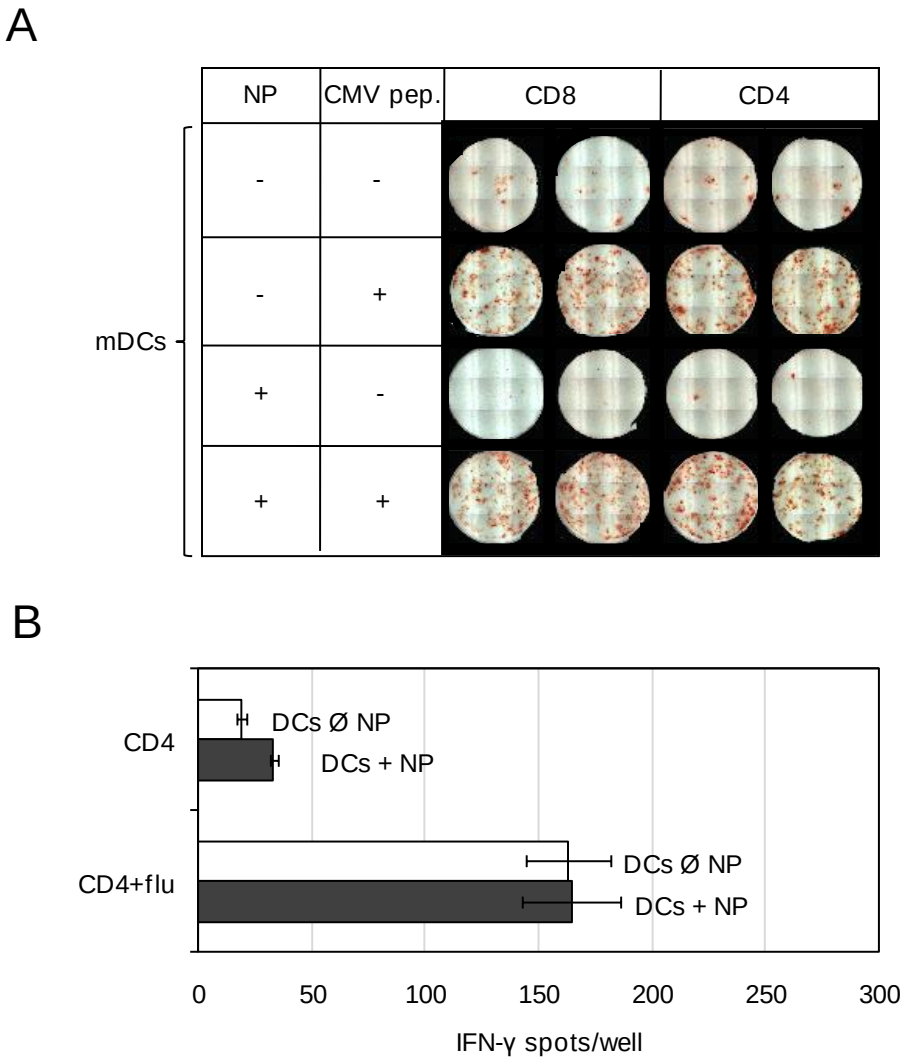

Figure 13: Processing and presentation of viral antigens. (A) For analyzing the antigen presentation capability of NP-loaded mDCs, immature dendritic cells of a CMV-seropositive donor were incubated with NP-2-NH_2 (25 µg/mL) for 16 h and were afterwards matured for 48 h. For IFN-γ ELISPOT assay, mature DCs with or without NP were pulsed with a CMV peptide mix (containing CD4 and CD8 epitopes) and were subsequently incubated with autologous $CD8^+$ and $CD4^+$ T cells, respectively for 24 h. Shown are the original ELISPOT results obtained with 10^4 mDCs incubated with $5x10^4$ effector cells per well. (B) For testing the antigen processing ability of NP-loaded mDCs, immature DCs were incubated with an inactivated whole virus preparation of an influenza A (H3N2 strain) virus, before maturation and use as antigen presenting cells in an IFN-γ ELISPOT assay (10^4 DCs per well). Effector cells were immunomagnetically isolated, autologous $CD4^+$ T cells ($2x10^5$/well). Data published in Zupke et al. 2010.

5 Results II: T lymphocytes

5.1 Loading of T cells with nanoparticles

5.1.1 Labeling efficiency of T cells with polystyrene nanoparticles

After developing a protocol for efficient labeling of human monocyte-derived DCs with amino-functionalized nanoparticles, we adapted this technique to human T lymphocytes. Allo-reactive T cell populations were used as the preferred model system to investigate the labeling of human T lymphocytes with NP. Primary $CD4^+$ and $CD8^+$ T cell lines were generated by mixed lymphocyte reaction (MLR) as shown in Figure 14. First, $CD4^+$ and $CD8^+$ T lymphocytes were immunomagnetically selected from PBMC of healthy blood donors. T cells were then stimulated with allogeneic, HLA-disparate, irradiated EBV-transformed B lymphoblastoid cell lines (B-LCL). The particle loading was performed by incubation with the cells at a defined time point during the weekly re-stimulation cycle (see below). After washing off NP that were not taken up, cells were analyzed for incorporation of PMI-containing particles by flow cytometry and in some experiments verified visually by cLSM/TEM. Alternatively, NP-loaded cells as well as unlabeled controls were used for functional evaluation.

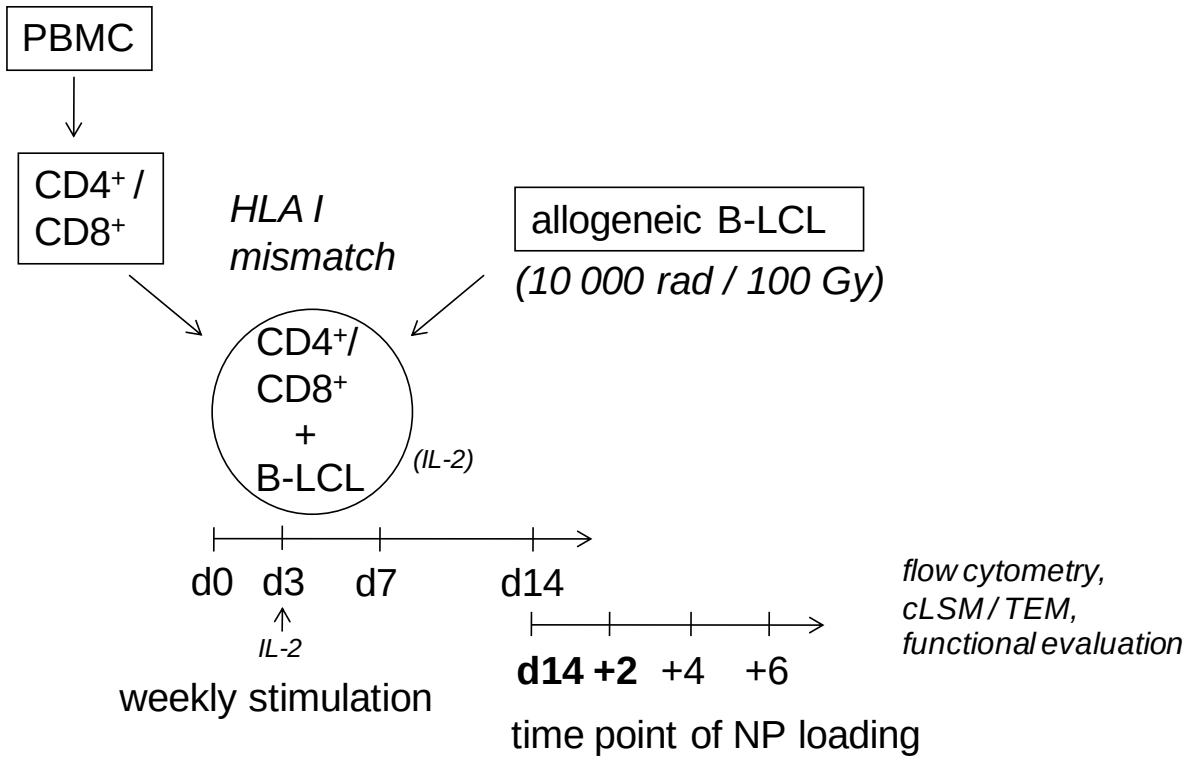

Figure 14: Generation of allo-HLA-reactive T lymphocytes and loading of the cells with polymeric nanoparticles.

Preliminary NP uptake studies with immortalized Jurkat T cells, used as a first model system for human T lymphocytes revealed that T cells demonstrate a considerably lower labeling efficiency compared to dendritic cells (Table 20).

Table 20: Overview of median fluorescence intensity (MFI) of DCs and Jurkat T cells after loading with different particles (conc.: 75 µg/mL, 16 h) as determined by flow cytometry.

Particle	Original name	MFI_{DC}	MFI_{Jurkat}	Proportion of MFI_{DC} (%)	Norm. Jurkat
NP-1	DB010-PS-(AA)g	5212	3862	74	(1)
NP-1-COOH	DB-010-PS-AA d	8585	3183	37	0.45
NP-2	DB011-PS-(AEMH) f	5966	5723	96	(1)
NP-2-NH_2	DB011-PS-AEMH c	32887	8390	26	1.09
NP-3	GB-PS-6	4205	2322	55	(1)
NP-3-COOH	GB-PS-8 AA	4530	2476	55	1.17
NP-3-NH_2	GB-PS-10 AEMH	3986	3563	89	1.57
NP-4-COOH	GB-PS-24 AA	4262	2231	52	1.06
NP-4-NH_2	GB-PS-26 AEMH	4451	4103	92	1.81

Norm.: Normalized data since particles contain different amounts of PMI (uptake of unfunctional NP were set to 1; reference particle for functionalized NP-4 was NP-3). MFIs are averages from at least two replicates. Uptake of NP pairs by DCs and Jurkat T cells was measured in different independent experiments.

Since incorporation of nanoparticles that were previously used for labeling of DCs was lower for T lymphocytes and furthermore, moderate fluorescence intensity could be attributed to extracellular attached NP, additional particles had to be tested for an effective uptake by Jurkat as well as allo-reactive T cells (NP-5 to NP-10, see Table 10). Flow cytometry screening using a broad panel of newly designed fluorochrome-containing NP formats (i.e. different surface functionalizations, detergents, diameters) showed that amino-functionalized polystyrene particles were taken up more efficiently by allo-reactive $CD4^+$ T lymphocytes than their carboxy-functionalized or unfunctionalized counterparts (Figure 15A, B) even if incorporation was only slightly improved. Another important factor for NP uptake into T cells was the surfactant used for synthesis that can be still present in small quantities on NP surface. Particles synthesized with CTMA chloride turned out to be more efficiently taken up than those which were produced in the presence of SDS or Lutensol. Slight differences in NP size played only a minor role in NP uptake. Thus, the amino-functionalized particle NP-9-NH_2 (507 NH_2 groups/particle, 65 nm in diameter, CTMA chloride as detergent) was chosen as a standard NP for all subsequent experiments if not noted otherwise. Because the labeling efficiency of T cells was initially lower compared to that of previously used dendritic cells, the loading protocol had to be adapted to the different conditions with T lymphocytes.

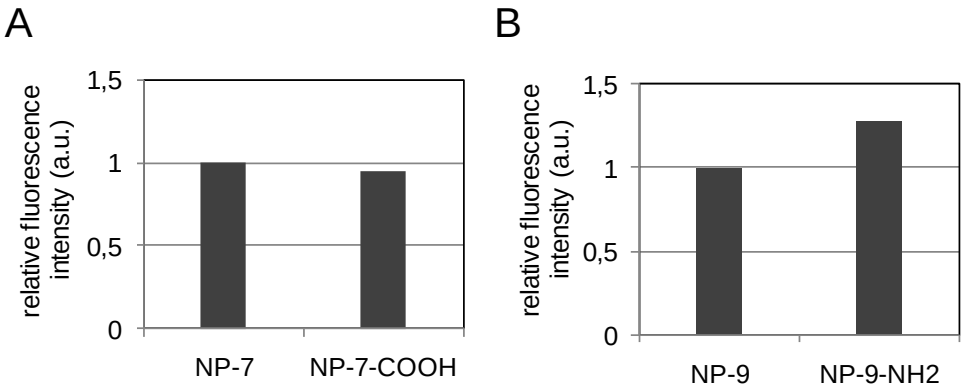

Figure 15: Uptake of unfunctionalized versus functionalized, fluorescent nanoparticles by CD4$^+$ T cells. Relative fluorescence intensity is shown in arbitrary units (a.u.). Cells were incubated with particles (conc. 75 µg/mL) for 16 h on day 2 after re-stimulation. (A) Uptake of nanoparticles unfunctionalized and functionalized with carboxyl groups (NP-7-COOH). (B) Uptake of the amino-functionalized particles (NP-9-NH_2) versus unfunctionalized particles.

5.1.2 Time point of NP loading during T cell re-stimulation cycle

As a first parameter, the day of NP pulse was changed during the antigen-specific re-stimulation cycle using the most suited particle NP-9-NH_2. Strongest NP uptake into allo-reactive CD4$^+$ and CD8$^+$ T cell lines was regularly observed on day 2 (compared to day 4 or day 6) after re-stimulation (Figure 16A). This finding was confirmed in the leukemia-reactive CTL clones 2A7 and 5B2 (Figure 16B).

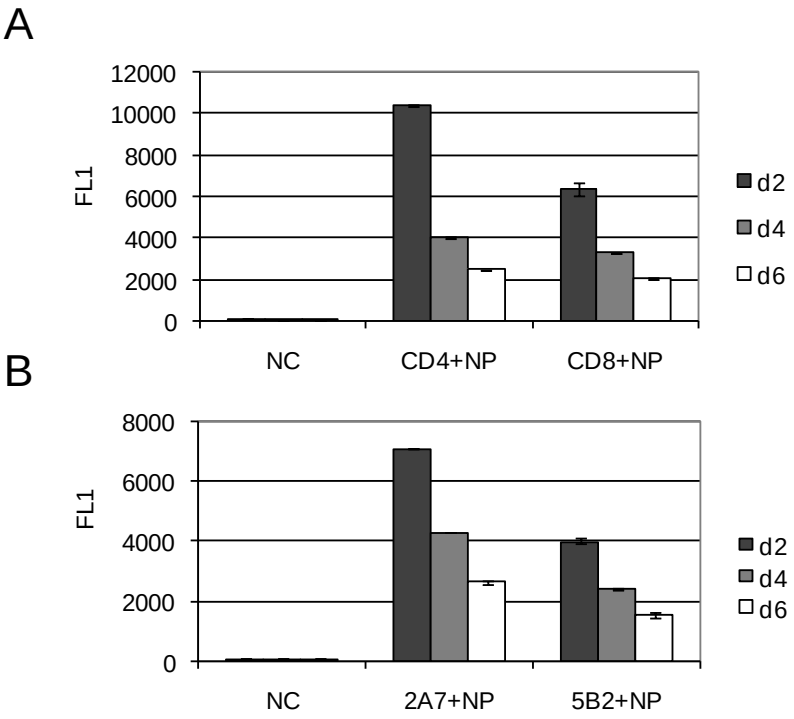

Figure 16: Optimal time point of NP loading during T cell re-stimulation cycle. (A, B) Allo-reactive CD4$^+$ and CD8$^+$ T cell lines (A; cultured for 21 d) as well as leukemia-reactive CD8$^+$ CTL clones 2A7 and 5B2 (B; cultured for 77 d and 42 d) were incubated with 500 µg/mL NP-9-NH_2 at d2, d4 or d6 after antigen-specific re-stimulation. FL1 is the median fluorescent intensity of PMI fluorochrome contained within T cells. NC, negative control (without NP).

Addition of NP on the day of re-stimulation (d 0) resulted in weak incorporation, similar to that obtained on d 6 after re-stimulation (data not shown). Since the second day after antigen-specific re-stimulation led to the highest NP uptake compared to other time points, subsequent tests were performed with particle loading to allo-reactive $CD4^+$ and $CD8^+$ T cell lines starting on day 2 after re-stimulation.

5.1.3 Influence of cell culture age on NP uptake capacity

For investigating the influence of cell culture age on NP uptake, $CD4^+$ and $CD8^+$ T cell lines were cultivated over two to four weeks with NP loading on the respective day 2 after antigen specific re-stimulation. Based on results obtained with cells from three different donors, it could be assumed that early cultured T cell lines (i.e. d 14+2) had an improved capability of taking-up NP compared to later cultures (d 21+2, d 28+2; Figure 17). Furthermore, incorporation of NP was slightly improved in $CD4^+$ T cell cultures versus $CD8^+$ counterparts. Therefore, d 14+2 was chosen as a standard condition for loading NP-9-NH_2 into allo-reactive $CD4^+$ or $CD8^+$ T cell populations, respectively (if not noted otherwise).

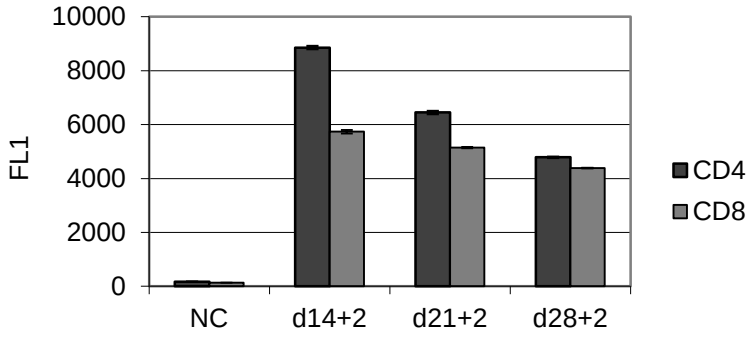

Figure 17: Influence of T cell culture age on particle uptake capacity. $CD4^+$ and $CD8^+$ T cell lines were incubated with NP after d14+2, d21+2, and d28+2 of culture. In all these experiments, T cells were incubated with 500 µg/mL of NP-9-NH_2 over 16 h, then washed and directly measured by flow cytometry for particle incorporation. Data shown are representative examples from one of three donors tested. Data are presented as described in Figure 16.

5.1.4 Optimization of NP concentration

An optimal protocol for labeling T lymphocytes with NP should allow for maximal cellular uptake along with minimal toxic effects. Dose titration experiments with NP-9-NH_2 in the range from 25 to 2400 µg/mL (16 h incubation) showed that a concentration of 500 µg/mL provided considerably high NP uptake without causing adverse effects on cell viability as determined by 7-AAD staining (Figure 18A, B). Although concentrations higher than 500

µg/mL led to even stronger fluorescence signals, they resulted in significant agglomeration of NP and increased cellular cytotoxicity (data not shown). Therefore, 500 µg/mL was used as a maximum concentration suitable for subsequent experiments.

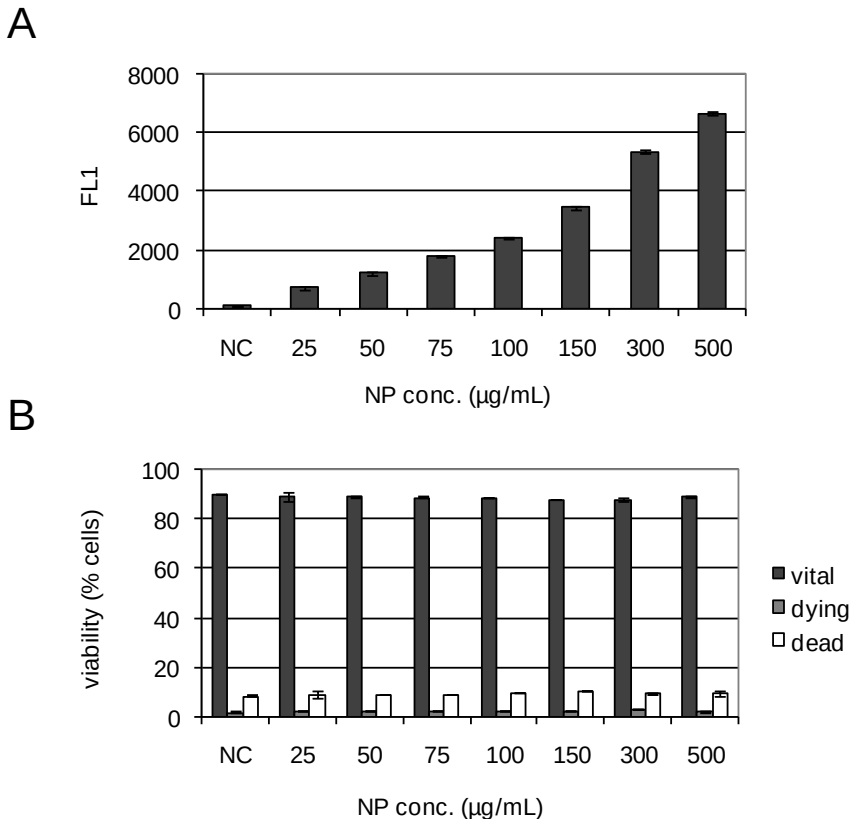

Figure 18: Optimization of NP concentration. $CD8^+$ T cell lines were incubated at day 2 after re-stimulation with varying NP-9-NH_2 concentrations over 16 h. Subsequently, cells were washed and measured by flow cytometry for NP uptake (A). 7-AAD co-stainings were performed to determine the percentage of viable, dying and dead cells, respectively (B). The results are representative for at least two independent experiments. Data are presented as described in Figure 7.

5.1.5 Optimization of incubation time

Subsequently, the impact of incubation time on uptake of NP-9-NH_2 by T cells was analyzed for different periods between 0.5 to 24 h at 37°C. T cells were incubated with 500 µg/mL NP on day 2 after antigen specific re-stimulation. As shown in Figure 19, maximum NP uptake was obtained after an incubation period of 16 h with a reasonable cell viability of 90% (data not shown). Since $CD4^+$ and $CD8^+$ T cell lines showed highest uptake after 16 h of incubation, subsequently performed experiments were done with this incubation period (if not mentioned otherwise).

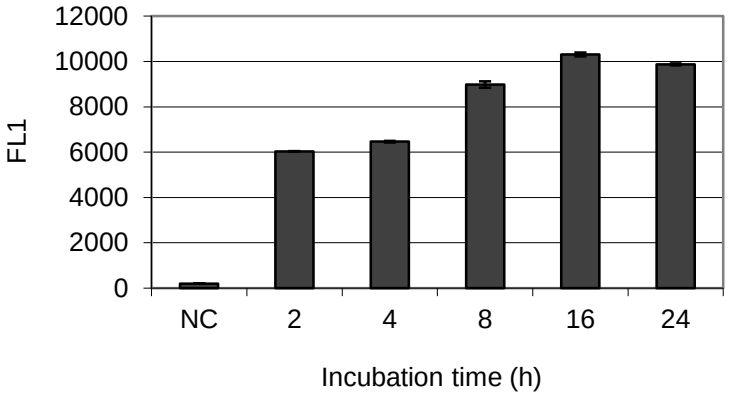

Figure 19: Optimization of incubation time. $CD4^+$ T cell lines were incubated for different time periods with 500 µg/mL NP-9-NH_2. After washing, the amount of incorporated NP was measured by flow cytometry. Results were very similar in a further experiment using $CD8^+$ T cell lines**.** Data are presented as described in Figure 16.

5.1.6 Influence of temperature on NP uptake

To analyze the temperature dependence of NP uptake, kinetic loading experiments were performed at 37°C and 4°C (Figure 20). Uptake level was inhibited by about 50% at 4°C compared to that at 37°C. While this uptake at 4°C remained largely unchanged after additional 12 h, uptake at 37°C continued to increase at 16 h and reached values that were four times higher than that at 4°C. Therefore, T cells were incubated with NP-9-NH_2 for 16 h at 37°C in all subsequent experiments.

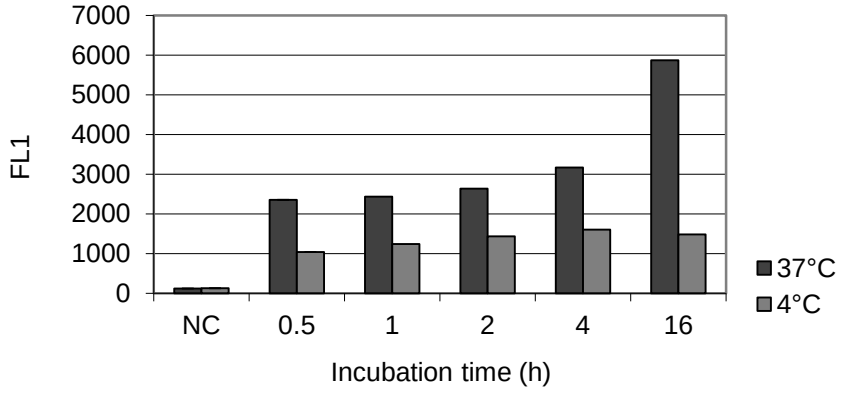

Figure 20: Temperature dependence of NP uptake. $CD4^+$ T cell lines were simultaneously incubated with NP-9-NH_2 for different time periods at 4° and 37°C before analyzing particle uptake by flow cytometry. The results are representative of two independent experiments with $CD4^+$ and $CD8^+$ T cells each. Data are presented as described in Figure 16.

5.1.7 Influence of human serum on NP uptake

In the next step, human serum usually added to T cell culture media as an essential supplement was investigated for its influence on NP uptake. Thus $CD4^+$ T cell lines cultured in medium containing 0 to 10% human serum were incubated for 16 h with NP-9-NH_2. After washing, the amount of incorporated particles was measured by flow cytometry. Figure 21A shows that NP uptake gradually decreased with rising serum concentrations. Maximal inhibition of about 70% was observed in the presence of 10% serum. Thus it can be concluded that human serum is a strong inhibitory factor for NP uptake although it is essential to maintain high T cell viability as determined by 7-AAD staining (Figure 21B). Therefore, a serum concentration of 1% was chosen during NP labeling in all subsequent experiments, because it allowed reliable NP uptake without significant loss of T cell viability. Additionally, the inhibitory influence of serum on NP uptake was observed to a similar extent by using four more NP with different modes of functionalizations (NP-9-NH_2 counterparts, not shown).

Further add-back experiments with titrated concentrations of human albumin and immunoglobulins excluded that these major serum components were responsible for the inhibitory effect (Figure 21C, D).

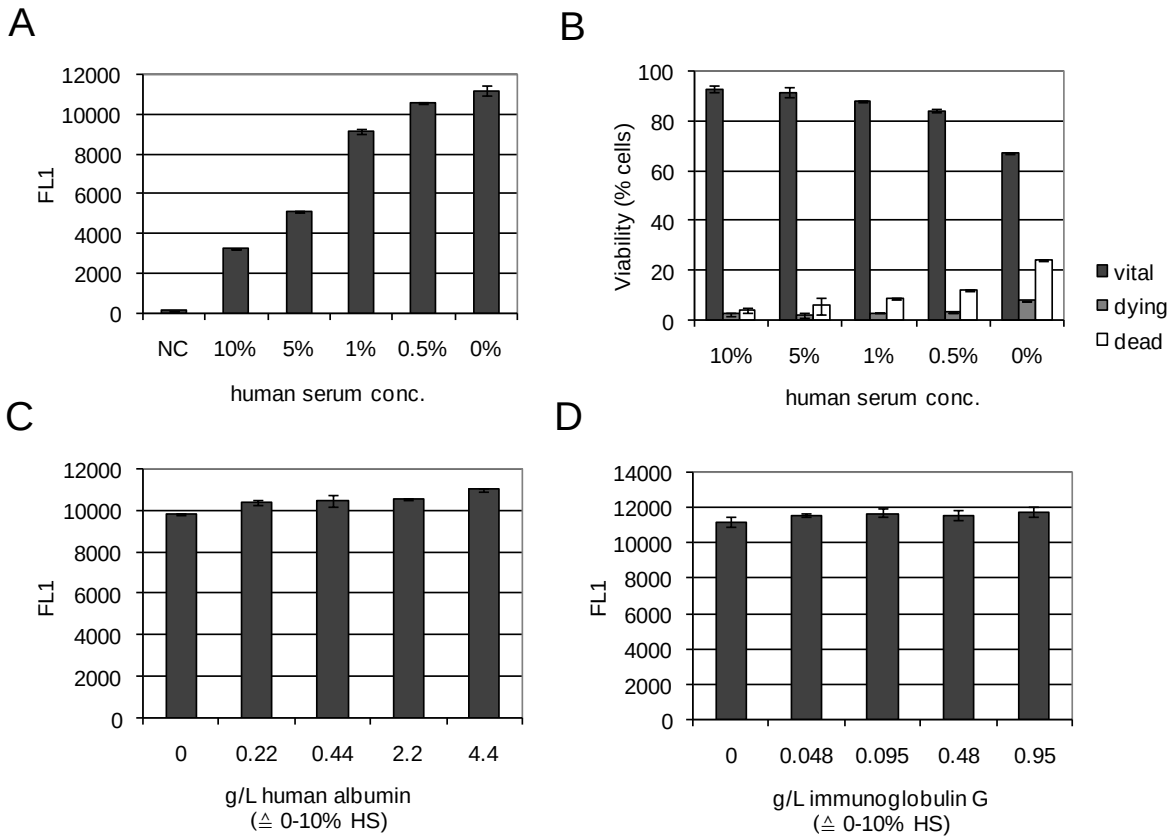

Figure 21: Influence of human serum concentration on NP uptake and T cell viability. $CD4^+$ T cell lines cultured in medium containing indicated percentages of human serum were incubated with NP-9-NH_2 (75 µg/mL) for 16 h. After washing, the amount of incorporated particles was directly measured by flow cytometry (A). 7-AAD stainings were performed to determine the percentage of viable, dying and dead cells (B). Further experiments were performed by using titrated concentrations of human albumin (C) and immunoglobulin G (D). The major serum components were added to serum free AIM-V medium in amounts corresponding to 0; 0,5; 1; 5; and 10% human serum, respectively. Data are presented as described in Figure 7.

5.1.8 Verification of NP uptake by cLSM

In order to confirm intracellular localization and to exclude mere attachment of NP at the cell surface, T lymphocytes loaded with NP-9-NH_2 were analyzed by confocal LSM. As shown in Figure 22, T cells incorporated intermediate to high amounts of green-fluorescent NP in the region between the nucleus and the cell membrane. Residual NP attachment at the outer cell surface was not observed. Therefore, it was confirmed that fluorescent signals measured by flow cytometry could definitively be attributed to incorporated NP.

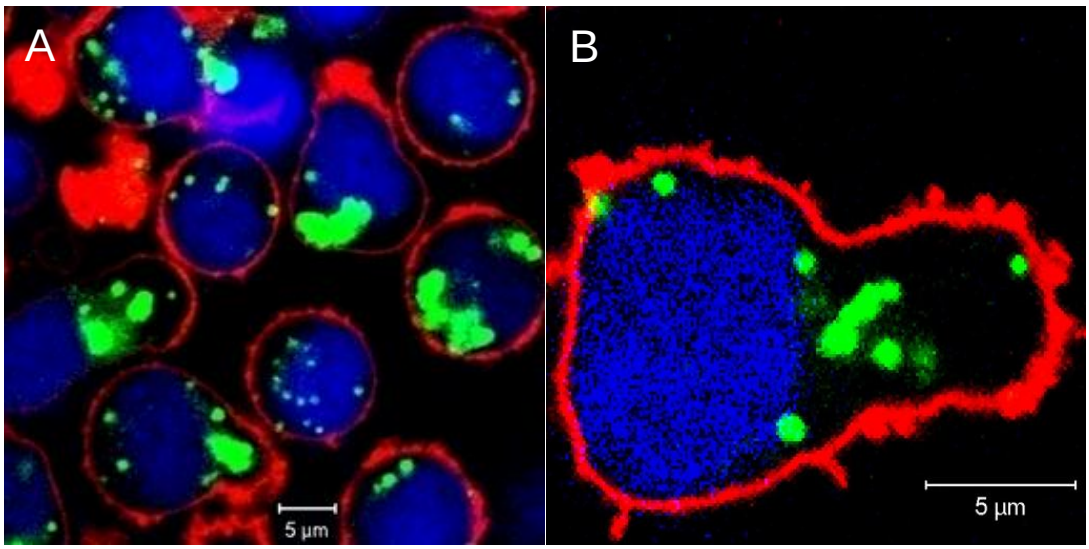

Figure 22: Confirmation of intracellular localization of NP by confocal laser scanning microscopy. $CD4^+$ (A) and $CD8^+$ (B) T cell lines were loaded with 500 µg/mL NP-9-NH_2 over 16 h. The particles contained PMI as green-fluorescent dye. Cell membranes were stained with CellMask™ Orange (red) and nuclei with Hoechst 33342™ (pseudocoloured blue), respectively. Representative examples from one of three donors are shown.

5.2 Functional evaluation of NP-loaded T lymphocytes: Recognition and lysis of target cells

The recognition and subsequent IFN-γ secretion as well as the specific lysis of target cells by antigen-specific T lymphocytes are fundamental prerequisites for an effective T-cell mediated immune response and should not be significantly inhibited by the nanoparticle freight. Functional evaluation of NP-loaded human T lymphocytes was performed using human leukemia-reactive and renal cell carcinoma (RCC)-reactive $CD8^+$ CTL clones as well as allo-reactive $CD4^+$ T cell lines in IFN-γ ELISPOT and chromium (^{51}Cr) cytotoxicity assays. After loading of T cells with different NP-9-NH_2 concentrations from 25 to 500 µg/mL, excess particles were removed by centrifugation and T cells were analyzed for NP uptake before using them in functional assays. As shown in Figure 23 (A, B) for leukemia-reactive $CD8^+$ CTL clone 8F11, specific IFN-γ production and cytolysis upon recognition of leukemia target cells was not significantly impaired at particle concentrations ranging from 25 to 150 µg/mL. However, higher NP concentrations (i.e. 500 µg/mL) clearly reduced antigen-specific IFN-γ production and cytotoxicity. Similar results were obtained with RCC-reactive $CD8^+$ CTL BC-V (Figure 23C, D) and two further leukemia-reactive $CD8^+$ CTL clones (data not shown). In $CD4^+$ T cell lines, strong inhibition of IFN-γ production (about 78%) occurred upon loading with 500 µg/mL NP (Figure 23E), while with NP concentrations up to 150 µg/mL functional impairment was not observed. In summary, these data suggested that loading with amino-functionalized NP-9-NH_2 at low to intermediate concentrations (25-150 µg/mL) does not adversely influence effector functions of T lymphocytes.

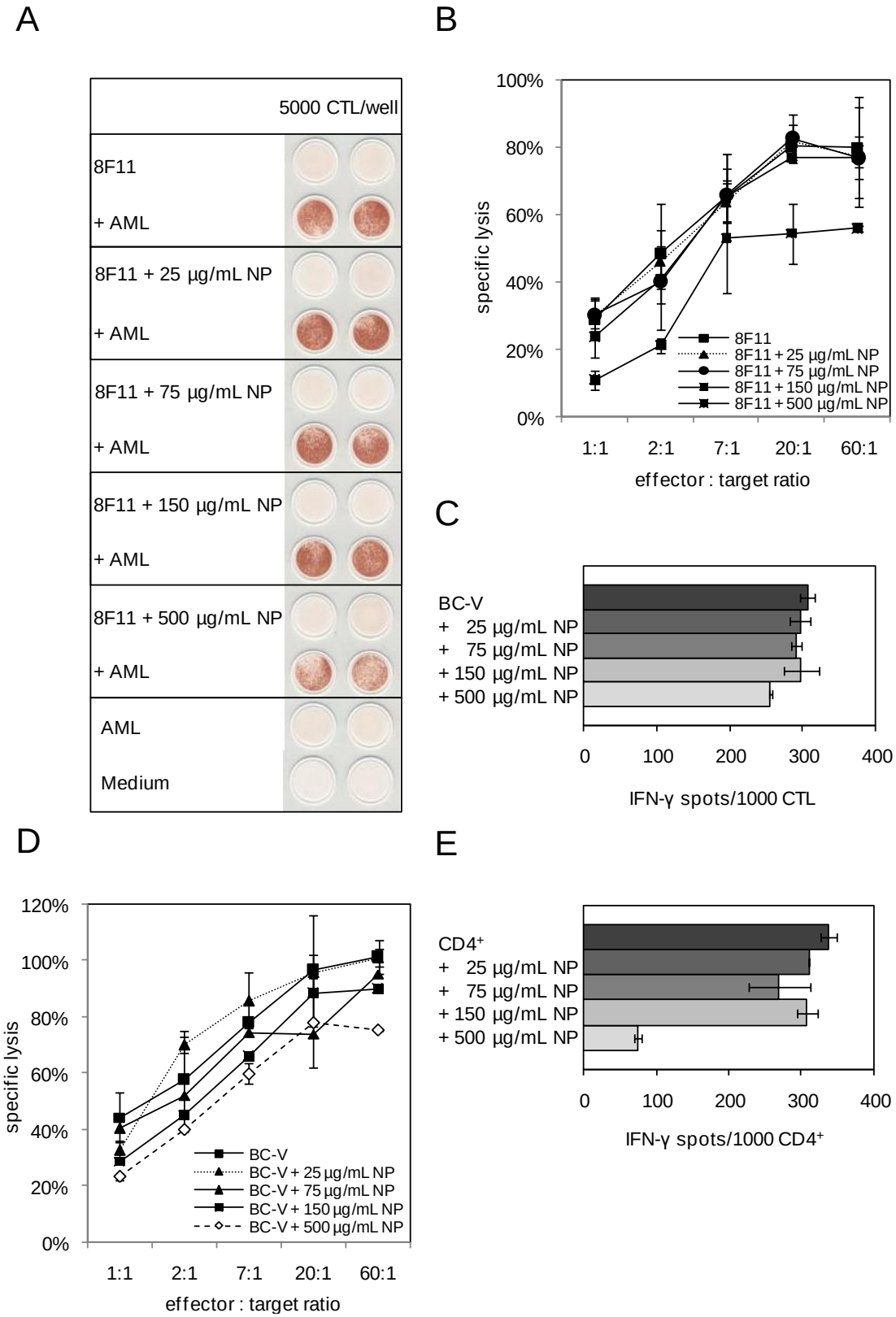

Figure 23: Analyzing effector functions of NP-loaded leukemia- and tumor-reactive CD8$^+$ CTL clones as well as of an allo-reactive CD4$^+$ T cell line. CD8$^+$ CTL clones 8F11 (anti-AML; cultured for 42 d) and BC-V (anti-RCC; cultured for 56 d) and also a CD4$^+$ T cell line (anti-EBV B-LCL, cultured for 14 d) were incubated with NP-9-NH_2 concentration from 25 to 500 µg/mL for 16 h on day 2 upon antigen-specific re-stimulation. After removal of excessive particles, NP-loaded T cells were analyzed for reactivity to target cells in IFN-γ ELISPOT (A, C, E) and ^{51}Cr cytotoxicity (B, D) assays, respectively.

5.3 Uptake mechanism in T cells

5.3.1 Influence of pharmacologic endocytosis inhibitors on NP uptake

To investigate the NP uptake mechanism, $CD4^+$ and $CD8^+$ T cell lines were incubated with NP-9-NH_2 in the presence of different drugs that are known to inhibit distinct components of major endocytic pathways. Inhibition studies were performed in the absence of human serum to prevent a possible interaction of serum proteins with the drugs or nanoparticles during the incubation period. Therefore, cells were seeded in PBS^+ (with $CaCl_2$ and $MgCl_2$), since Ca^{2+} and Mg^{2+} are necessary cofactors for different enzymes that could be potentially involved in NP uptake. In preliminary dose finding studies T cells were incubated with titrated concentrations of individual drugs to determine the maximum non-toxic concentration that could be used in later inhibition experiments (data not shown). Since dead and dying cells may bind particles non-specifically, they were identified in flow cytometry by 7-AAD staining and were excluded from all analyses. As shown in Figure 24 (A, B), treatment of $CD4^+$ T cell lines with chlorpromazine, an inhibitor of clathrin-dependent endocytosis, and also with the dynamin-inhibitor dynasore, during NP loading resulted in a slight dose-dependent diminishing effect with maximum inhibition of 23% and 18%, respectively. In contrast, inhibition of actin-polymerization by cytochalasin D and also of endosomal Na^+/H^+ exchange by EIPA failed to reduce NP incorporation (Figure 24C, D). Similar data were observed when $CD8^+$ T cell lines were treated with endocytosis inhibitors during NP loading (data not shown).

Confocal LSM was regularly used to confirm intracellular localization of NP in the presence of inhibitors. 7-AAD staining applied throughout all analyses revealed a cell viability exceeding 70-80% in all inhibition experiments (data not shown).

Additionally, the effect of Golgi inhibitors Brefeldin A and Monensin was analyzed, but no influence on NP incorporation by $CD4^+$ T cell lines could be observed (data not shown).

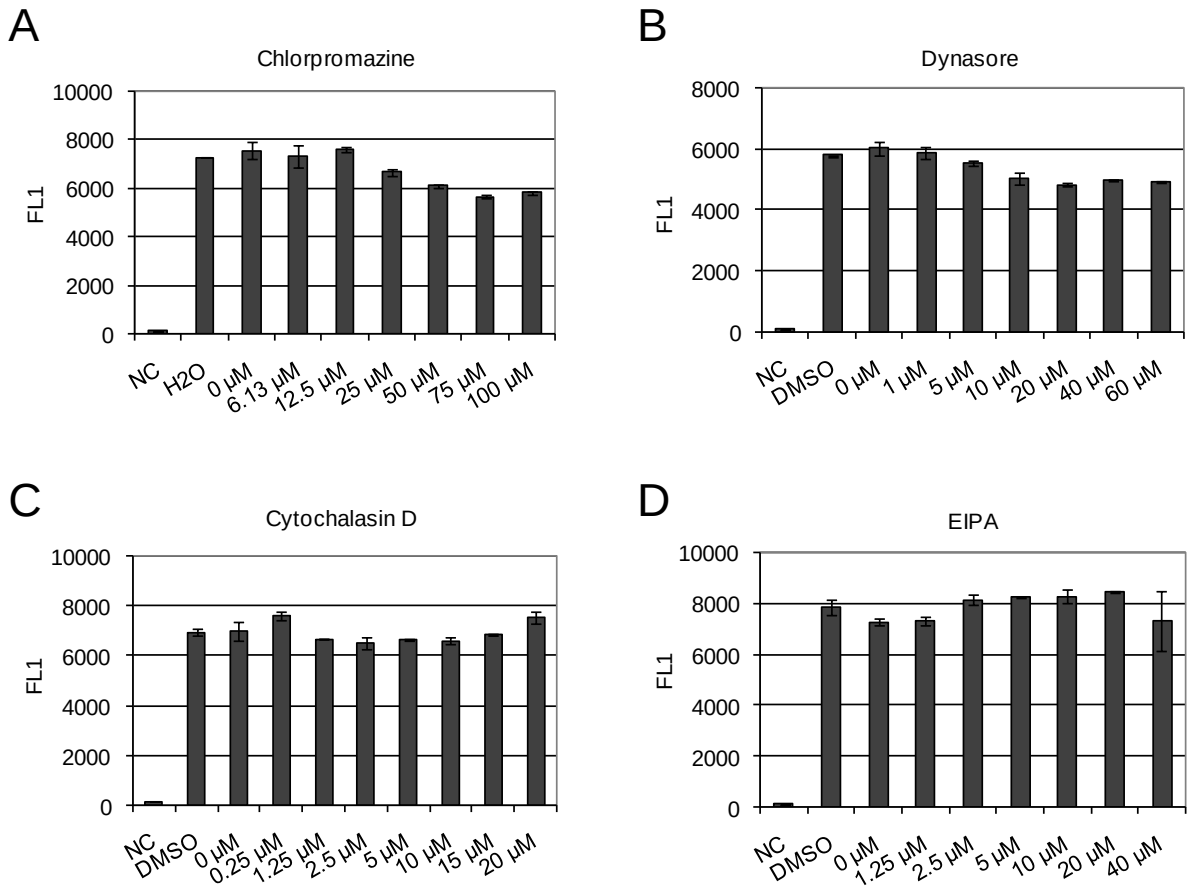

Figure 24: NP uptake by CD4$^+$ T cell lines in the presence of endocytosis inhibitors. T cells were pre-incubated with chlorpromazine (A), dynasore (B), cytochalasin D (C) or EIPA (D) at indicated concentrations for 30 min before NP-9-NH_2 were added and incubated in the presence of inhibitors for another 60 min. After washing the cells, particle incorporation was determined by flow cytometry analysis. Representative data from one out of three donors are shown. H_2O and DMSO mean treatment by drug solvent only (without inhibitor). FL1 is the median fluorescent intensity of PMI fluorochrome contained within T cells. NC, negative control (without NP/inhibitor).

5.3.2 Intracellular localization of NP by TEM

To investigate the precise intracellular localization of amino-functionalized NP, transmission electron microscopy (TEM) was performed after sectioning of labeled T cells and subsequent staining of polymers with ruthenium tetroxide. As shown in Figure 25A, incorporated nanoparticles were found to be localized in membrane-surrounded vesicles in the cytoplasmic region between nucleus and the cell membrane. Figure 25B shows vesicle formation and potential internalization process of NP that appeared to be captured between membrane protrusions of T cells. Additionally, the number of NP-loaded endosomes and particles per endosome rose with increasing NP concentrations from 500 to 2000 µg/mL (not shown).

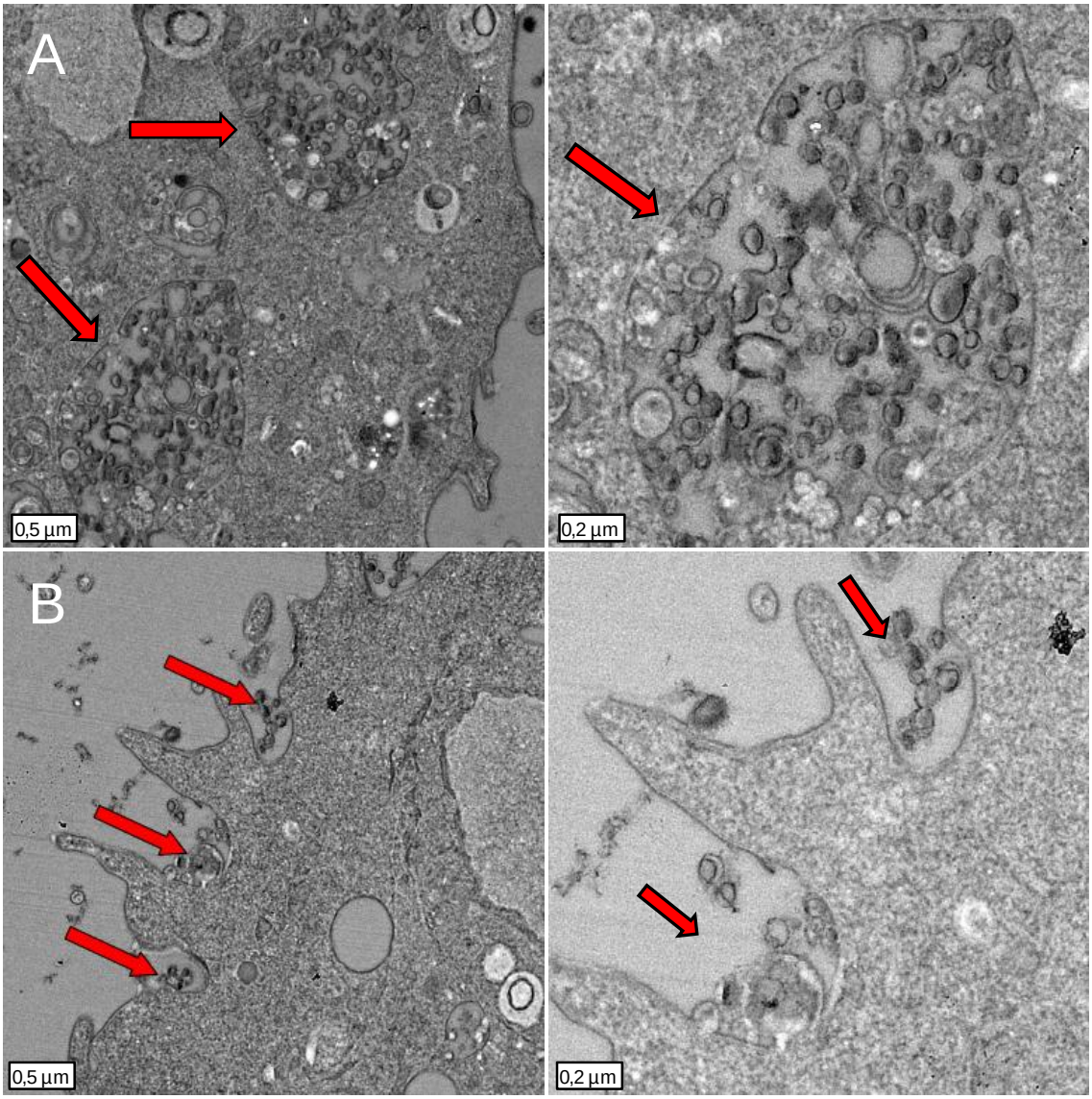

Figure 25: TEM analysis on $CD4^+$ T cells after 16 h incubation with NP-9-NH_2 at 1500 µg/mL to allow for maximal loading of intracellular compartments. (A) Red arrows show particles intracellularly localized in membrane-surrounded vesicles. (B) Vesicle formation and possible internalization scenario for NP. Red arrows show extracellular particles between membrane protrusions of $CD4^+$ T cells.

Because the membrane-surrounded vesicles resembled compartments of the endolysosomal system, co-staining experiments of NP and endolysosomal markers such as EEA1 (early endosome antigen 1), LAMP1 (lysosomal-associated membrane protein 1) and the small GTPases Rab5 and Rab7 were performed in collaboration with Dr. Anna Jürchott. Surprisingly, co-localization between intracellular nanoparticles and any of these endosomal proteins was not found. The GTPase Rab11, described to be involved in endocytic recycling pathways (Ward et al. 2005), could not be detected in T cell lines by a similar staining procedure (data not shown).

5.4 Release of NP by T cells

5.4.1 Long-term follow-up of NP-loaded T cells

The release of NP by $CD4^+$ T lymphocytes was monitored up to five days after labeling with 500 µg/mL for 16 h at 37°C. These data showed that T lymphocytes lost over 90% of incorporated particles during the first 24 h after re-culture in particle free medium supplemented with 10% HS (Figure 26). Already three days after NP loading the fluorescence intensity of labeled cells was almost as low as the background signal caused by auto fluorescence of the cells. Similar results were obtained by using unfunctionalized NP (not shown). In general, T lymphocytes appeared to lose incorporated NP more quickly than DCs.

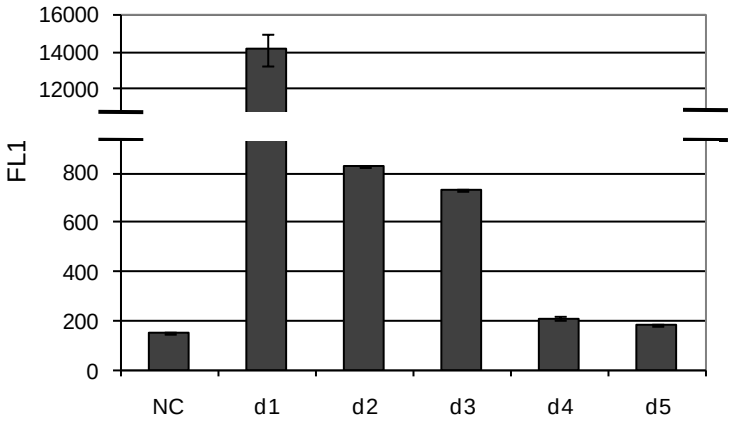

Figure 26: Long-term follow-up of NP-loaded T cells over five days. After 16 h incubation, cells were washed and measured by flow cytometry for NP uptake (value d1). Residual NP-loaded cells were re-cultured in particle free medium for monitoring NP release at indicated time points (values d2-d5). Data are presented as described in Figure 16.

5.4.2 Influence of human serum on NP release

Not only particle uptake, but also particle release was strongly influenced by human serum (Figure 27). In these experiments NP-loaded $CD4^+$ T cell lines (500 µg/mL; 16 h; 1% HS) were re-cultured in particle-free medium that contained titrated amounts of human serum. Intracellular NP content was analyzed after 24 h by flow cytometry. There was a clear inverse correlation between serum concentration and residual NP incorporation. Since 7-AAD staining showed that T cell viability was reduced about 10% at a serum concentration of <1% (not shown), subsequent experiments concerning the release of particles by labeled T cells were performed in the presence of 1% human serum supplement in the medium if not noted otherwise.

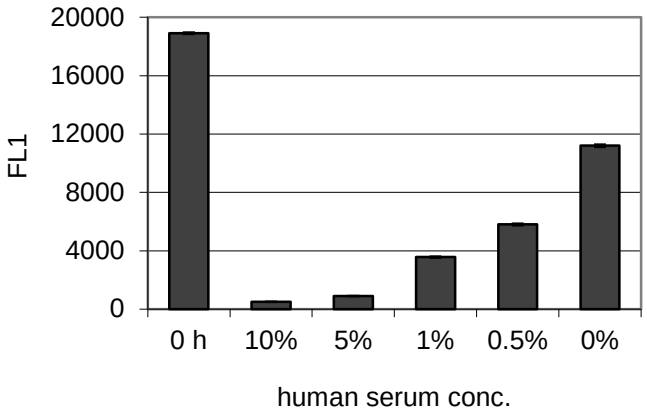

Figure 27: Influence of human serum concentration on NP release. To investigate NP release, $CD4^+$ T cell lines pulsed over 16 h with high NP-9-NH_2 concentration (500 µg/mL) in medium containing 1% human serum were first washed to remove excess particles. After immediate determination of NP incorporation (0 h), labeled T cells were re-cultured in medium supplemented with indicated percentages of human serum for another 24 h and were then analyzed for NP content. The results are representative of at least two independent experiments each. Data are presented as described in Figure 16.

5.4.3 NP release during the first 24 h and influence of cell proliferation

For monitoring NP release within the first 24 h of re-culture, $CD4^+$ T cell lines were pulsed with NP-9-NH_2 (75 µg/mL, 16 h) in the presence of 1% HS. After removal of excess particles, labeled cells were re-cultured in medium supplemented with 1% HS for different time periods at 37°C. Release of NP was stopped by centrifugation and subsequent fixation of the labeled cells with PBS containing 1% PFA and 0.1% BSA since fixation results in a preservation of fluorescence intensity to approximately 100% for at least 24 h (not shown). Subsequently, intracellular NP content was analyzed by flow cytometry (Figure 28). Fluorescence intensity of labeled cells decreased to about 50% already 4 h after re-culture at 37°C. 24 h after NP-

loading fluorescent intensity was only 20-30% of the initial value. Monitoring of cell numbers showed that T cell growth did not exceed a factor of 2 during the first 24 h after NP loading. Additionally, parallel studies at 4°C versus 37°C revealed a considerably faster release of incorporated NP at 37°C with an approximately 30% lower NP content compared to 4°C after re-culturing of labeled cells for 24 h (data not shown).

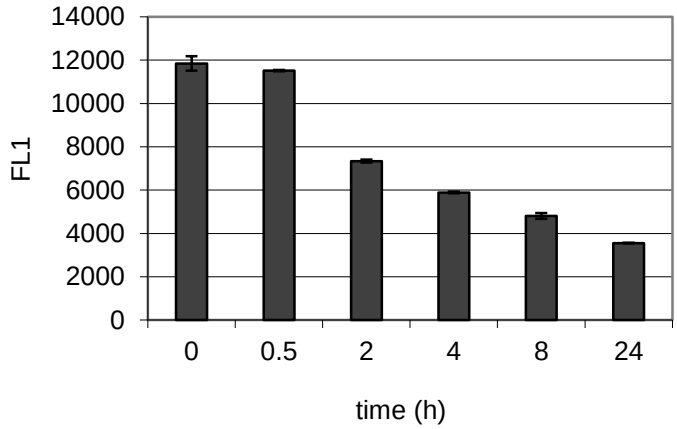

Figure 28: NP release during the first 24 h after re-culture of labeled T cells. For monitoring NP release within the first 24 h, $CD4^+$ T cell lines were loaded with 75 µg/mL NP over 16 h. After removal of excess particles, labeled cells were re-cultured in medium supplemented with 1% HS for different time periods at 37°C. In order to investigate a possible correlation between cellular proliferation and NP release, labeled cells were counted manually after staining of dead cells with Trypan Blue (prior to fixation). The results are representative of two independent experiments each. Data are presented as described in Figure 16.

5.4.4 Influence of adenosine triphosphate binding cassette (ABC)-transporter on NP release

NP uptake and release were studied in $CD4^+$ and $CD8^+$ memory T cells that were sorted from PBMC according to characteristic phenotypic markers (CCR7, CD45RA; Sallusto et al. 2004) by flow cytometry (Figure 29A). Central and effector memory (CM/EM) T cells have been described to express high ABC transporter activity and thus this as well as other pathways relevant for exocytosis of foreign materials are expected to be up-regulated (Turtle et al. 2009). However, there was no significant difference in NP uptake and release in central ($CCR7^+$ $CD45RA^-$) or effector ($CCR7^-$ $CD45RA^-$) memory T cells compared to naïve ($CCR7^+$ $CD45RA^+$) T cells (Figure 29B). Each population showed a decrease of the median fluorescent intensity to approximately 10% of the initial value 24 h after re-culture at 37°C in particle free medium supplemented with 1% HS.

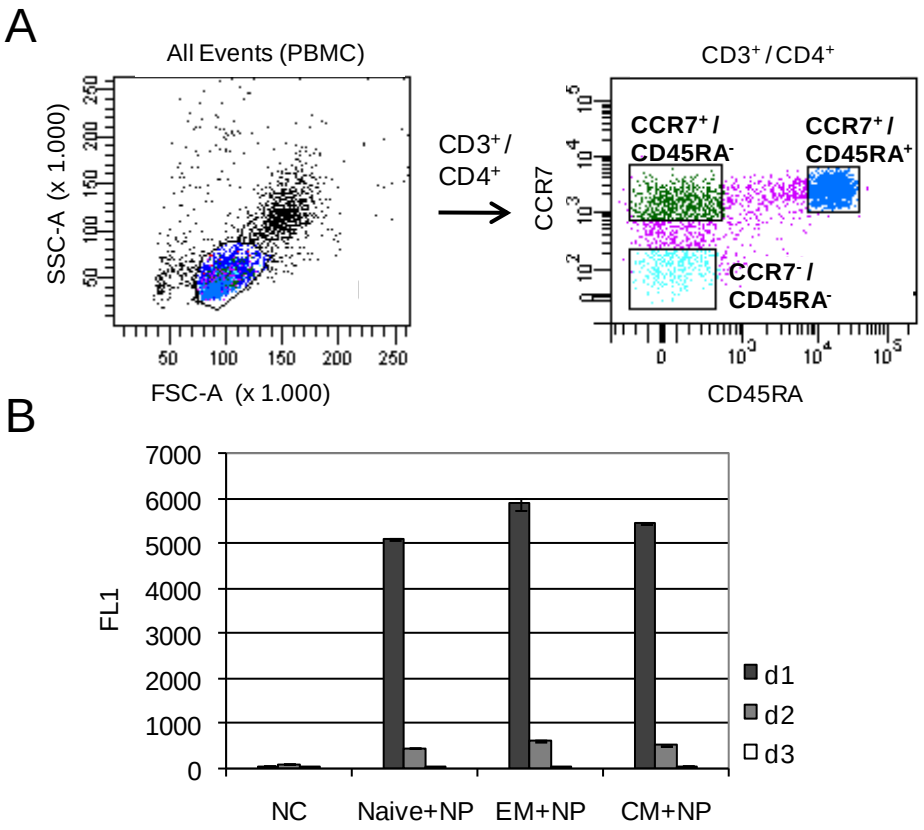

Figure 29: Influence of ABC-transporter activity on NP release. Flow cytometric sorted naive, central memory (CM) and effector memory (EM) $CD4^+$ T cells (A) were stimulated for 72 h using anti-CD3/CD28 beads in AIM-V medium supplemented with 5% HS and 50 U/mL IL-2 before labeling with 75 µg/mL NP-9-NH_2 for 16 h. NP-loaded $CD4^+$ T cells were re-cultured in NP free medium for monitoring NP release. (B) Uptake (value d1) and release (values d2, d3) of NP in T-cell subsets. Results were reproduced with sorted central and effector memory $CD8^+$ T cells. FL1 is the median fluorescent intensity of PMI fluorochrome contained within T cells. NC, negative control (without NP).

5.5 Release of NP by human B cells and murine T cell lines

To investigate if NP release is attributable either to the lymphocytic origin of T cells or to the missing APC function, EBV-B LCLs that combine both features were loaded with 75 µg/mL NP-9-NH_2 for 16 h and subsequently re-cultured in particle free AIM-V medium supplemented with 1% HS (Figure 30A). In contrast to myeloid-derived DCs, NP incorporation and release behavior of antigen presenting but lymphatic-originated B lymphocytes resembled that of T cells resulting in a signal loss of about 80% during the first 24 h after re-culture of labeled cells. Furthermore, to exclude that NP release is a species specific property of human T lymphocytes, murine $CD4^+$ and $CD8^+$ T cell lines were also analyzed for NP release after labeling with 75 µg/mL NP-9-NH_2 for 16 h. As shown in Figure 30B, murine T cell lines behave like their human counterparts upon loading with NP, showing a notable decrease of the median fluorescent intensity to approximately 25% of the initial value 24 h after re-culture at 37°C in particle free RPMI medium supplemented with 5% FCS

and 100 U/mL IL-2. Simultaneous monitoring of the cell number revealed that the loss of fluorescence could not be merely attributed to cell division (data not shown). Intracellular localization of NP was confirmed by cLSM (not shown).

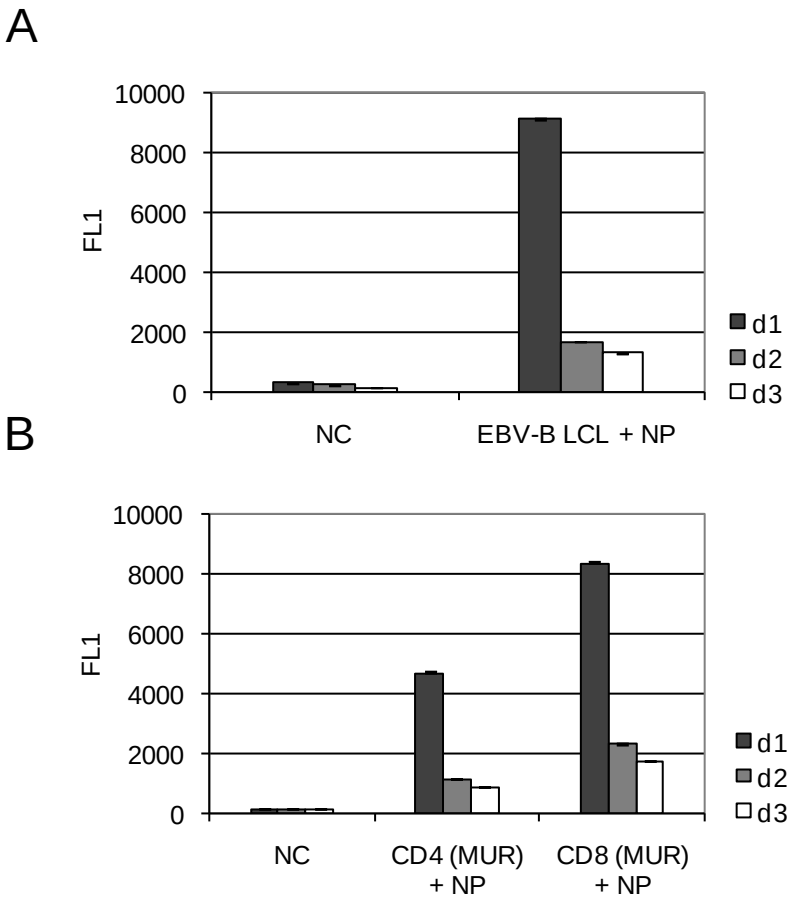

Figure 30: Uptake and release of NP-9-NH_2 by antigen presenting human B lymphocytes (A) and murine $CD4^+$ and $CD8^+$ T cell lines (B). NP loading to murine T cell lines was performed 72 h after isolation and polyclonally stimulation with anti-CD3 beads in AIM-V supplemented with 5% FCS and 100 U/mL IL-2. After incubation with NP, cells were washed and measured by flow cytometry for NP uptake (value d1). Residual NP-loaded cells were re-cultured in particle free medium for monitoring NP release at indicated time points. The results are representative of at least two independent experiments each. MUR, murine. Data are presented as described in Figure 16.

5.6 Optimizing NP incorporation and duration of labeling in human T cell lines

Several strategies were investigated in order to improve NP uptake and to avoid the rapid release of NP from T cells upon loading.

5.6.1 Transfection agents

5.6.1.1 Protamine sulfate and Lipofectamine

The cationic transfection agents protamine sulfate and Lipofectamine are frequently used for achieving an enhanced uptake of nanoparticles into cells (Arbab et al. 2004, Niemeyer et al. 2010). For pretreatment of NP with transfection agents protamine sulfate and Lipofectamine, negatively, positively and uncharged particles were preincubated with 1, 3 and 5 µg/mL protamine sulfate or 5, 10 or 20 µg/mL Lipofectamine for 15 min at 37°C since the surface charge of the particles could be an important factor for complex formation. Here, instead of 65 nm-sized NP-9-NH_2, particles of similar sizes (about 120 nm) were used in order to minimize variables that might influence complex formation. After preincubation, complexes were added to $CD8^+$ T cells for 16 h incubation at 37°C in AIM-V+10% HS. As shown in Figure 31, pretreatment of particles with protamine sulfate or Lipofectamine did not result in a stronger uptake by $CD8^+$ T cells, irrespective of the surface charge of nanoparticles. Most efficient incorporation was achieved with positively charged amino-functionalized NP-5-NH_2 while negatively charged carboxy-functionalized NP-7-COOH as well as uncharged NP-7 showed low uptake by $CD8^+$ T cells as already observed before. 7-AAD staining revealed no toxic effects of transfection agents on T cell viability (data not shown). In addition, cLSM analysis of NP loaded cells confirmed that these transfection agents had no significant influence on NP incorporation by T cells while agglomeration of extracellular NP rose with increasing concentrations of the cationic agents (not shown).

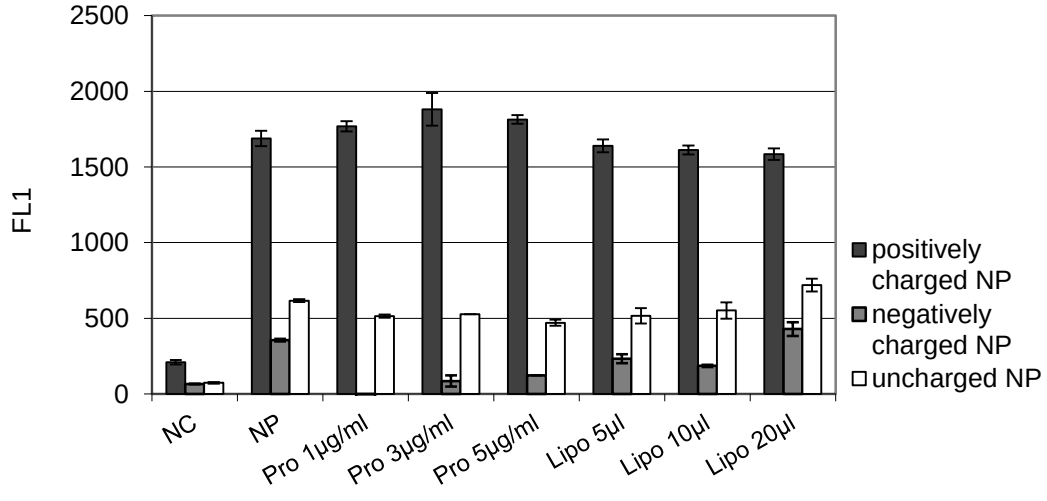

Figure 31: Uptake of differently charged nanoparticles after pretreatment with cationic transfection agents protamine sulfate and Lipofectamine at various concentrations. Complexes were incubated with $CD8^+$ T cells for 16 h at 37°C before analyzing NP incorporation by flow cytometry. Data are presented as described in Figure 16. NC, negative control (without NP); NP, nanoparticle control (untreated, without transfection agent). Since NP loading of carboxyfunctionalized NP to cells after treatment with 1 µg/mL protamine sulfate led to a negative median fluorescent intensity, this value was set to 0.

5.6.1.2 PULSIn™

PULSin™ is an aqueous formulation of cationic lipids (dioctadecylamidoglycylspermine) arranged into cationic liposomes of 100 nm in diameter able to form noncovalent complexes that interact with the cell surface by binding to heparan sulfate proteoglycans before endocytic internalization (Weiss et al. 2011, Weill et al. 2008). PULSIn™ is usually intended for delivery of proteins into the cytoplasm but was also used by another group to deliver Quantum Dots (QD) into the cytoplasm of COS-1 and HEK 293T/17 cells after complex formation (Delehanty et al. 2010). In preliminary experiments, 4 µL, 20 µL and 40 µL of PULSin™ reagent were preincubated with 75 µg/mL NP-9-NH_2 for 15 min at room temperature allowing a complex formation before adding the mixture to the T cell culture for further 16 h incubation at 37°C. After the incubation period excess NP were removed and cells re-cultured in NP free medium. Since PULSin™ was very toxic even at its lowest dose (data not shown) concentration was reduced to 1 µL, 4µL and 20 µL. Additionally, the incubation period of cells with NP-PULSin™ complexes was shortened to 4 h and 1 h for minimizing toxicity. As shown in Figure 32A, pretreatment of particles with PULSin™ and a subsequent incubation with cells for 1 h resulted in a threefold higher fluorescent intensity compared to the respective H_2O control. A longer incubation period of 4 h even led to a fourfold higher fluorescent intensity, while an increase of concentration from 1 µL to 4 µL PULSin™ showed no stronger fluorescence signal. 7-AAD staining revealed no considerably toxicity until a PULSin™ dose of 4 µL (70-80% vital cells) while incubation with 20 µL PULSin™ resulted in a decrease of T cell viability to about 30% indicating remarkable toxicity at higher concentrations (not shown). In the next step, NP-PULSin™ treated cells were analyzed by cLSM. As demonstrated in Figure 32B, the majoriy of the particles was attached to the outer cell surface appearing like a cap structure on one cell pole, while only a minority of NP is localized intracellularly showing a punctuate distribution of NP in the cytoplasmic region between nucleus and cell membrane.

A

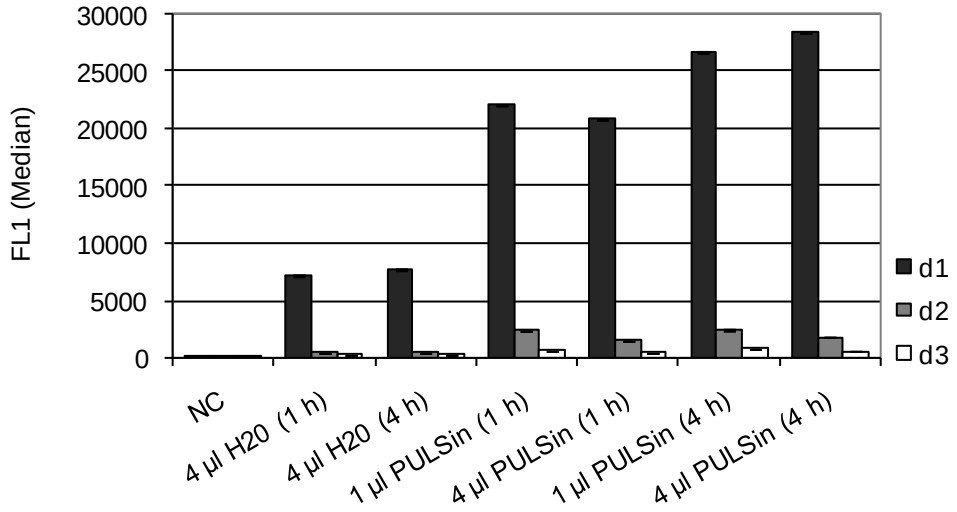

B

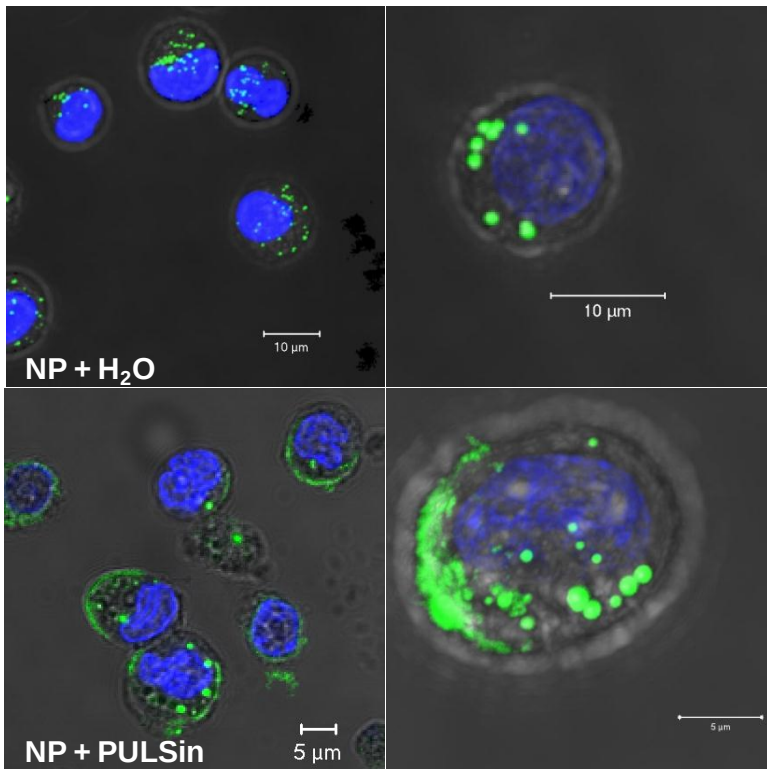

Figure 32: Fluorescence intensity of CD4$^+$ T cells after incubation with PULSin treated NP. After NP pulsing, cells were washed and measured by flow cytometry for NP uptake (value d1). Residual NP-loaded cells were re-cultured in particle free medium for monitoring NP release at indicated time points. (A) FL1 is the median fluorescent intensity of PMI fluorochrome associated with T cells. NC, negative control; H_2O, solvent (without PULSin, but with NP). Cells were subsequently analyzed by cLSM indicating a strong attachment of NP (75 µg/mL NP, 4 µL PULSin, 4 h) at the outer cell surface (B). Particles are shown in green. Representative cLSM images show all particles from different layers in a 3D view.

5.6.2 Electroporation

For direct delivery of particles to the cytoplasm via electric field induced membrane pores, T cells were electroporated in the presence of particles at different conditions. Preliminary experiments with Jurkat T cells at different electric puls conditions revealed that stronger pulses (500 V, 5 ms duration; 350 V, 12 ms) did not led to considerably higher fluorescent values compared to milder pulses (350 V, 5 ms; 50 V, 5 ms; 50 V, 5 ms, 5 pulses, 100 ms interval between pulses). At the same time, toxicity rose strongly as observed by a decrease of cell viability of about 20% after application of strong pulses (not shown) and subsequent 7-AAD staining. Therefore, further experiments were performed with those untoxic, mild electroporation conditions at 350 V for 5 ms. Since NP delivery to T cells was very weak compared to incubation with cells for 16 h at 37°C, further protocol optimization experiments were performed. First, electroporated cells were stored at 4°C for 15 min immediately after electroporation since resealing of membranes can be delayed at low temperatures. However, fluorescence intensity was not considerably higher than after 15 min regeneration of electroporated cells at 37°C. Furthermore, the usage of smaller particles NP-10 (32 nm) did also not result in a stronger fluorescence intensity of electroporated cells. In contrast, NP incorporation increased with higher NP concentrations (not shown) and also by using lower number of cells in the cuvette (Figure 33A). Since the NP control showed similar strong fluorescent values without previous application of an electric pulse and additionally, incorporated NP seemed to be distributed punctuate in the cytoplasmic region of electroporated cells as determined by cLSM (Figure 33B), it can be assumed that most particles were taken up by an endocytic process during the short incubation phase in the cuvette but not due to application of the electric pulse. In summary, electroporation of T cells in the presence of NP using various electric pulse conditions did neither result in an enhancement of NP uptake nor in a prolonged duration of cell labeling.

A

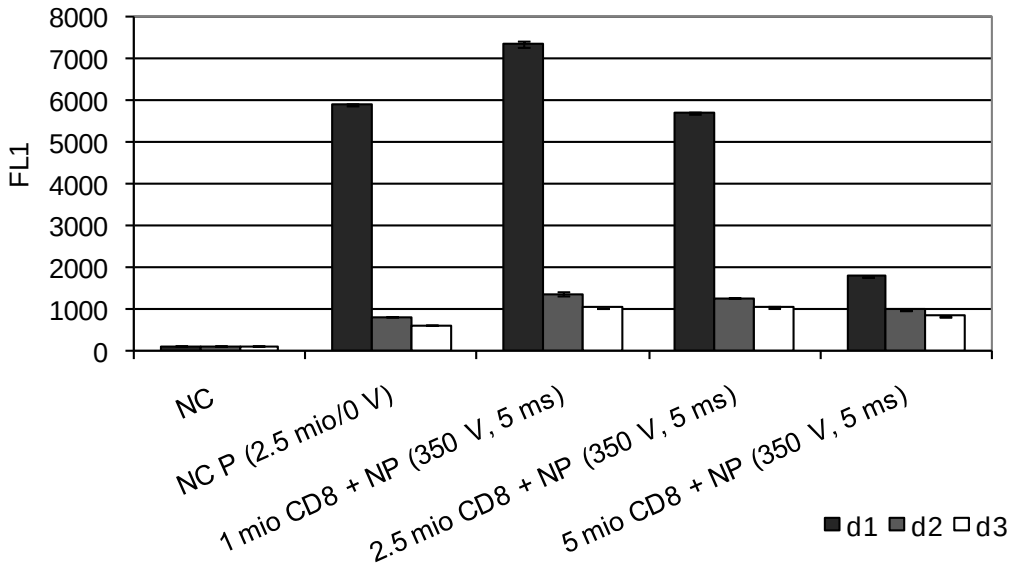

B

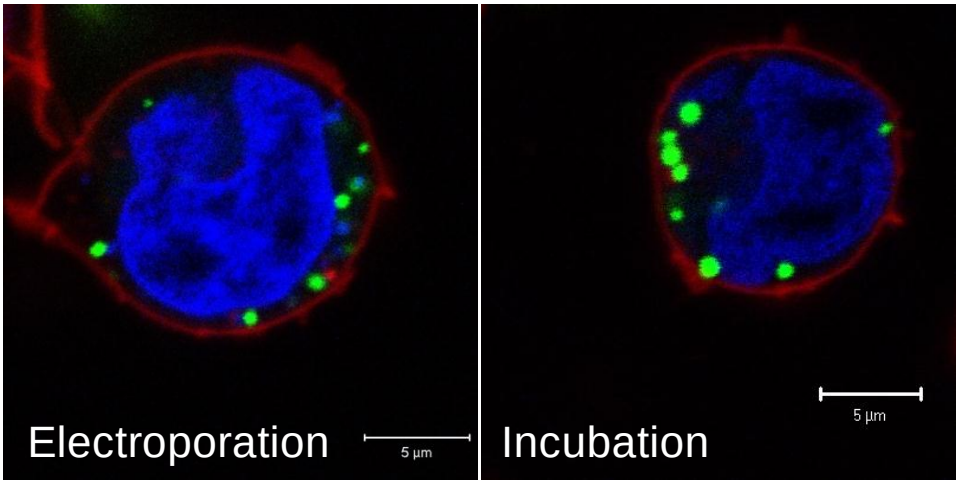

Figure 33: NP delivery to T cell lines by electroporation. Fluorescence intensity of T cells after electroporation at 350 V for 5 ms in the presence of 750 µg/mL NP-9-NH_2 (A). For protocol optimization different numbers of allo-reactive $CD8^+$ T cells (d14+3) were electroporated with particles. After electroporation, cells were analyzed by flow cytometry for NP incorporation (value d1). Residual NP-loaded cells were re-cultured in particle free medium for monitoring NP release at indicated time points. FL1 is the median fluorescent intensity of PMI fluorochrome contained within T cells. NC, negative control (without NP; 350 V, 5 ms); NC P, particle control (no electric pulse, $2.5x10^6$ cells + 750 µg/mL NP). (B) cLSM of Jurkat T cells after electroporation ($2.5x10^6$ cells/350 V, 5 ms/750 µg/mL NP; left picture) and 16 h incubation with 75 µg/mL NP at 37°C (right picture). The particles contain PMI as green-fluorescent dye; cell membranes were stained with CellMask™ Orange (red) and nuclei with Hoechst 33342™ (pseudocoloured blue), respectively.

5.6.3 Selection of strongly labeled cells by cell sorting

CD4$^+$ T cells were incubated with particles for 16 h or electroporated in the presence of 750 µg/mL NP by application of an electric pulse of 350 V for 5 ms. After NP loading, cells with high NP uptake behavior were separated by flow cytometric cell sorting (Figure 34A) at 4°C for subsequent monitoring of NP release over three days. As shown in Figure 34B, C, sorted cells with high NP uptake behavior did not retain more particles over time than poorly labeled counterparts, irrespective of NP delivery method. After NP loading by incubation (Figure 34B) as well as by electroporation (Figure 34C), the content of residual NP was below 10% in both sorted populations after re-culture in NP free medium indicating a similar NP release behavior by strongly as well as weakly labeled T cells.

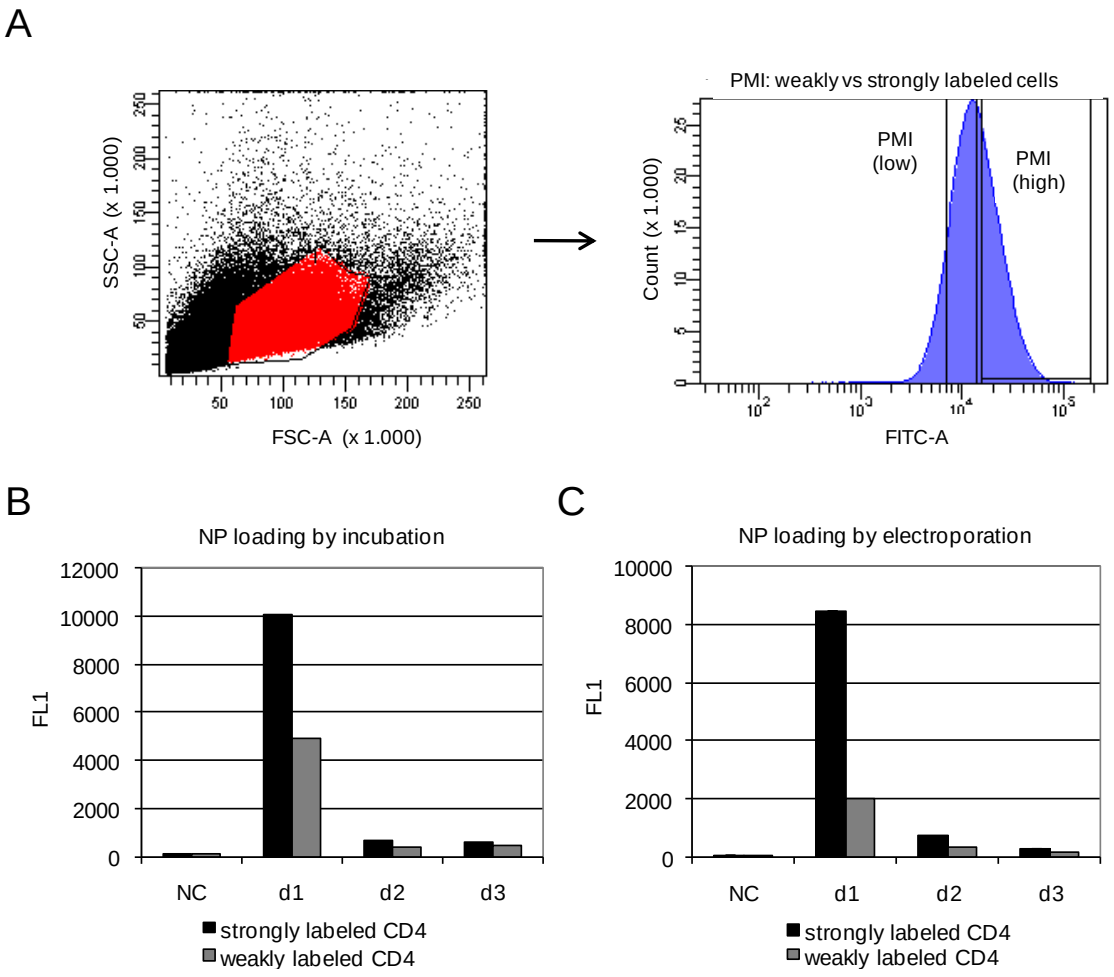

Figure 34: Selection of strongly and weakly labeled T cells by flow cytometric cell sorting and monitoring of NP release. Gating strategy (A) and median fluorescence intensity of flow cytometric sorted CD4$^+$ T cells with a high or low NP uptake behaviour after incubation (B) or electroporation (C) with NP. FACS plots show T lymphocytes after NP loading by incubation. After sorting, cells were washed and measured by flow cytometry for NP uptake (value d1). Residual NP-loaded cells were re-cultured in particle free medium for monitoring NP release at indicated time points. FL1 is the median fluorescent intensity of PMI fluorochrome contained within T cells. NC, negative control (without NP).

5.6.4 Chloroquine

Chloroquine is a lysosomotropic reagent that accumulates in endosomes and lysosomes of treated cells and prevents acidification by inhibition of an ion-transporting ATPase resulting in a disruption of the endosome (Wadia et al. 2004). Therefore it can also be used for delivery of nanoparticles into the cytoplasm since an endosomal disruption results in a floating out of the vesicles enabling an endosomal escape of loaded particles (Sêe et al. 2009). For this purpose, $CD4^+$ T cells were incubated with NP-9-NH_2 for 3 h at 37°C in the presence of 10 µM, 100 µM and 200 µM chloroquine in serum free medium. After incubation excess particles and chloroquine were removed by centrifugation and labeled cells were re-cultured in AIM-V+1% HS for monitoring NP release over three days by flow cytometry. As shown in Figure 35, uptake of particles was not affected by chloroquine, while NP release of labeled cells was slightly influenced by the endosome maturation inhibitor during the 48 h period of re-culture. After 24 h a slightly inhibitory effect was observed showing an elevated content of residual NP of about 9% and 10%, respectively in the presence of 100 µM and 200 µM chloroquine compared to the control without inhibitor (6%). Furthermore, NP content after 48 h was still 5% (10 µM), 6% (100 µM), and 8% (200 µM) of the initial fluorescence intensity after NP loading compared to the control (4%). 7-AAD staining revealed a slightly toxic effect not until after 24 h resulted in a lower viability of chloroquine treated cells of about 15% (not shown).

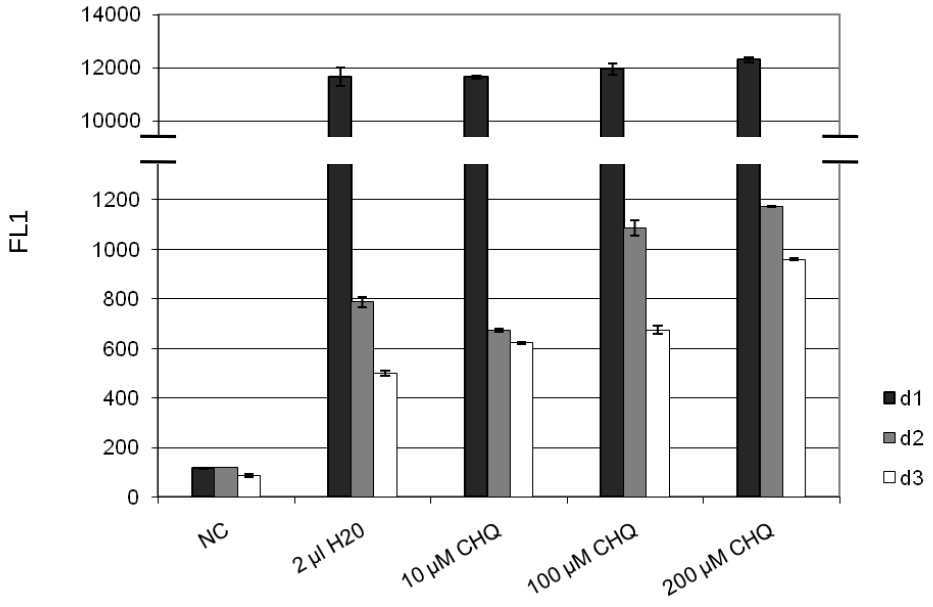

Figure 35: Inhibition of maturation of NP-loaded endodomes by chloroquine. After 3 h incubation of T cells with chloroquine at different concentrations, cells were washed and measured by flow cytometry for NP uptake (value d1). Residual NP-loaded cells were re-cultured in particle free medium for monitoring NP release at indicated time points. Data are presented as described in Figure 16. NC, negative control; H_2O, solvent (without chloroquine, but with NP).

5.6.5 Transferrin-conjugated nanoparticles

The transferrin (Tf)-conjugated particle NP-9-Tf was produced and obtained from Dr. Umaporn Paiphansiri, Max Planck Institute for Polymer Research, Mainz. Human holo-Tf was conjugated to NP-9-NH_2 (372 molecules per particle) aiming at uptake via the transferrin receptor CD71 highly expressed on activated T cells. For this purpose, $CD4^+$ and $CD8^+$ T cells were incubated with NP for 16 h at day 2 after antigen-specific stimulation (Figure 36) in serum-free culture medium. Positively charged and neutral polyethylene glycol (PEG)-coated particles as well as the regularly used amino-functionalized NP-9-NH_2 served as controls. Although incorporation of transferrin-conjugated NP-9-Tf by T cells was slightly improved in comparison to PEG-modified control particles, NP loading was not as efficient as when untreated NP-9-NH_2 was used.

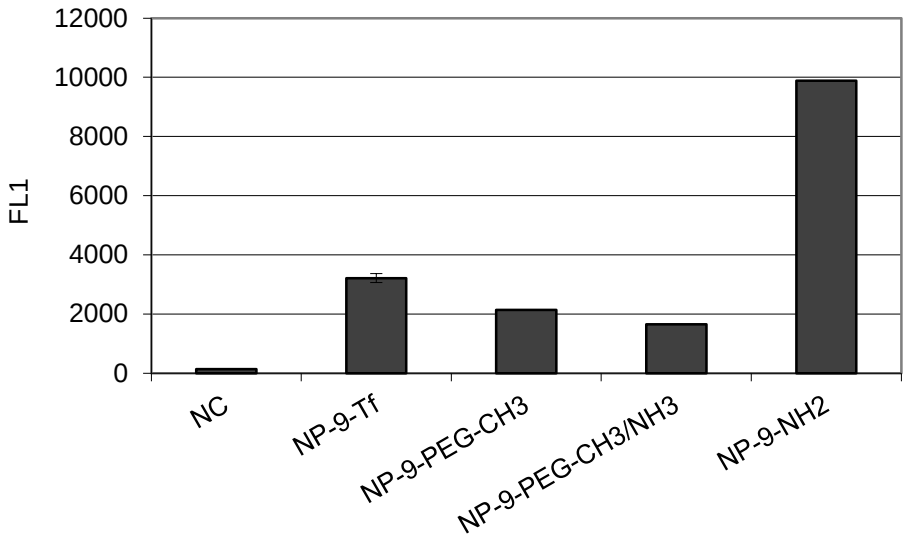

Figure 36: Incorporation of transferrin-conjugated NP. Particles (75 µg/mL) were incubated with $CD4^+$ T cells (day 14+2) for 16 h at 37°C in serum-free AIM-V medium. After washing off non-incorporated NP, uptake was quantified by flow cytometry. The results are representative of at least two independent experiments with $CD4^+$ and $CD8^+$ T cells. Data are presented as described in Figure 16.

5.6.6 Biocoating of NP with Influenza whole virus

Amino-functionalized NP-9-NH_2 was preincubated with a 244.5 µg/mL (i.e. hemagglutinin protein concentration) preparation of an inactivated influenza A (H3N2) whole virus vaccine for 0.5 h at 37°C allowing an electrostatic attachment of virus on NP surface. Higher concentrations of virus were also tested but led to a strong NP agglomeration (not shown). The newly formed NP-virus complexes were incubated with either T cells or with DC serving as control cells for further 2 h at 37°C. As shown in Figure 37A, the “biocoating” of NP with inactivated whole virus resulted in a moderately but significantly enhanced uptake by T cells.

However, the consistent increase of about 30% was low compared to that observed with DC which showed a remarkable enhancement of 400% if NP were coated with virus material (Figure 37B). In release studies the particle content of T cells labeled with NP-virus complexes was still 20% higher after 2 to 3 days than in control samples without virus material. As expected, DC retained incorporated NP-virus complexes much more effectively than T lymphocytes. Long-term follow up at day 9 after NP pulsing showed that nearly half of DC still contained nanoparticles.

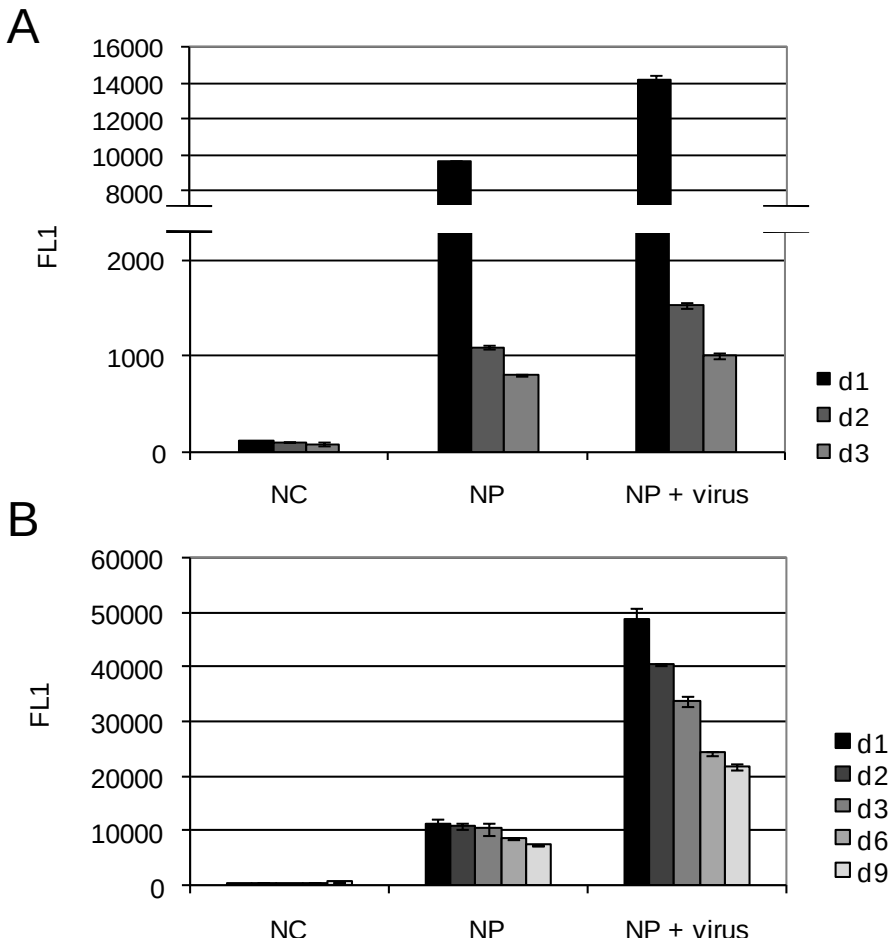

Figure 37: Improved delivery of NP to dendritic cells and T lymphocytes after 'biocoating' with whole virus particles. NP-9-NH_2 (75 µg/mL) were pre-treated with an influenza inactivated whole virus vaccine preparation for 0.5 h at 37°C and were then incubated with immune cells for further 2 h at 37°C. After removal of non-incorporated NP, cells were measured by flow cytometry for NP uptake (value d1). Residual NP-loaded cells were re-cultured in particle free medium for monitoring NP release at indicated time points. Data in (A) and (B) are derived from $CD4^+$ T cell lines and DC, respectively. Results are representative of at least two independent experiments. Data are presented as described in Figure 16.

Subsequently, incorporation of NP-virus complexes by T cells and DCs was analyzed by cLSM (Figure 38). Based on these results, it could be confirmed that fluorescent signals

previously measured by flow cytometry can definitively be attributed to incorporated NP. Therefore, biocoating of particles with inactivated whole virus resulted in an enhanced uptake without a detectable attachment of NP-virus complexes at the outer cell surface. NP incorporation by T cells was not as strong than by dendritic cells. Despite the strong uptake of NP-virus complexes, no significant toxicity could be observed (not shown). Additionally, intracellular particles appeared as a globular formation next to the nucleus of DCs, while T cells showed a more dispersed distribution of incorporated particles as observed by cLSM.

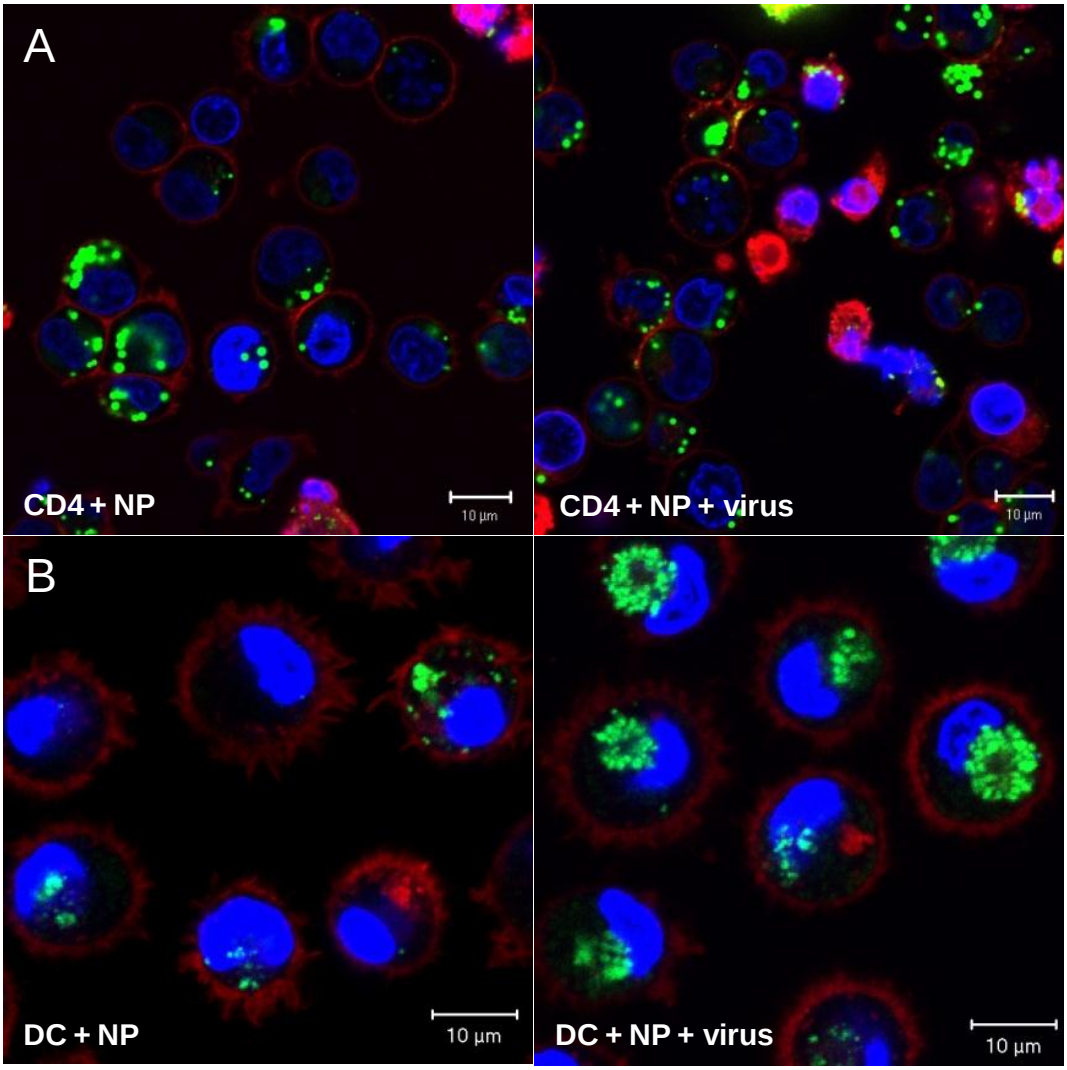

Figure 38: cLSM of cells loaded with "biocoated" NP. NP labeled $CD4^+$ T cells (A) as well as dendritic cells (B) were analyzed by cLSM indicating a stronger uptake of NP after pretreatment with virus without a detectable attachment on the outer cell surface. Left pictures show controls with untreated NP. The particles contain PMI as green-fluorescent dye; cell membranes were stained with CellMask™ Orange (red) and nuclei with Hoechst 33342™ (pseudocoloured blue), respectively.

5.7 Delivery of Cy5-oligonucleotides with biodegradable PBCA nanocapsules

Biodegradable poly(n-butylcyanoacrylate) (PBCA)-capsules containing Cy5 labeled oligonucleotides as freight molecules were produced and obtained from Dr. Grit Baier, Max Planck Institute for Polymer Research, Mainz. Notably with an average diameter of 325 nm they were larger than the nanoparticles used before, but had been applied previously in HeLa and mesenchymal stem cells. Therefore uptake was expected also to occur for T cells. Briefly, the enzymatic biodegradability of the PBCA-shell allowed a gradually release of the oligonucleotide fright molecules after incorporation of the capsules by cells as observed in HeLa cells and mesenchymal stem cells (Baier et al. 2011). The Cy5 labeled oligonucleotides were thought to act as a model system for short RNA molecules that can be encapsulated in PBCA and delivered to a specific cell population *in vitro* as well as *in vivo* enabling a gently, genetically modification of the addressed cells.

For studying the uptake of PBCA capsules by T lymphocytes, $CD4^+$ T cells were incubated with 150 µg/mL capsules for 24 h at 37°C. After the incubation period excess capsules were removed by centrifugation and cells were prepared for cLSM as described in Materials and Methods. Preliminary experiments showed a successful endosomal escape of Cy5 labeled oligonucleotides into the mitochondria (Figure 39) already after 24 h incubation with 150 µg/mL capsules at 37°C.

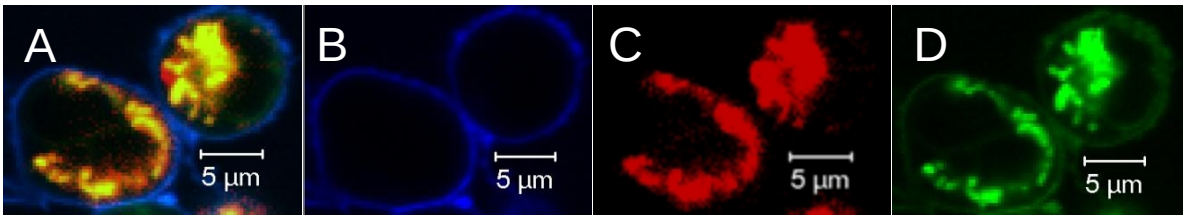

Figure 39: Colocalization studies of Cy5 labeled oligonucleotides delivered by PBCA nanocapsules in T cells with mitochondria by cLSM. Merged picture is shown in (A); (B) cell membrane stained by CellMask ™ orange and shown in blue; (C) Cy5 labeled oligonucleotides pseudocolored in red; (D) counterstaining of mitochondria with MitoTracker green FM (shown in green).

As shown in Figure 40A, a reduction of incubation time to 1 and 8 h led to a considerably lower mitochondrial Cy5 signal suggesting that the enzymatic degradation of PBCA capsules had not progressed far enough yet. In contrast, prolonging of incubation time to 48 h or 72 h resulted in a notably stronger fluorescent signal due to accumulation of released Cy5 labeled oligonucleotids in the mitochondria as observed in a further experiment (Figure 40B). Additionally, no cytotoxic effects could be observed even after 72 h incubation with PBCA capsules at 37°C (not shown).

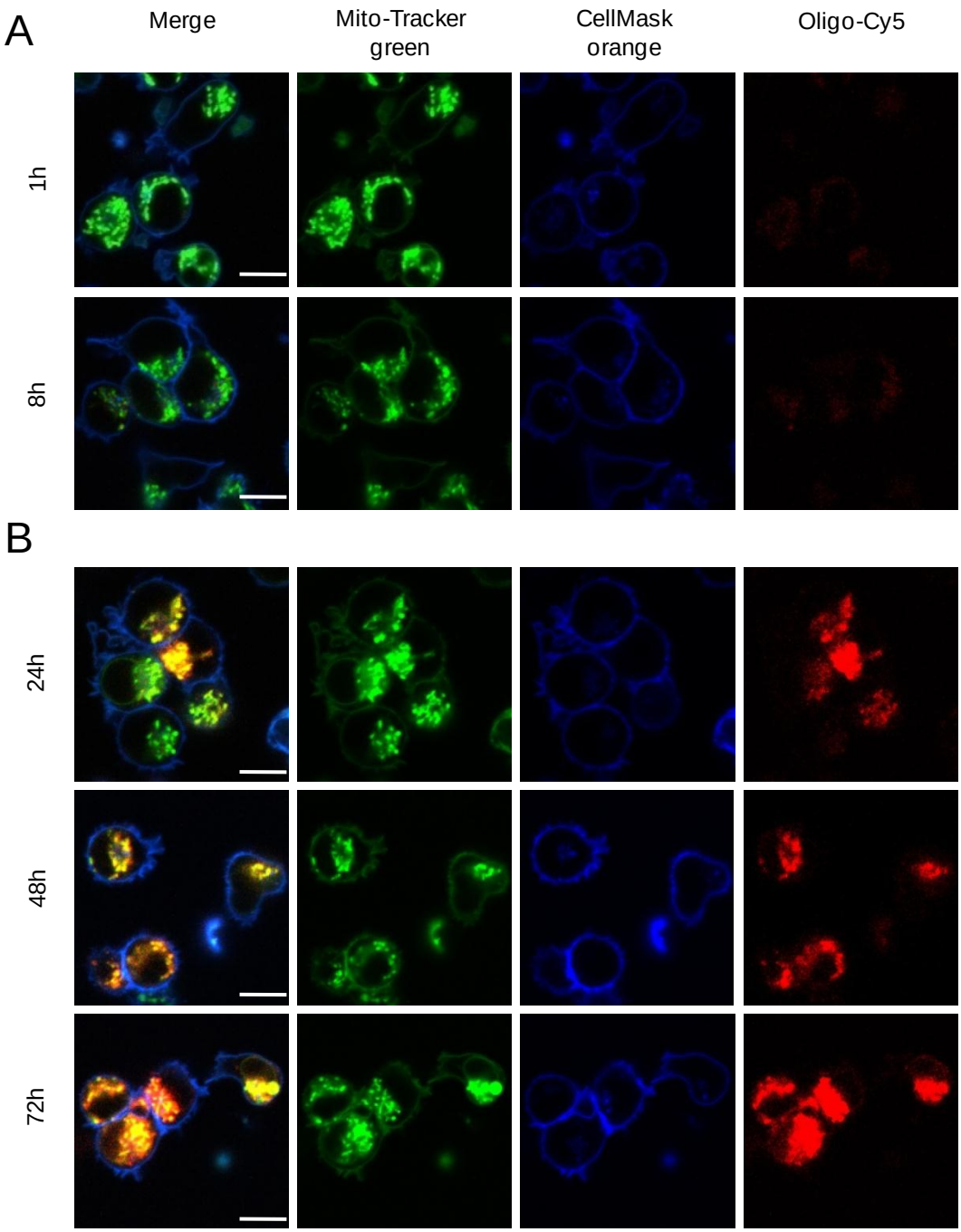

Figure 40: cLSM of T lymphocytes incubated with PBCA capsules for different time periods. The images show the time dependent release of Cy5-labeled oligonucleotides (stained in red). Counterstaining of mitochondria with Mito-Tracker is shown in green, the cell membrane stained by CellMask orange is coloured blue. Within the first 8 h of incubation (2 h, 4 h: not shown) release of Cy5-labeled oligonucleotides was weak (A), while a longer incubation period up to 72 h led to a strong mitochondrial Cy5 signal (B). Scale bar is 10 µm.

6 Discussion

6.1 Labeling of dendritic cells with nanoparticles

Dendritic cells are the most potent antigen presenting cells. Therefore they are interesting targets for vaccination strategies – either in-vivo or expanded and manipulated ex-vivo as for immune therapy of malignant diseases. They are also key cellular components in graft versus host disease (GvHD). After allogeneic hematopoetic transplantation the activation of DCs and the presentation of graft derived antigens is an important step in the development of GvHD. A thorough understanding of DC migration from tissues to the lymph nodes is essential for further developments of these cells as cellular therapeutics and for influencing GvHD. Fluorescent nanoparticles in the range of 20 to 200 nm are ideal markers for cells as they can be synthesized according to the need of the application.

Influence of surface functionalization on NP uptake by DCs. In order to investigate the influence of different NP parameters like surface functionalization on the labeling efficiency, all NP should be synthesized by the same process. Therefore the miniemulsion process was chosen which can provide functionalized and unfunctionalized polymeric nanoparticles just by the addition of a co-monomer (Musyanovych et al. 2007). With these, the specific contributions of a modification (e.g. carboxy-functionalization) can be investigated. In contrast to other cell types carboxy-functionalization did not enhance the uptake of NP into DCs and amino-functionalization enhanced the uptake only by a factor of 3-4. With mesenchymal stem cells an enhancement of 70x for amino-functionalized NP was reported (Lorenz et al. 2006). A possible explanation for this might be that internalization by phagocytosis by professional APC is less specific in comparison to other endocytic pathways (e.g. receptor-mediated endocytosis), and therefore the modification of the NP surface only played a minor role during phagocytosis of NP. In accordance with the results in this work, Fischer et al. showed that surface functionalization of poly(lactide-co-glycolide) microparticles by adsorption of positively charged polyelectrolytes did not have a significant influence on particle uptake into DCs (Fischer et al. 2007). This demonstrates that not only NP properties but also the target cell type is an important variable for NP uptake.

NP size and uptake mechanism. Further characterization of the NP showed that they were in the range between 60 and 150 nm. We did not analyze the uptake mechanism into DCs by detailed endocytosis inhibitor experiments. Rejman et al. found that for the internalization of particles with a diameter <200 nm the clathrin-coated pits pathway was the main uptake

mechanism (Rejman et al. 2004). Additionally, Macho-Fernandez et al. reported that incorporation of 90 nm-sized NP by DCs preferentially occured via clathrin-mediated endocytosis (Macho-Fernandez et al. 2012). Only well below (probably somewhere below 20-50 nm) or above (probably somewhere above 200 to 300 nm) other endocytic mechanisms were expected to be operational in the uptake of NP (Rejman et al. 2004, He et al. 2010). With increasing size, a shift to a caveolae-mediated internalization mechanism occurred as shown by these authors and that was predominant for particles with 500 nm in size. As professional antigen presenting cells, DCs are also capable of ingesting NP efficiently by phagocytosis (Elamanchili et al. 2004). Therefore NP synthesized for this study seem to be ideal for DC labeling as they can carry a high amount of fluorochrome while they should be taken up by clathrin-coated pits as well as by phagocytosis. The influence of the size on NP trafficking has also been investigated *in vivo*. Manolova et al. demonstrated for subcutaneous *in vivo* application of NP that large particles (500-2000 nm) were mostly associated with DCs detected at the injection site while small (20-200 nm) nanoparticles were also found in lymph node resident DCs and macrophages, suggesting free drainage of these particles to the lymph nodes (Manolova et al. 2008). Therefore the synthesized nanoparticles tested in this work could also be used for *in vivo* applications outside of lymphatic tissue, which is a significant advantage over larger microparticles.

Toxicity. While there was an enhancement of NP toxicity at a dose of 25 µg/mL in the initial dose finding studies, cytotoxicity in the following experiments could not be observed and also in long-term settings, where more than 95% of labeled DCs were still alive after 8 days. The slight enhancement of toxicity at a dose of 25 µg/mL did not seem to be due to the surface charge or the inert polymeric materials itself, but seemed to be caused by surfactant which was not removed vigorously enough (data not shown). This and other studies revealed that toxicity of polymeric NP is a minor problem compared to some inorganic NP like quantum dots (Wang et al. 2008). Nevertheless, future studies should also investigate possible long-term effects after chronic exposure to NP (e.g. genotoxicity).

Phenotypical and functional evaluation of NP-loaded DCs. While acute toxicity of NP may be screened with many cell types, specific functions should also not be altered when using a nanoparticular material for labeling of DCs. The main functions of DCs are antigen uptake, processing, presentation and stimulation of an immune response. All these functions should not be altered by a labeling procedure. As uptake of NP takes place into intracellular compartments where antigens are usually processed, it was surprising that this did not lead to a “danger” signal and an increase in costimulatory molecules. Studies with biodegradable poly-L-lysine nanoparticles have shown that the nanoparticles themselves enhance

expression of MHC class II as antigen presenting molecule and also to a lesser extent the expression of the costimulatory molecule CD86 (Elamanchili et al. 2004). This effect could be further increased by incorporating stimulatory substances like monophosphoryl lipid A. Phenotypic evaluation revealed that amino-functionalized NP do not alter the expression of MHC Class II and other immunostimulatory surface molecules on DCs (Zupke et al. 2010). This has also been shown in DCs for superparamagnetic iron oxide NP and other preparations of poly(lactide-co-glycolide) NP (Fischer et al. 2007, de Vries et al. 2005). Thus, the reported alteration of surface molecules by NP (Elamanchili et al. 2004) might be related to the materials used for synthesis. Different applications therefore may opt to choose different materials for their purposes (enhanced or unaltered expression of DCs relevant proteins). Surface molecules on DCs are only one aspect of DC function and as the quantitative uptake of NP in this work is substantial, an important question is if this loading of intracellular compartments would interfere with other functions of DCs, namely allo-stimulation, antigen uptake and antigen processing. No differences in the immunostimulatory capacity of mDCs in an allogeneic mixed lymphocyte reaction (MLR) could be found in this work either in the absence or presence of NP. The uptake of virus peptides and the stimulation of T cells as shown by the production of IFN-γ in the ELISPOT assay was not influenced by the presence of NP in DCs in this study. De Vries et al. have shown similar results for supernatant of DC/T cell co-cultures and Fischer et al. have demonstrated an influence of NP functionalization only for polyethyleneimide on the production of IL-12p70 (De Vries et al. 2005, Fischer et al. 2007). While peptides can be loaded directly onto the peptide presenting MHC complex larger proteins first need to be processed to oligomers in intracellular compartments. In this work it could be demonstrated that even this delicate task of antigen processing of an influenza whole virus preparation is not disturbed despite the high load of NP in intracellular compartments (Zupke et al. 2010). To our knowledge this has not been shown before for NP in DCs. Since the loading process did not adversely affect the cellular phenotype and function of DCs as antigen-presenting cells, this type of NP is ideally suited for delivery of reporters, antigens, and other freight molecules into DCs. Future studies should assess the *in vivo* trafficking of transferred NP-labeled cells in humanized mouse model by using bioluminescence and fluorescence imaging, or in the case of magnetic particles, by MRI.

6.2 Loading of T lymphocytes with nanoparticles

Besides active vaccination with dendritic cells, adoptive immunotherapy using virus-, leukemia- or tumor-reactive T cells has emerged as a promising approach for the treatment of malignant diseases. Here, nanoparticles offer great potential to deliver therapeutic agents into human T lymphocytes. Only limited literature is dealing with NP loading into T cells. Most studies focussed on murine T cells that were loaded with iron oxide-particles *in vitro* to demonstrate homing of adoptively transferred T cells into sites of tumor infiltration or autoimmune disease by MRI in animals *in vivo* (Moore et al. 2002, Kircher et al. 2003, Anderson et al. 2004). Since the incubation with NP alone mostly resulted in a weak uptake by T cells, transfection agents (e.g. Lipofectamine) as well as surface functionalization with cell penetrating peptides (e.g. HIV-TAT peptide) were used to improve NP incorporation, even if those are not approved for clinical application in humans (Beer et al. 2008, Anderson et al. 2004, Moore et al. 2002).

Optimizing NP parameters for efficient uptake by T cells. Preliminary NP loading experiments with the human T lymphoblastoid cell line Jurkat that was used as a first model system for T lymphocytes showed that these cells demonstrate a considerably lower NP-labeling efficiency compared to dendritic cells, which have a much stronger phagocytic capability and also a larger cytoplasm to nuclear ratio. For that reason, novel NP with different properties and surface modifications like functional groups or protein conjugates (e.g. for targeting the transferrin receptor, CD71) were synthesized and tested for improved uptake by primary T lymphocytes. In fact, results with newly designed NP demonstrated that amino-functionalized NP are very efficiently taken up also by human T cells. After increasing NP concentration we even reached almost the same level of incorporation as shown for human professional APC such as DCs. In contrast, uptake in T cells was lower for many other NP preparations including those that carried surface carboxyl groups. Furthermore, slight differences in particle size turned out to be not as important as surface properties (e.g. functionalization, residual surfactant) for efficient NP incorporation. These observations underline the importance of surface functionalization as a major determinant for the entry of NP into cells (Lunov et al. 2011, Lorenz et al. 2006, Weiss et al. 2007). The amino-functionalization process may especially facilitate the incorporation of NP that are designed as nanocarriers to transport labeling agents or nucleic acids inside T cells and other immune cell types, allowing their tracking or genetic manipulation (Lorenz et al. 2006, Mailänder&Landfester 2009, Kircher et al. 2003, Weinstein&Peer 2010). Additional surface functionalization with antigen-specific T-cell recognition receptors such as HLA-peptide multimers would offer the unique opportunity to target NP to certain T cell subsets and to use

NP-based strategies for modulation of T cells not only *in vitro* but also *in vivo* (Klenerman et al. 2002, Clemente-Cesares et al. 2011).

Optimizing cellular parameters during the NP loading process. In addition to the NP surface, several cellular factors appeared to influence particle uptake. It could be shown that pre-stimulation of T cells with specific antigen over 2 days strongly increased the incorporation of NP. A similar enhancing effect has been described by several investigators using polyclonal activation of T cells with concanavalin A, anti-CD3, anti-CD28, and IL-2 (Kircher et al. 2003, Smirnov et al. 2006, Dodd et al. 2001). However, these agents are non-physiological stimuli and do not specifically target those T cells that are activated by natural antigen. Moreover, we observed that $CD4^+$ T cells are slightly superior compared to $CD8^+$ T cells in the ability to take up NP. The reason for this observation remains unclear at this point. Interestingly, it could be demonstrated that NP uptake in T cells gradually decreased beyond the 3rd week of *in vitro* stimulation, indicating the need to label them during early culture periods. This would also maintain important *in vivo* properties of T cells, considering that long-term *in vitro* culture has been shown to correlate with impaired homing, persistence and effector function of tumor- and virus-reactive T cell lines after adoptive transfer *in vivo* (Hinrichs et al. 2006, 2011). Together, antigen-specific T cell lines expanded over few weeks *in vitro* appear optimally suited for NP uptake as well as for mediating T-cell functions upon transfer into patients.

Functional evaluation. Loading of T cells with polymeric NP might have an adverse impact on T-cell function, particularly if T cells are heavily filled with particle material. Some studies showed that $CD8^+$ CTL moderately labeled with SPIO-NP did retain the ability to recognize and to kill target cells *in vitro* as well as *in vivo* (Dodd et al. 2001, Kircher et al. 2003, Iida et al. 2008, Janic et al. 2009), while strong labeling of T cells with iron oxide-NP and Lipofectamine resulted in a reduced T cell proliferation capacity *in vitro* (Beer et al. 2008). In dose-response experiments, we observed that pulsing T cells with low to intermediate (up to 150 µg/mL) NP concentrations did not impair antigen-induced IFN-γ production and cytotoxicity. This was true for both $CD4^+$ and $CD8^+$ T cell lines as well as for $CD8^+$ CTL clones that recognize leukemia or tumor antigens. In contrast, higher NP concentrations (i.e. >150 µg/mL) significantly inhibited T-cell function. Therefore, T cells intended for clinical use should undergo careful pre-testing to determine optimal loading conditions, where NP do not adversely affect T-cell function.

Influence of pharmacologic endocytosis inhibitors on NP uptake. Endocytic mechanisms involved in the uptake of the amino-functionalized particle NP-9-NH_2 into T lymphocytes were investigated. In contrast to DCs, there is only very few literature dealing with T cells. Consistent with other cell types (Dausend et al. 2008, Panyam et al. 2002, Davda&Labhasetwar 2002), T cells showed decreased NP incorporation at 4°C compared to 37°C during the loading period. This finding suggested that the uptake process is energy-dependent and that conventional pathways of endocytosis might be involved. The next step was to identify the mechanism of NP uptake in T cells by pharmacologic endocytosis inhibitors, as successfully demonstrated in HeLa cells (Dausend et al. 2008). Although some inhibition (i.e. <20%) could be observed for chlorpromazine and dynasore at non-toxic concentrations and thus would conclude that clathrin- and dynamin-mediated endocytosis is involved in NP incorporation, the impairment was much less impressive than in HeLa cells. Thus single or multiple hitherto unidentified uptake mechanisms appear to be involved in human T cells and may play an even more important role than endocytic functions mediated by clathrin and dynamin, respectively.

Intracellular localization of NP. As the further fate of NP depends very much on their intracellular localization, TEM as well as confocal LSM studies including co-staining of major endolysosomal compartments were performed. The TEM data clearly showed that NP were located in intracellular membrane-surrounded vesicles of T cells. In contrast, particles were not detected in the cytoplasm or nucleus as described for other cell types upon loading with polymeric NP (Lorenz et al. 2006). In confocal LSM experiments, any co-localization of NP with major endolysosomal markers such as EEA1 and LAMP1 as well as the small GTPases Rab5 and Rab7 could not be found. This result was somewhat surprising since these markers define compartments that the NP should at least pass through. Therefore, one might speculate that NP localize in recycling endosomes that express the small GTPase Rab11 protein. However, Rab11 was not detected in T cell lines despite several attempts and modifications in the staining protocol including the use of different antibody clones.

Release of nanoparticles. We furthermore investigated the release of NP from T cells. Here, we found that 70-90% of intracellular particle material was already exported to the outside during the first 24 h after loading was stopped. Most NP were even lost within 2 to 4 hours, indicating that this rapid release cannot be merely attributed to cell division. In contrast to our results, some studies showed that labeling is durable even after days (Kircher et al. 2003, Kaufman et al. 2003), while others reported significant loss of MRI signal by approximately 40% during 24 h, but which was attributed to ongoing division of T cells during this period (Smirnov et al. 2006). Additionally, parallel studies at 4°C versus 37°C revealed a

considerably faster release of incorporated NP at 37°C suggesting that not only uptake but also the export of NP is an energy-dependent process. When the cell metabolism was completely blocked by paraformaldehyde fixation, NP release did not occur. These findings support the hypothesis of an active export mechanism for incorporated NP.

NP release was observed in all T cell populations analyzed, namely entire $CD4^+$ and $CD8^+$ T cells as well as that of naïve, central memory, and effector memory differentiation, respectively. Memory T cells have been reported to protect themselves much better than other subtypes from the influence of material outside of the cell (Turtle et al. 2009). However, no difference in the uptake and release of NP in central or effector memory T cells versus naïve T cells could be found.

Additional analysis on B lymphocytes showed that B cells behave much more like T cells upon loading with NP. This may indicate that the lymphocytic origin of B cells is a more determining factor for interaction with NP compared to the nature as professional APC that B cells share with myeloid DCs. Furthermore, it can be excluded that NP release is a species specific property of human T lymphocytes since murine $CD4^+$ and $CD8^+$ T cell lines showed similar behaviour upon labeling with a loss of NP signal of 80% during 48 h of re-cultivation. This is interesting because it was reported that still 70% of initially labeled murine T cells contain intracellular HIV-TAT conjugated NP even 72 h after labeling (Kaufman et al. 2003). The strong retainment of incorporated NP can therefore potentially be attributed to the surface functionalization with TAT peptide leading to an endosomal escape of NP into the cytoplasm.

Influence of human serum on NP uptake and release. The most important factor that influenced the import and export of NP in human T cells turned out to be serum. Notably, the serum concentration of media used during loading or maintenance of T cells was inversely correlated with NP uptake and intracellular retention, respectively. Previous studies have shown that NP are capable of binding a broad panel of serum proteins including albumin (Tenzer et al. 2011, Röcker et al. 2009). Therefore, human albumin and immunoglobulins as the two major serum components were added to serum-free medium during NP loading of T cells, which however were completely unable to substitute for the inhibitory effect of entire human serum. Another study (Simberg et al. 2009), using SPIO-NP and murine plasma, has shown that mainly minor plasma proteins were strongly enriched on the NP surface after short incubation with particles, while enrichment of albumin, immunoglobulins, and transferrin as the most abundant components was not as significant. In contrast to our study, SPIO-NP incorporation by macrophages was not inhibited by the “corona” of directly and indirectly bound proteins (Simberg et al. 2009). A possible explanation for this observation might be the strong phagocytic activity of macrophages resulting in a more effective internalization of

protein-particle conjugates compared to T cells. Sensitive approaches such as 2D gel electrophoresis and mass spectrometry are clearly needed to identify the serum component that interferes with the uptake and release of NP in T lymphocytes.

Strategies to improve NP uptake and to prolong the duration of intracellular NP labeling. Several strategies were investigated in order to improve NP uptake and to avoid the rapid release of NP from T cells upon loading. First, NP were loaded to cells after pretreatment with protamine sulfate and Lipofectamine, since those transfection agents have been reported to enhance NP uptake into different cell lines (Arbab et al. 2004, Matuszewski et al. 2005). However, NP incorporation by T cells could not be improved significantly by using differently charged NP for complex formation with polymers.

Delehanty et al. reported an enhanced uptake, and subsequently a modest cytosolic dispersal of NP that were pretreated with PULSin^{TM} reagent before loading them to cells (Delehanty et al. 2010). These results could not be confirmed by using T cells, since those NP-PULSin^{TM} complexes mainly attached to the outer cell membrane while intracellular NP content was not significantly enhanced compared to the untreated controls.

Furthermore, T lymphocytes were incubated with NP in the presence of Golgi inhibitors Brefeldin A and Monensin that block endosomal transport processes towards the membrane (Qiu et al. 1995). Since no influence on intracellular NP content could be observed, it can be assumed that NP-loaded endosomes are being transported towards the plasma membrane for exosomal release of NP even before reaching the Golgi complex.

In order to inject particles through electric field induced membrane pores directly into the cytoplasm, T cell lines were electroporated in the presence of different particles at various conditions. The results are consistent with those of previous reports showing that electroporation is an inefficient and toxic NP delivery method compared to other loading strategies (Delehanty et al. 2010, Steinfeld et al. 2006). Additionally, T cells with high NP uptake behavior did not retain considerably more particles over time than their poorly labeled counterparts, irrespective of NP delivery by electroporation or incubation. Thus, NP seem to be incorporated and stored in the endolysosomal compartment where they are trapped until their release to the extracellular environment.

Furthermore, NP were loaded to T lymphocytes in presence of chloroquine that accumulates in endosomes and lysosomes, and prevents acidification by inhibition of an ion-transporting ATPase leading to a disruption of the endosome (Wadia et al. 2004). Sêe et al. reported a successful cytoplasmic delivery of NP in HeLa cells by using chloroquine since endosomal disruption results in a floating out of the vesicles with subsequent escape of the NP load into the cytoplasm (Sêe et al. 2009). In contrast to this work, NP uptake and release by T cells in our study could not be improved considerably by chloroquine treatment.

Moreover, NP surface was functionalized with transferrin molecules for achieving an improved uptake via the transferrin receptor highly expressed on activated T cells. However, NP uptake by T cells was weak in comparison to the standard particle NP-9-NH_2. These results are contrary to those of previous reports that showed a strongly improved uptake of transferrin-conjugated NP into different human, but malignant cell lines (Yang et al. 2005; Li et al. 2009).

Because influenza viruses have developed efficient means to escape the endolysosomal pathway (Bender et al. 1995), an inactivated influenza whole virus vaccine preparation was added during NP loading to T lymphocytes. This procedure increased uptake of NP into T cells by 30% and had a small, but unimpressive influence on the release. Interestingly, the whole virus vaccine strategy strongly enhanced intracellular uptake and long-term retention of NP in the DC control by a factor of 3 to 4, suggesting that the interactions between NP, virus material, and cellular pathways are different in DCs and T cells.

Nanocapsules for intracellular delivery of nucleic acids. Novel biodegradable nanocapsules were tested for their suitability to deliver nucleic acids into T lymphocytes. Initial experiments using PBCA capsules containing Cy5 labeled oligonucleotides (Cy5-20mer) as cargo revealed a successful endosomal escape of the load in T cells with a subsequent localization in the mitochondria as determined by cLSM. In accordance with the results in this work, it was shown that those oligonucleotide cargo molecules were gradually released within MSCs after incubation with the capsules (Baier et al. 2011). While release in MSCs occurred already after 4-6 h, the endosomal escape as well as the mitochondrial accumulation of such freight molecules in T lymphocytes was considerably slower with a notable colocalization signal not until 24 h of incubation. The Cy5 labeled oligonucleotides were thought to act as a model system for short RNA molecules that can be encapsulated in PBCA and delivered to a specific cell population *in vitro* as well as *in vivo*. Here, the administration of small interfering RNA (siRNA) to knockdown negative immunoregulatory molecules such as PD-1 and the Casitas B-cell lymphoma (CBL) family protein CBL-B would be a promising approach. The results in this work demonstrate that PBCA capsules are well suited as vehicles for nucleic acids allowing a non-toxic, genetic modification of T lymphocytes to be used in cellular immunotherapy. Another advantage of these biocompatible capsules is that polycyanoacrylates are already approved for clinical use (Eskandari et al. 2006, Faria et al. 2005).

7 Conclusions

In the first part of this work we developed an *in vitro* protocol allowing a strong labeling of human monocyte-derived DCs with amino-functionalized fluorescent polymeric NP. Protocol optimization experiments revealed that already a relative low dose of NP (25 µg/mL), incubated with DCs for 16 h, is sufficient to label DCs efficiently. Long-term follow up of NP loaded cells showed that even after 8 days 95% of DCs retained nanoparticles with a fluorescence intensity of 67% compared to day 1. Toxic effects could not be observed. The expression of several markers for maturation, homing and co-stimulation molecules, which are indispensable for the function of DCs as professional antigen-presenting cells, was not adversely affected by NP. Furthermore, a potential negative influence of NP loading on the allo-immunostimulatory capacity of DCs for T lymphocytes could be excluded. Additionally, neither the capacity of labeled DCs for peptide presentation, nor their ability to process viral proteins was inhibited by the NP load. Since the loading process did not adversely affect the function of DCs as antigen-presenting cells, this type of NP appears ideally suited for delivery of reporters, antigens, and other freight molecules into DCs.

In the second part of this work we showed that amino-functionalized NP were taken up also by human $CD4^+$ and $CD8^+$ T lymphocytes. However, T cells demonstrated a considerably lower labeling efficiency compared to dendritic cells. Therefore, the NP loading protocol had to be adapted to the different conditions. Nevertheless, after increasing NP concentration we even reached almost the same level of incorporation as shown for human professional APC such as DCs. The second day after antigen-specific stimulation resulted in the strongest NP uptake by T-cells. We further observed that short-term cultured T cells (i.e. day 14) had an improved capability of taking-up NP compared to T cells from ‘older’ cultures. Functional testing of NP-loaded T cells showed that IFN-γ production and specific cytolysis toward target cells were not adversely affected by NP at low to intermediate concentrations. cLSM and TEM studies indicated that NP were localized in membrane-surrounded vesicles. Although clathrin- and dynamin-mediated endocytosis was involved in NP incorporation, most NP were taken up by a hitherto unidentified, but energy dependent mechanism. Analysis of culture medium with different additives revealed that human serum strongly influenced NP uptake and also NP release. T cells released intracellular NP very rapidly (70-90% during the first 24 hours), which points to the need to escape from vesicles before export to the outside can occur. Preliminary data with biodegradable PBCA capsules revealed that encapsulated cargo molecules can, in principle, escape from the endolysosomal compartment after loading into T lymphocytes. Therefore, those nanovehicles appear as a well-suited tool for the delivery of drugs and other molecules into T lymphocytes for enhancing immunity or to reduce existing misdirected function.

8 References

Ahern, T., Taylor, G. A. and Sanderson, C. J. (1976). An evaluation of an assay for DNA synthesis in lymphocytes with [3H]thymidine and harvesting on to glass fibre filter discs. J Immunol Methods 10(4): 329-336.

Albert, M. L., Jegathesan, M. and Darnell, R. B. (2001). Dendritic cell maturation is required for the cross-tolerization of CD8+ T cells. Nat Immunol 2(11): 1010-1017.

Albrecht, J., Frey, M., Teschner, D., Carbol, A., Theobald, M., Herr, W. and Distler, E. (2011). IL-21-treated naive CD45RA+CD8+ T cells represent a reliable source for producing leukemia-reactive cytotoxic T lymphocytes with high proliferative potential and early differentiation phenotype. Cancer Immunol Immunother 60(2): 235-248.

Andersen, M. H., Schrama, D., thor Straten, P. and Becker, J. C. (2006). Cytotoxic T Cells. J Invest Dermatol 126(1): 32-41.

Anderson, R. (1998). The caveolae membrane system. Annu Rev Biochem 67: 199-225.

Anderson, S. A., Shukaliak-Quandt, J., Jordan, E. K., Arbab, A. S., Martin, R., McFarland, H. and Frank, J. A. (2004). Magnetic resonance imaging of labeled T-cells in a mouse model of multiple sclerosis. Annals Neurol 55(5): 654-659.

Arbab, A. S., Bashaw, L. A., Miller, B. R., Jordan, E. K., Bulte, J. W. M. and Frank, J. A. (2003). Intracytoplasmic tagging of cells with ferumoxides and transfection agent for cellular magnetic resonance imaging after cell transplantation: methods and techniques. Transplantation 76(7): 1123-1130.

Arbab, A. S., Yocum, G. T., Kalish, H., Jordan, E. K., Anderson, S. A., Khakoo, A. Y., Read, E. J. and Frank, J. A. (2004). Efficient magnetic cell labeling with protamine sulfate complexed to ferumoxides for cellular MRI. Blood 104(4): 1217-1223.

Baier, G., Musyanovych, A., Dass, M., Theisinger, S. and Landfester, K. (2010). Cross-Linked Starch Capsules Containing dsDNA Prepared in Inverse Miniemulsion as “Nanoreactors” for Polymerase Chain Reaction. Biomacromolecules 11(4): 960-968.

Baier, G., Musyanovych, A., Landfester, K., Best, A., Lorenz, S. and Mailänder, V. (2011). DNA Amplification via Polymerase Chain Reaction Inside Miniemulsion Droplets with Subsequent Poly(n-butylcyanoacrylate) Shell Formation and Delivery of Polymeric Capsules into Mammalian Cells. Macromol Biosci 11(8): 1099-1109.

Basu, S., Harfouche, R., Soni, S., Chimote, G., Mashelkar, R. A. and Sengupta, S. (2009). Nanoparticle-mediated targeting of MAPK signaling predisposes tumor to chemotherapy. Proc Nat Acad Sci 106(19): 7957-7961.

Baumjohann, D. and Lutz, M. B. (2006). Non-invasive imaging of dendritic cell migration in vivo. Immunobiol 211(6-8): 587-597.

Beer, A., Holzapfel, K., Neudorfer, J., Piontek, G., Settles, M., Krönig, H., Peschel, C., Schlegel, J., Rummeny, E. and Bernhard, H. (2008). Visualization of antigen-specific human cytotoxic T lymphocytes labeled with superparamagnetic iron-oxide particles. European Radiology 18(6): 1087-1095.

Beilhack, A., Schulz, S., Baker, J., Beilhack, G. F., Nishimura, R., Baker, E. M., Landan, G., Herman, E. I., Butcher, E. C., Contag, C. H. and Negrin, R. S. (2008). Prevention of acute graft-versus-host disease by blocking T-cell entry to secondary lymphoid organs. Blood 111(5): 2919-2928.

Bender, A., Bui, L., Feldman, M., Larsson, M. and Bhardwaj, N. (1995). Inactivated influenza virus, when presented on dendritic cells, elicits human CD8+ cytolytic T cell responses. J Exp Med. 182 (6): 1663-71.

Bettelli, E., Korn, T. and Kuchroo, V. K. (2007). Th17: the third member of the effector T cell trilogy. Curr Opin Immunol 19(6): 652-657.

Blattman, J. and Greenberg, P. (2004). Cancer immunotherapy: a treatment for the masses. Science 305(5681): 200-5.

Bleakley, M. and Riddell, S. R. (2004). Molecules and mechanisms of the graft-versus-leukaemia effect. Nat Rev Cancer 4(5): 371-380.

Bollard, C. M., Aguilar, L., Straathof, K. C., Gahn, B., Huls, M. H., Rousseau, A., Sixbey, J., Gresik, M. V., Carrum, G., Hudson, M., Dilloo, D., Gee, A., Brenner, M. K., Rooney, C. M. and Heslop, H. E. (2004). Cytotoxic T Lymphocyte Therapy for Epstein-Barr Virus+ Hodgkin's Disease. J Exp Med 200(12): 1623-1633.

Britten, C. M., Meyer, R. G., Kreer, T., Drexler, I., Wölfel, T. and Herr, W. (2002). The use of HLA-A*0201-transfected K562 as standard antigen-presenting cells for CD8+ T lymphocytes in IFN-γ ELISPOT assays. J Immunol Methods 259: 95-110.

Burgdorf, S., Scholz, C., Kautz, A., Tampe, R. and Kurts, C. (2008). Spatial and mechanistic separation of cross-presentation and endogenous antigen presentation. Nat Immunol 9(5): 558-566.

Cambi, A., Lidke, D. S., Arndt-Jovin, D. J., Figdor, C. G. and Jovin, T. M. (2007). Ligand-Conjugated Quantum Dots Monitor Antigen Uptake and Processing by Dendritic Cells. Nano Lett 7(4): 970-977.

Casella, J. F., Flanagan, M. D. and Lin, S. (1981). Cytochalasin D inhibits actin polymerization and induces depolymerization of actin filaments formed during platelet shape change. Nature 293(5830): 302-305.

Chithrani, B. D. and Chan, W. C. W. (2007). Elucidating the Mechanism of Cellular Uptake and Removal of Protein-Coated Gold Nanoparticles of Different Sizes and Shapes. Nano Lett 7(6): 1542-1550.

Chithrani, B. D., Ghazani, A. A. and Chan, W. C. W. (2006). Determining the Size and Shape Dependence of Gold Nanoparticle Uptake into Mammalian Cells. Nano Lett 6(4): 662-668.

Clemente-Casares, X., Tsai, S., Yang, Y. and Santamaria, P. (2011). Peptide-MHC-based nanovaccines for the treatment of autoimmunity: a “one size fits all” approach? J Mol Med 89(8): 733-742.

Conner, S. D. and Schmid, S. L. (2003). Regulated portals of entry into the cell. Nature 422(6927): 37-44.

Creusot, R. m. J., Yaghoubi, S. S., Chang, P., Chia, J., Contag, C. H., Gambhir, S. S. and Fathman, C. G. (2009). Lymphoid tissue-specific homing of bone marrow-derived dendritic cells. Blood 113(26): 6638-6647.

Cvetanovich, G. L. and Hafler, D. A. (2010). Human regulatory T cells in autoimmune diseases. Curr Opin Immunol 22(6): 753-760.

Dausend, J., Musyanovych, A., Dass, M., Walther, P., Schrezenmeier, H., Landfester, K. and Mailänder, V. (2008). Uptake Mechanism of Oppositely Charged Fluorescent Nanoparticles in HeLa Cells. Macromol Biosci 8(12): 1135-1143.

Davda, J. and Labhasetwar, V. (2002). Characterization of nanoparticle uptake by endothelial cells. Int J Pharm 233: 51-59.

Davis, M. E., Chen, Z. and Shin, D. M. (2008). Nanoparticle therapeutics: an emerging treatment modality for cancer. Nat Rev Drug Discov 7(9): 771-782.

De Vries, I. J. M., Lesterhuis, W. J., Barentsz, J. O., Verdijk, P., van Krieken, J. H., Boerman, O. C., Oyen, W. J. G., Bonenkamp, J. J., Boezeman, J. B., Adema, G. J., Bulte, J. W. M., Scheenen, T. W. J., Punt, C. J. A., Heerschap, A. and Figdor, C. G. (2005). Magnetic resonance tracking of dendritic cells in melanoma patients for monitoring of cellular therapy. Nat Biotech 23(11): 1407-1413.

Delehanty, J. B., Bradburne, C. E., Boeneman, K., Susumu, K., Farrell, D., Mei, B. C., Blanco-Canosa, J. B., Dawson, G., Dawson, P. E., Mattoussi, H. and Medintz, I. L. (2010). Delivering quantum dot-peptide bioconjugates to the cellular cytosol: escaping from the endolysosomal system. Integr Biol 2: 265-277.

Delves, P. J. and Roitt, I. M. (2000). The Immune System. New Engl J Med 343(1): 37-49.

Delves, P. J. and Roitt, I. M. (2000). The Immune System. New Engl J Med 343(2): 108-117.

Demento, S. L., Eisenbarth, S. C., Foellmer, H. G., Platt, C., Caplan, M. J., Mark Saltzman, W., Mellman, I., Ledizet, M., Fikrig, E., Flavell, R. A. and Fahmy, T. M. (2009). Inflammasome-activating nanoparticles as modular systems for optimizing vaccine efficacy. Vaccine 27(23): 3013-3021.

Distler, E., Bloetz, A., Albrecht, J., Asdufan, S., Hohberger, A., Frey, M., Schnürer, E., Thomas, S., Theobald, M., Hartwig, U. F. and Herr, W. (2011). Alloreactive and leukemia-reactive T cells are preferentially derived from naive precursors in healthy donors: implications for immunotherapy with memory T cells. Haematologica 96(7): 1024-1032.

Distler, E., Wölfel, C., Köhler, S., Nonn, M., Kaus, N., Schnürer, E., Meyer, R. G., Wehler, T. C., Huber, C., Wölfel, T., Hartwig, U. F. and Herr, W. (2008). Acute myeloid leukemia (AML)-reactive cytotoxic T lymphocyte clones rapidly expanded from CD8+ CD62L(high)+ T cells of healthy donors prevent AML engraftment in NOD/SCID IL2Rγ(null) mice. Exp Hematol 36(4): 451-463.

Dodd, C. H., Hsu, H.-C., Chu, W.-J., Yang, P., Zhang, H.-G., Mountz Jr, J. D., Zinn, K., Forder, J., Josephson, L., Weissleder, R., Mountz, J. M. and Mountz, J. D. (2001). Normal T-cell response and in vivo magnetic resonance imaging of T cells loaded with HIV transactivator-peptide-derived superparamagnetic nanoparticles. J Immunol Methods 256(2001): 89-105.

Dörrschuck, A., Schmidt, A., Schnürer, E., Glückmann, M., Albrecht, C., Wölfel, C., Lennerz, V., Lifke, A., Di Natale, C., Ranieri, E., Gesualdo, L., Huber, C., Karas, M., Wölfel, T. and Herr, W. (2004). CD8+ cytotoxic T lymphocytes isolated from allogeneic healthy donors recognize HLA class Ia/Ib–associated renal carcinoma antigens with ubiquitous or restricted tissue expression. Blood 104(8): 2591-2599.

Dudley, M. E. and Rosenberg, S. A. (2003). Adoptive-cell-transfer therapy for the treatment of patients with cancer. Nat Rev Cancer 3(9): 666-675.

Elamanchili, P., Diwan, M., Cao, M. and Samuel, J. (2004). Characterization of poly(d,l-lactic-co-glycolic acid) based nanoparticulate system for enhanced delivery of antigens to dendritic cells. Vaccine 22(19): 2406-2412.

Elamanchili, P., Lutsiak, C. M. E., Hamdy, S., Diwan, M. and Samuel, J. (2007). Pathogen-Mimicking Nanoparticles for Vaccine Delivery to Dendritic Cells. J Immunother 30(4): 378-395 10.1097/CJI.0b013e31802cf3e3.

Eskandari, M., Ozturk, O., Eskandari, H., Balli, E. and Yilmaz, C. (2006). Cyanoacrylate adhesive provides efficient local drug delivery. Clin Orthop Relat Res (451): 242-250.

Faria, M. C. F., de Almeida, F. M., Serrao, M. L., de Oliveira Almeida, N. K. and Labarthe, N. (2005). Use of cyanoacrylate in skin closure for ovariohysterectomy in a population control programme. J Feline Medi Surg 7(2): 71-75.

Fischer, S., Uetz-von Allmen, E., Waeckerle-Men, Y., Groettrup, M., Merkle, H. P. and Gander, B. (2007). The preservation of phenotype and functionality of dendritic cells upon phagocytosis of polyelectrolyte-coated PLGA microparticles. Biomaterials 28(6): 994-1004.

Gekle, M., Freudinger, R. and Mildenberger, S. (2001). Inhibition of Na+-H+ exchanger-3 interferes with apical receptor-mediated endocytosis via vesicle fusion. J Physiol 531(3): 619-629.

Gilboa, E. (2007). DC-based cancer vaccines. J Clin Invest 117(5): 1195-1203.

Goulmy, E. (2006). Minor Histocompatibility Antigens: from Transplantation Problems to Therapy of Cancer. Hum Immunol 67(6): 433-438.

Greenwald, R. J., Freeman, G. J. and Sharpe, A. H. (2005). The B7 family revisited. Annu Rev Immunol 23: 515-548.

Greiner, J., Schmitt, M., Li, L., Giannopoulos, K., Bosch, K., Schmitt, A., Dohner, K., Schlenk, R. F., Pollack, J. R., Dohner, H. and Bullinger, L. (2006). Expression of tumor-associated antigens in acute myeloid leukemia: implications for specific immunotherapeutic approaches. Blood 108(13): 4109-4117.

Haag, R. and Kratz, F. (2006). Polymer Therapeutics: Concepts and Applications. Angewandte Chemie International Edition 45(8): 1198-1215.

Hammer, G. E., Gonzalez, F., Champsaur, M., Cado, D. and Shastri, N. (2006). The aminopeptidase ERAAP shapes the peptide repertoire displayed by major histocompatibility complex class I molecules. Nat Immunol 7(1): 103-112.

Han, T. H., Jin, P., Ren, J., Slezak, S., Marincola, F. M. and Stroncek, D. F. (2009). Evaluation of 3 Clinical Dendritic Cell Maturation Protocols Containing Lipopolysaccharide and Interferon-γ. J Immunother 32(4): 399-407

He, C., Hu, Y., Yin, L., Tang, C. and Yin, C. (2010). Effects of particle size and surface charge on cellular uptake and biodistribution of polymeric nanoparticles. Biomaterials 31(13): 3657-3666.

Heath, W. R., Belz, G. T., Behrens, G. M. N., Smith, C. M., Forehan, S. P., Parish, I. A., Davey, G. M., Wilson, N. S., Carbone, F. R. and Villadangos, J. A. (2004). Cross-presentation, dendritic cell subsets, and the generation of immunity to cellular antigens. Immunol Rev 199(1): 9-26.

Herr, W., Linn, B., Leister, N., Wandel, E., Meyer zum Büschenfelde, K.-H. and Wölfel, T. (1997). The use of computer-assisted video image analysis for the quantification of CD8+ T lymphocytes producing tumor necrosis factor α spots in response to peptide antigens. J Immunol Methods 203(2): 141-152.

Herr, W., Ranieri, E., Olson, W., Zarour, H., Gesualdo, L. and Storkus, W. J. (2000). Mature dendritic cells pulsed with freeze-thaw cell lysates define an effective in vitro vaccine designed to elicit EBV-specific CD4+ and CD8+ T lymphocyte responses. Blood 96(5): 1857-1864.

Hinrichs, C. S., Borman, Z. A., Gattinoni, L., Yu, Z., Burns, W. R., Huang, J., Klebanoff, C. A., Johnson, L. A., Kerkar, S. P., Yang, S., Muranski, P., Palmer, D. C., Scott, C. D., Morgan, R. A., Robbins, P. F., Rosenberg, S. A. and Restifo, N. P. (2011). Human effector CD8+ T cells derived from naive rather than memory subsets possess superior traits for adoptive immunotherapy. Blood 117(3): 808-814.

Hinrichs, C. S., Gattinoni, L. and Restifo, N. P. (2006). Programming CD8+ T cells for effective immunotherapy. Curr Opin Immunol 18(3): 363-370.

Holzapfel, V., Lorenz, M., Weiss, C. K., Landfester, H. S. and Mailänder, V. (2006). Synthesis and biomedical applications of functionalized fluorescent and magnetic dual reporter nanoparticles as obtained in the miniemulsion process. J Phys: Condens Matter 18(38): 2581-2594.

Holzapfel, V., Musyanovych, A., Landfester, K., Lorenz, M. R. and Mailänder, V. (2005). Preparation of Fluorescent Carboxyl and Amino-functionalized Polystyrene Particles by Miniemulsion Polymerization as Markers for Cells. Macromol Chem Phys 206(24): 2440-2449.

Iida, H., Takayanagi, K., Nakanishi, T., Kume, A., Muramatsu, K., Kiyohara, Y., Akiyama, Y. and Osaka, T. (2008). Preparation of human immune effector T cells containing iron-oxide nanoparticles. Biotechnol Bioeng 101(6): 1123-1128.

Ishimoto, H., Yanagihara, K., Araki, N., Mukae, H., Sakamoto, N., Izumikawa, K., Seki, M., Miyazaki, Y., Hirakata, Y., Mizuta, Y., Yasuda, K. and Kohno, S. (2008). Single-cell observation of phagocytosis by human blood dendritic cells. Jpn J Infect Dis 61(4): 294-97.

Issa, F., Schiopu, A. and Wood, K. J. (2010). Role of T cells in graft rejection and transplantation tolerance. Exp Rev Clin Immunol 6(1): 155-169.

Ito, A. and Kobayashi, T. (2008). Intracellular Hyperthermia Using Magnetic Nanoparticles : A Novel Method for Hyperthermia Clinical Applications. Therm Med 24(4): 113-129.

Iversen, T.-G., Skotland, T. and Sandvig, K. (2011). Endocytosis and intracellular transport of nanoparticles: Present knowledge and need for future studies. Nano Today 6(2): 176-185.

Janeway, C. (2008). Immunobiology. Garland Science New York.

Janic, B., Rad, A. M., Jordan, E. K., Iskander, A. S. M., Ali, M. M., Varma, N. R. S., Frank, J. A. and Arbab, A. S. (2009). Optimization and Validation of FePro Cell Labeling Method. PLoS ONE 4(6): e5873.

Jiang, H. and Chess, L. (2006). Regulation of Immune Responses by T Cells. New Engl J Med 354(11): 1166-1176.

Jiang, X., Musyanovych, A., Rocker, C., Landfester, K., Mailander, V. and Nienhaus, G. U. (2011). Specific effects of surface carboxyl groups on anionic polystyrene particles in their interactions with mesenchymal stem cells. Nanoscale 3(5): 2028-2035.

Johannsen, M., Gneveckow, U., Eckelt, L., Feussner, A., Waldöfner, N., Scholz, R., Deger, S., Wust, P., Loening, S. and Jordan, A. (2005). Clinical hyperthermia of prostate cancer using magnetic nanoparticles: presentation of a new interstitial technique. Int J Hyperthermia 21(7): 637-47.

Kaufman, C. L., Williams, M., Madison Ryle, L., Smith, T. L., Tanner, M. and Ho, C. (2003). Superparamagnetic iron oxide particles transactivator protein-fluorescein isothiocyanate particle labeling for in vivo magnetic resonance imaging detection of cell migration: uptake and durability. Transplantation 76(7): 1043-1046.

Kavurma, M. M. and Khachigian, L. M. (2002). Signaling and transcriptional control of Fas ligand gene expression. Cell Death Differ 10(1): 36-44.

Kircher, M. F., Allport, J. R., Graves, E. E., Love, V., Josephson, L., Lichtman, A. H. and Weissleder, R. (2003). In Vivo High Resolution Three-Dimensional Imaging of Antigen-Specific Cytotoxic T-Lymphocyte Trafficking to Tumors. Cancer Res 63(20): 6838-6846.

Kirkham, M. and Parton, R. G. (2005). Clathrin-independent endocytosis: New insights into caveolae and non-caveolar lipid raft carriers. BBA - Mol Cell Res 1746(3): 350-363.

Kitawaki, T., Kadowaki, N., Kondo, T., Ishikawa, T., Ichinohe, T., Teramukai, S., Fukushima, M., Kasai, Y., Maekawa, T. and Uchiyama, T. (2008). Potential of dendritic cell immunotherapy for relapse after allogeneic hematopoietic stem cell transplantation, shown by WT1 peptide- and keyhole limpet hemocyanin-pulsed, donor-derived dendritic cell vaccine for acute myeloid leukemia. Am J Hematol 83(4): 315-317.

Klebanoff, C. A., Gattinoni, L. and Restifo, N. P. (2006). CD8+ T-cell memory in tumor immunology and immunotherapy. Immunol Rev 211(1): 214-224.

Klein, J. and Sato, A. (2000). The HLA System. New Engl J Med 343(11): 782-786.

Klein, J. and Sato, A. (2000). The HLA System. New Engl J Med 343(10): 702-709.

Klenerman, P., Cerundolo, V. and Dunbar, P. R. (2002). Tracking T cells with tetramers: new tales from new tools. Nat Rev Immunol 2(4): 263-272.

Kolb, H.-J. (2008). Graft-versus-leukemia effects of transplantation and donor lymphocytes. Blood 112(12): 4371-4383.

Kolb, H. J., Schattenberg, A., Goldman, J. M., Hertenstein, B., Jacobsen, N., Arcese, W., Ljungman, P., Ferrant, A., Verdonck, L. and Niederwieser, D. (1995). Graft-versus-leukemia effect of donor lymphocyte transfusions in marrow grafted patients. Blood 86(5): 2041-2050.

Lacroix, L. M., Malaki, R. B., Carrey, J., Lachaize, S., Respaud, M., Goya, G. F. and Chaudret, B. (2009). Magnetic hyperthermia in single-domain monodisperse FeCo nanoparticles: Evidences for Stoner--Wohlfarth behavior and large losses. J Appl Phys 105(2): 023911-4.

Lai, S. K., Hida, K., Man, S. T., Chen, C., Machamer, C., Schroer, T. A. and Hanes, J. (2007). Privileged delivery of polymer nanoparticles to the perinuclear region of live cells via a non-clathrin, non-degradative pathway. Biomaterials 28(18): 2876-2884.

Landfester, K. (2001). Polyreactions in Miniemulsions. Macromol Rapid Comm 22(12): 896-936.

Landfester, K. (2009). Miniemulsion Polymerization and the Structure of Polymer and Hybrid Nanoparticles. Angewandte Chemie International Edition 48(25): 4488-4507.

Li, J.-L., Wang, L., Liu, X.-Y., Zhang, Z.-P., Guo, H.-C., Liu, W.-M. and Tang, S.-H. (2009). In vitro cancer cell imaging and therapy using transferrin-conjugated gold nanoparticles. Cancer Letters 274(2): 319-326.

Lim, Y. T., Noh, Y.-W., Han, J. H., Cai, Q.-Y., Yoon, K.-H. and Chung, B. H. (2008). Biocompatible Polymer-Nanoparticle-Based Bimodal Imaging Contrast Agents for the Labeling and Tracking of Dendritic Cells. Small 4(10): 1640-1645.

Limbach, L., Bereiter, R., Müller, E., Krebs, R., Galli, R. and Stark, W. (2008). Removal of oxide nanoparticles in a model wastewater treatment plant: influence of agglomeration and surfactants on clearing efficiency. Environ Sci Technol. 42(15): 5828-33.

Lorenz, M. R., Holzapfel, V., Musyanovych, A., Nothelfer, K., Walther, P., Frank, H., Landfester, K., Schrezenmeier, H. and Mailänder, V. (2006). Uptake of functionalized, fluorescent-labeled polymeric particles in different cell lines and stem cells. Biomaterials 27(14): 2820-2828.

Lorenz, M. R., Kohnle, M.-V., Dass, M., Walther, P., Höcherl, A., Ziener, U., Landfester, K. and Mailänder, V. (2008). Synthesis of Fluorescent Polyisoprene Nanoparticles and their Uptake into Various Cells. Macromol Biosci 8(8): 711-727.

Lorenz, S., Tomcin, S. and Mailänder, V. (2011). Staining of Mitochondria with Cy5-Labeled Oligonucleotides for Long-Term Microscopy Studies. Microscopy and Microanalysis 17(03): 440-445.

Lu, J. J., Langer, R. and Chen, J. (2009). A Novel Mechanism Is Involved in Cationic Lipid-Mediated Functional siRNA Delivery. Mol Pharm 6(3): 763-771.

Lunov, O., Syrovets, T., Loos, C., Beil, J., Delacher, M., Tron, K., Nienhaus, G. U., Musyanovych, A., Mailänder, V., Landfester, K. and Simmet, T. (2011). Differential Uptake of Functionalized Polystyrene Nanoparticles by Human Macrophages and a Monocytic Cell Line. ACS Nano 5(3): 1657-1669.

Macho-Fernandez, E., Chang, J., Fontaine, J., Bialecki, E., Rodriguez, F., Werkmeister, E., Krieger, V., Ehret, C., Heurtault, B. a., Fournel, S., Frisch, B., Betbeder, D., Faveeuw, C. and Trottein, F. (2012). Activation of invariant Natural Killer T lymphocytes in response to the galactosylceramide analogue KRN7000 encapsulated in PLGA-based nanoparticles and microparticles. Int J Pharm 423(1): 45-54.

Macia, E., Ehrlich, M., Massol, R., Boucrot, E., Brunner, C. and Kirchhausen, T. (2006). Dynasore, a Cell-Permeable Inhibitor of Dynamin. Develop Cell 10(6): 839-850.

Mackensen, A., Herbst, B., Chen, J.-L., Köhler, G., Noppen, C., Herr, W., Spagnoli, G. C., Cerundolo, V. and Lindemann, A. (2000). Phase I study in melanoma patients of a vaccine with peptide-pulsed dendritic cells generated in vitro from CD34+ hematopoietic progenitor cells. Int J Cancer 86(3): 385-392.

Mailänder, V. and Landfester, K. (2009). Interaction of Nanoparticles with Cells. Biomacromolecules 10(9): 2379-2400.

Manolova, V., Flace, A., Bauer, M., Schwarz, K., Saudan, P. and Bachmann, M. F. (2008). Nanoparticles target distinct dendritic cell populations according to their size. Eur J Immunol 38(5): 1404-1413.

Marijt, E., Wafelman, A., van der Hoorn, M., van Bergen, C., Bongaerts, R., van Luxemburg-Heijs, S., van den Muijsenberg, J., Wolbers, J. O., van der Werff, N., Willemze, R. and Falkenburg, F. (2007). Phase I/II feasibility study evaluating the generation of leukemia-reactive cytotoxic T lymphocyte lines for treatment of patients with relapsed leukemia after allogeneic stem cell transplantation. Haematologica 92(1): 72-80.

Masilamani, M., Narayanan, S., Prieto, M., Borrego, F. and Coligan, J. E. (2008). Uncommon Endocytic and Trafficking Pathway of the Natural Killer Cell CD94/NKG2A Inhibitory Receptor. Traffic 9(6): 1019-1034.

Matuszewski, L., Persigehl, T., Wall, A., Schwindt, W., Tombach, B., Fobker, M., Poremba, C., Ebert, W., Heindel, W. and Bremer, C. (2005). Cell Tagging with Clinically Approved Iron Oxides: Feasibility and Effect of Lipofection, Particle Size, and Surface Coating on Labeling Efficiency1. Radiology 235(1): 155-161.

Merad, M., Hoffmann, P., Ranheim, E., Slaymaker, S., Manz, M. G., Lira, S. A., Charo, I., Cook, D. N., Weissman, I. L., Strober, S. and Engleman, E. G. (2004). Depletion of host Langerhans cells before transplantation of donor alloreactive T cells prevents skin graft-versus-host disease. Nat Med 10(5): 510-517.

Miltenyi, S., Müller, W., Weichel, W. and Radbruch, A. (1990). High gradient magnetic cell separation with MACS. Cytometry 11(2): 231-238.

Moore, A., Zhe Sun, P., Cory, D., Högemann, D., Weissleder, R. and Lipes, M. A. (2002). MRI of insulitis in autoimmune diabetes. Magnet Reson Med 47(4): 751-758.

Mou, Y., Hou, Y., Chen, B., Hua, Z., Zhang, Y., Xie, H., Xia, G., Wang, Z., Huang, X., Han, W., Ni, Y. and Hu, Q. (2011). In vivo migration of dendritic cells labeled with synthetic superparamagnetic iron oxide. Int J Nanomed 6(1): 2633-2640.

Muro, S., Cui, X., Gajewski, C., Murciano, J.-C., Muzykantov, V. R. and Koval, M. (2003). Slow intracellular trafficking of catalase nanoparticles targeted to ICAM-1 protects endothelial cells from oxidative stress. Am J Physiol - Cell Physiol 285(5): C1339-C1347.

Musyanovych, A. and Landfester, K. (2008). Synthesis of Poly(butylcyanoacrylate) Nanocapsules by Interfacial Polymerization in Miniemulsions for the Delivery of DNA Molecules. Prog Coll Pol Sci 134: 120-127.

Musyanovych, A., Rossmanith, R., Tontsch, C. and Landfester, K. (2007). Effect of Hydrophilic Comonomer and Surfactant Type on the Colloidal Stability and Size Distribution of Carboxyl- and Amino-Functionalized Polystyrene Particles Prepared by Miniemulsion Polymerization. Langmuir 23(10): 5367-5376.

Musyanovych, A., Schmitz-Wienke, J., Mailänder, V., Walther, P. and Landfester, K. (2008). Preparation of Biodegradable Polymer Nanoparticles by Miniemulsion Technique and Their Cell Interactions. Macromol Biosci 8(2): 127-139.

Nagel, J. and Scarpulla, M. (2010). Enhanced absorption in optically thin solar cells by scattering from embedded dielectric nanoparticles. Opt Express 18(S2): 139-146.

Nel, A., Xia, T., Mädler, L. and Li, N. (2006). Toxic Potential of Materials at the Nanolevel. Science 311(5761): 622-627.

Niemeyer, M., Oostendorp, R., Kremer, M., Hippauf, S., Jacobs, V., Baurecht, H., Ludwig, G., Piontek, G., Bekker-Ruz, V., Timmer, S., Rummeny, E., Kiechle, M. and Beer, A. (2010). Non-invasive tracking of human haemopoietic CD34+ stem cells in vivo in immunodeficient mice by using magnetic resonance imaging. Eur Radiol 20(9): 2184-2193.

Noh, Y.-W., Lim, Y. T. and Chung, B. H. (2008). Noninvasive imaging of dendritic cell migration into lymph nodes using near-infrared fluorescent semiconductor nanocrystals. FASEB J 22(11): 3908-3918.

Nylander, S. and Kalies, I. (1999). Brefeldin A, but not monensin, completely blocks CD69 expression on mouse lymphocytes: efficacy of inhibitors of protein secretion in protocols for intracellular cytokine staining by flow cytometry. J Immunol Methods 224(1-2): 69-76.

O'Neill, D. (2010). Dendritic cells and T cells in immunotherapy. J Drugs Dermatol. 9(11): 1383-92.

O'Neill, D. W., Adams, S. and Bhardwaj, N. (2004). Manipulating dendritic cell biology for the active immunotherapy of cancer. Blood 104(8): 2235-2246.

Palucka, K., Ueno, H., Zurawski, G., Fay, J. and Banchereau, J. (2010). Building on dendritic cell subsets to improve cancer vaccines. Curr Opin Immunol 22(2): 258-263.

Panyam, J. and Labhasetwar, V. (2003). Biodegradable nanoparticles for drug and gene delivery to cells and tissue. Adv Drug Del Rev 55(3): 329-347.

Panyam, J., Zhou, W.-Z., Prabha, S., Sahoo, S. K. and Labhasetwar, V. (2002). Rapid endo-lysosomal escape of poly(DL-lactide-co-glycolide) nanoparticles: implications for drug and gene delivery. FASEB J 16(10): 1217-1226.

Parkin, J. and Cohen, B. (2001). An overview of the immune system. The Lancet 357(9270): 1777-1789.

Pedrazzoli, P., Comoli, P., Montagna, D., Demirer, T. and Bregni, M. (2011). Is adoptive T-cell therapy for solid tumors coming of age? Bone Marrow Transplant: 1-7; doi: 10.1038/bmt.2011.155

Petros, R. A. and DeSimone, J. M. (2010). Strategies in the design of nanoparticles for therapeutic applications. Nat Rev Drug Discov 9(8): 615-627.

Philpott, N. J., Turner, A. J., Scopes, J., Westby, M., Marsh, J. C., Gordon-Smith, E. C., Dalgleish, A. G. and Gibson, F. M. (1996). The use of 7-amino actinomycin D in identifying apoptosis: simplicity of use and broad spectrum of application compared with other techniques. Blood 87(6): 2244-2251.

Pinzon-Charry, A., Maxwell, T. and Lopez, J. A. (2005). Dendritic cell dysfunction in cancer: A mechanism for immunosuppression. Immunol Cell Biol 83(5): 451-461.

Porter, D. L., Levine, B. L., Kalos, M., Bagg, A. and June, C. H. (2011). Chimeric Antigen Receptor-Modified T Cells in Chronic Lymphoid Leukemia. New Engl J Med 365(8): 725-733.

Pure, E., Allison, J. P. and Schreiber, R. D. (2005). Breaking down the barriers to cancer immunotherapy. Nat Immunol 6(12): 1207-1210.

Qiu, Z., Tufaro, F. and Gillam, S. (1995). Brefeldin A and monensin arrest cell surface expression of membrane glycoproteins and release of rubella virus. J Gen Virol 76(4): 855-863.

Quinn, P. J. (2010). A lipid matrix model of membrane raft structure. Prog Lipid Res 49(4): 390-406.
Rabolli, V., Thomassen, L. C. J., Princen, C., Napierska, D., Gonzalez, L., Kirsch-Volders, M., Hoet, P. H., Huaux, F. o., Kirschhock, C. E. A., Martens, J. A. and Lison, D. (2010). Influence of size, surface area and microporosity on the in vitro cytotoxic activity of amorphous silica nanoparticles in different cell types. Nanotoxicology 4(3): 307-318.

Ranieri, E., Herr, W., Gambotto, A., Olson, W., Rowe, D., Robbins, P., Salvucci Kierstead, L., Watkins, S., Gesualdo, L. and Storkus, W. (1999). Dendritic Cells Transduced with an Adenovirus Vector Encoding Epstein-Barr Virus Latent Membrane Protein 2B: a New Modality for Vaccination. J Virol. 73(12): 10416-25.

Raynal, I., Prigent, P., Peyramaure, S., Najid, A., Rebuzzi, C. c. and Corot, C. (2004). Macrophage Endocytosis of Superparamagnetic Iron Oxide Nanoparticles: Mechanisms and Comparison of Ferumoxides and Ferumoxtran-10. Invest Radiol 39(1): 56-63.

Rejman, J., Oberle, V., Zuhorn, I. and Hoekstra, D. (2004). Size-dependent internalization of particles via the pathways of clathrin- and caveolae-mediated endocytosis. Biochem J 377(1): 159-169.

Röcker, C., Potzl, M., Zhang, F., Parak, W. J. and Nienhaus, G. U. (2009). A quantitative fluorescence study of protein monolayer formation on colloidal nanoparticles. Nat Nano 4(9): 577-580.

Rooney, C. M., Smith, C. A., Ng, C. Y. C., Loftin, S. K., Sixbey, J. W., Gan, Y., Srivastava, D.-K., Bowman, L. C., Krance, R. A., Brenner, M. K. and Heslop, H. E. (1998). Infusion of Cytotoxic T Cells for the Prevention and Treatment of Epstein-Barr Virus Induced Lymphoma in Allogeneic Transplant Recipients. Blood 92(5): 1549-1555.

Rosenberg, S. A. (2004). Shedding Light on Immunotherapy for Cancer. New Engl J Med 350(14): 1461-1463.

Rosenberg, S. A., Packard, B. S., Aebersold, P. M., Solomon, D., Topalian, S. L., Toy, S. T., Simon, P., Lotze, M. T., Yang, J. C., Seipp, C. A., Simpson, C., Carter, C., Bock, S., Schwartzentruber, D., Wei, J. P. and White, D. E. (1988). Use of Tumor-Infiltrating Lymphocytes and Interleukin-2 in the Immunotherapy of Patients with Metastatic Melanoma. New Engl J Med 319(25): 1676-1680.

Rosenberg, S. A., Restifo, N. P., Yang, J. C., Morgan, R. A. and Dudley, M. E. (2008). Adoptive cell transfer: a clinical path to effective cancer immunotherapy. Nat Rev Cancer 8(4): 299-308.

Sallusto, F., Geginat, J. and Lanzavecchia, A. (2004). Central Memory and Effector Memory T Cell Subsets: Function, Generation, and Maintenance. Annu Rev Immunol 22(1): 745-763.

Savina, A. and Amigorena, S. (2007). Phagocytosis and antigen presentation in dendritic cells. Immunol Rev 219(1): 143-156.

Schneider, U., Schwenk, H.-U. and Bornkamm, G. (1977). Characterization of EBV-genome negative “null” and “T” cell lines derived from children with acute lymphoblastic leukemia and leukemic transformed non-Hodgkin lymphoma. Int J Cancer 19(5): 621-626.

Scientific Committee on Emerging and Newly Identified Health Risks (SCENIHR; 2010). Scientific basis for the definition of the term "nanomaterial". From: http://ec.europa.eu/health/scientific_committees/emerging/docs/scenihr_o_030.pdf

Sêe, V., Free, P., Cesbron, Y., Nativo, P., Shaheen, U., Rigden, D. J., Spiller, D. G., Fernig, D. G., White, M. R. H., Prior, I. A., Brust, M., Lounis, B. and Lêvy, R. (2009). Cathepsin L Digestion of Nanobioconjugates upon Endocytosis. ACS Nano 3(9): 2461-2468.

Sen, D., Deerinck, T. J., Ellisman, M. H., Parker, I. and Cahalan, M. D. (2008). Quantum Dots for Tracking Dendritic Cells and Priming an Immune Response in Vitro and in Vivo. PLoS ONE 3(9): e3290, 1-13.

Sieczkarski, S. B. and Whittaker, G. R. (2002). Dissecting virus entry via endocytosis. J Gen Virol 83(7): 1535-1545.

Simberg, D., Park, J.-H., Karmali, P. P., Zhang, W.-M., Merkulov, S., McCrae, K., Bhatia, S. N., Sailor, M. and Ruoslahti, E. (2009). Differential proteomics analysis of the surface heterogeneity of dextran iron oxide nanoparticles and the implications for their in vivo clearance. Biomaterials 30(23-24): 3926-3933.

Smirnov, P., Lavergne, E., Gazeau, F., Lewin, M., Boissonnas, A., Doan, B.-T., Gillet, B., Combadière, C., Combadière, B. and Clément, O. (2006). In vivo cellular imaging of lymphocyte trafficking by MRI: A tumor model approach to cell-based anticancer therapy. Magn Reson Med 56(3): 498-508.

Steinfeld, U., Pauli, C., Kaltz, N., Bergemann, C. and Lee, H.-H. (2006). T lymphocytes as potential therapeutic drug carrier for cancer treatment. Int J Pharm 311(1-2): 229-236.

Steinman, R. M. and Banchereau, J. (2007). Taking dendritic cells into medicine. Nature 449(7161): 419-426.

Tacken, P. J., de Vries, I. J. M., Torensma, R. and Figdor, C. G. (2007). Dendritic-cell immunotherapy: from ex vivo loading to in vivo targeting. Nat Rev Immunol 7(10): 790-802.

Tatsumi, E. (1992). Epstein-Barr virus (EBV) and human hematopoietic cell lines: a review. Hum Cell 5(1): 79-86.

Tenzer, S., Docter, D., Rosfa, S., Wlodarski, A., Kuharev, J., Rekik, A., Knauer, S. K., Bantz, C., Nawroth, T., Bier, C., Sirirattanapan, J., Mann, W., Treuel, L., Zellner, R., Maskos, M., Schild, H. and Stauber, R. H. (2011). Nanoparticle Size Is a Critical Physicochemical Determinant of the Human Blood Plasma Corona: A Comprehensive Quantitative Proteomic Analysis. ACS Nano 5(9): 7155-7167.

Torchilin, V. (2000). Drug targeting. Eur J Pharm Sci 11(S2): 81-91.

Thomas, S. and Herr, W. (2011). Natural and adoptive T-cell immunity against herpes family viruses after allogeneic hematopoietic stem cell transplantation. Immunotherapy 3(6): 771-788.

Trent, J. S., Scheinbeim, J. I. and Couchman, P. R. (1983). Ruthenium tetraoxide staining of polymers for electron microscopy. Macromolecules 16(4): 589-598.
Trowsdale, J. (1995). Both man & bird & beast: comparative organization of MHC genes. Immunogenetics 41(1): 1-17.

Turtle, C. J., Swanson, H. M., Fujii, N., Estey, E. H. and Riddell, S. R. (2009). A Distinct Subset of Self-Renewing Human Memory CD8+ T Cells Survives Cytotoxic Chemotherapy. Immunity 31(5): 834-844.

Verdijk, P., Aarntzen, E. H. J. G., Lesterhuis, W. J., Boullart, A. C. I., Kok, E., van Rossum, M. M., Strijk, S., Eijckeler, F., Bonenkamp, J. J., Jacobs, J. F. M., Blokx, W., vanKrieken, J. H. J. M., Joosten, I., Boerman, O. C., Oyen, W. J. G., Adema, G., Punt, C. J. A., Figdor, C. G. and de Vries, I. J. M. (2009). Limited Amounts of Dendritic Cells Migrate into the T-Cell Area of Lymph Nodes but Have High Immune Activating Potential in Melanoma Patients. Clin Cancer Res 15(7): 2531-2540.

Villadangos, J. (2001). Presentation of antigens by MHC class II molecules: getting the most out of them. Mol Immunol 38(5): 329-346.

Villadangos, J. A. and Schnorrer, P. (2007). Intrinsic and cooperative antigen-presenting functions of dendritic-cell subsets in vivo. Nat Rev Immunol 7(7): 543-555.

Volpe, E., Servant, N., Zollinger, R., Bogiatzi, S. I., Hupe, P., Barillot, E. and Soumelis, V. (2008). A critical function for transforming growth factor-[beta], interleukin 23 and proinflammatory cytokines in driving and modulating human TH-17 responses. Nat Immunol 9(6): 650-657.

Wadia, J. S., Stan, R. V. and Dowdy, S. F. (2004). Transducible TAT-HA fusogenic peptide enhances escape of TAT-fusion proteins after lipid raft macropinocytosis. Nat Med 10(3): 310-315.

Walter, E. A., Greenberg, P. D., Gilbert, M. J., Finch, R. J., Watanabe, K. t. S., Thomas, E. D. and Riddell, S. R. (1995). Reconstitution of Cellular Immunity against Cytomegalovirus in Recipients of Allogeneic Bone Marrow by Transfer of T-Cell Clones from the Donor. New Engl J Med 333(16): 1038-1044.

Wang, Y. (2011). Superparamagnetic iron oxide based MRI contrast agents: Current status of clinical application. Quant Imaging Med Surg 1: 35-40.

Wang, L., Nagesha, D., Selvarasah, S., Dokmeci, M. and Carrier, R. (2008). Toxicity of CdSe Nanoparticles in Caco-2 Cell Cultures. J Nanobiotechnol 6(1): 11.

Wang, L.-H., Rothberg, K. G. and Anderson, R. G. W. (1993). Mis-assembly of clathrin lattices on endosomes reveals a regulatory switch for coated pit formation. J Cell Biol 123(5): 1107-1117.

Ward, E. S., Martinez, C., Vaccaro, C., Zhou, J., Tang, Q. and Ober, R. J. (2005). From Sorting Endosomes to Exocytosis: Association of Rab4 and Rab11 GTPases with the Fc Receptor, FcRn, during Recycling. Mol Biol Cell 16(4): 2028-2038.

Warren, E. H., Fujii, N., Akatsuka, Y., Chaney, C. N., Mito, J. K., Loeb, K. R., Gooley, T. A., Brown, M. L., Koo, K. K. W., Rosinski, K. V., Ogawa, S., Matsubara, A., Appelbaum, F. R. and Riddell, S. R. (2010). Therapy of relapsed leukemia after allogeneic hematopoietic cell transplantation with T cells specific for minor histocompatibility antigens. Blood 115(19): 3869-3878.

Weaver, C. T., Hatton, R. D., Mangan, P. R. and Harrington, L. E. (2007). IL-17 family cytokines and the expanding diversity of effector T cell lineages. Annu Rev Immunol 25: 821-852.

Weill, C., Biri, S. and Erbacher, P. (2008). Cationic lipid–mediated intracellular delivery of antibodies into live cells. BioTechniques 44(7): 7-11.

Weinstein, S. and Peer, D. (2010). RNAi nanomedicines: challenges and opportunities within the immune system. Nanotechnology 21(23): 232001-232001.

Weiss, C. and Landfester, K. (2010). Miniemulsion Polymerization as a Means to Encapsulate Organic and Inorganic Materials. Adv Polym Sci 233: 185-236.

Weiss, C. K., Lorenz, M. R., Landfester, K. and Mailänder, V. (2007). Cellular Uptake Behavior of Unfunctionalized and Functionalized PBCA Particles Prepared in a Miniemulsion. Macromol Biosci 7(7): 883-896.

Weiss, A., Neuberg, P., Philippot, S., Erbacher, P. and Weill, C. O. (2011). Intracellular peptide delivery using amphiphilic lipid-based formulations. Biotechnol Bioeng 108(10): 2477-2487.

Williams, A., Peh, C. A. and Elliott, T. (2002). The cell biology of MHC class I antigen presentation. Tissue Antigens 59(1): 3-17.

Yang, P.-H., Sun, X., Chiu, J.-F., Sun, H. and He, Q.-Y. (2005). Transferrin-Mediated Gold Nanoparticle Cellular Uptake. Bioconjugate Chemistry 16(3): 494-496.

Yee, C. (2005). Adoptive T cell therapy: Addressing challenges in cancer immunotherapy. J Translat Med 3(1): 17.

Zahr, A. S., Davis, C. A. and Pishko, M. V. (2006). Macrophage Uptake of Core-Shell Nanoparticles Surface Modified with Poly(ethylene glycol). Langmuir 22(19): 8178-8185.

Zhang, N. and Bevan, M. (2011). CD8+ T Cells: Foot Soldiers of the Immune System. Immunity 35(2): 161-168.

Zhao, F., Zhao, Y., Liu, Y., Chang, X., Chen, C. and Zhao, Y. (2011). Cellular Uptake, Intracellular Trafficking, and Cytotoxicity of Nanomaterials. Small 7(10): 1322-1337.

Zhu, J. and Paul, W. E. (2008). CD4 T cells: fates, functions, and faults. Blood 112(5): 1557-1569.

Zupke, O., Distler, E., Baumann, D., Strand, D., Meyer, R. G., Landfester, K., Herr, W. and Mailänder, V. (2010). Preservation of dendritic cell function upon labeling with amino-functionalized polymeric nanoparticles. Biomaterials 31: 7086-7095.

9 Danksagung

10 Veröffentlichungen

Teile dieser Arbeit wurden bereits publiziert und in Postervorträgen auf wissenschaftlichen Tagungen präsentiert.

10.1 Publikationen

Zupke, O., Distler, E., Baumann, D., Strand, D., Meyer, R. G., Landfester, K., Herr, W., Mailänder, V. (2010). Preservation of dendritic cell function upon labeling with amino-functionalized polymeric nanoparticles. Biomaterials. 31: 7086-7095

Zupke, O., et al. (in Vorbereitung). Nanoparticles and T cells: a comprehensive study on uptake and release.

10.2 Postervorträge

Zupke, O., Distler, E., Baumann, D., Strand, D., Meyer, R. G., Landfester, K., Mailänder, V., Herr, W. Nanoparticles for efficient labeling of dendritic cells to be used in cellular immunotherapy. CIMT Annual Meeting Mai 2010, Mainz, Germany

Zupke, O., Distler, E., Baumann, D., Strand, D., Meyer, R. G., Landfester, K., Mailänder, V., Herr, W. Preservation of dendritic cell function upon labeling with amino-functionalized polymeric nanoparticles. DGfI Annual Meeting September 2010, Leipzig, Germany

Mailänder, V., **Zupke, O.**, Distler, E., Baumann, D., Landfester, K., Herr, W. Labeling of Dendritic Cell Populations with fluorescent Nanoparticles: Feasibility and Influence on Cellular Functions. DGTI Annual Meeting Juni 2010, Berlin, Germany

Zupke, O., Distler, E., Paiphansiri, U., Strand, D., Dass, M., Theobald, M., Landfester, K., Mailänder, V., Herr, W. Nanoparticles for efficient labeling of human T lymphocytes to be used in adoptive immunotherapy. Cellular Therapy Meeting März 2011, Erlangen, Germany

Zupke, O., Distler, E., Paiphansiri, U., Strand, D., Dass, M., Theobald, M., Landfester, K., Mailänder, V., Herr, W. Nanoparticles for efficient labeling of human T lymphocytes to be used in adoptive immunotherapy. CIMT Annual Meeting Mai 2011, Mainz, Germany

Zupke, O., Jürchott, A., Distler, E., Paiphansiri, U., Strand, D., Dass, M., Theobald, M., Landfester, K., Mailänder, V., Herr, W. Labeling of human T lymphocytes with amino-functionalized nanoparticles for use in adoptive immunotherapy trials. DGHO Annual Meeting Oktober 2011, Basel, Schweiz

Sommer, M., **Zupke, O.**, Diken, M., Baier, G., Wolff, D., Distler, E., Theobald, M., Sahin, U., Landfester, K., Herr, W., Mailänder, V., Meyer, R. G. Targeting dendritic cells with functionalized nanoparticles. Cellular Therapy Meeting März 2011, Erlangen, Germany

Hofmann, D., Baumann, D., **Zupke, O.**, Distler, E., Herr, W., K. Landfester, V. Mailänder. Interaction of hydroxyethyl starch nanocapsules with primary cells from whole blood. BioNanoResponse Meeting (SPP1313), März 2012, Fulda, Germany

Sommer, M., Okwieka, P., **Zupke, O.**, Diken, M., Baier, G., Wolff, D., Distler, E., Theobald, Landfester, K., Herr, W., Mailänder, V., Meyer, R. G. Targeting dendritic cells with functionalized nanoparticles. CIMT Annual Meeting Mai 2012, Mainz, Germany

11 Lebenslauf